WNT7A and EGF Alter Myogenic Differentiation in hiPSCs Derived from Duchenne Muscular Dystrophy Patients

MARIA MADANA

Thesis submitted to the University of Ottawa
in partial Fulfillment of the requirements for the
M.Sc. program in Cellular and Molecular Medicine

Department of Cellular and Molecular Medicine
Faculty of Medicine
University of Ottawa

ABSTRACT

Duchenne Muscular Dystrophy (DMD) is a disorder caused by loss-of-function mutations in dystrophin, a critical protein that maintains muscle fiber integrity. Our lab discovered that dystrophin-deficient skeletal muscle stem cells, also known as satellite cells, cannot generate enough myogenic progenitors for proper muscle regeneration. Previously, we demonstrated that WNT7A, a protein expressed during muscle regeneration, stimulates symmetric division of satellite cells, and gives rise to two daughter satellite cells. Conversely, epidermal growth factor (EGF) induces asymmetric division, which generates one daughter satellite cell and one committed precursor cell. We aimed to investigate these satellite cell division mechanisms following WNT7A or EGF treatment in a human model using healthy and DMD-patient derived hiPSCs differentiated into the myogenic lineage. The presence of satellite-like cells was confirmed in both lines by their characteristic expression of PAX7 and other myogenic markers. Intriguingly, DMD-patient hiPSCs precociously differentiated compared to healthy control human induced pluripotent stem cells (hiPSCs). More notably, WNT7A treatment had a potent effect on the DMD differentiated cells. High content analysis revealed an expansion of the satellite-like cell pool as observed by a higher number of PAX7+ cells within the total population and gene expression analysis demonstrated a significant increase in global *PAX7* expression. In contrast, EGF treatment reduced the number of PAX7+ cells and increased the proportion of MYOG+ cells within the myogenic population, indicating an increase in myogenic progenitors. Taken together, WNT7A and EGF can alter the myogenic differentiation program of healthy and DMD-patient derived hiPSCs by modulating the satellite-like cell division dynamics.

TABLE OF CONTENTS

LIST OF FIGURES

LIST OF ABBREVIATIONS

AURKA – Aurora Kinase A

BRACHT – Brachyury or T-box transcription factor

CONT1-3 – Healthy control human induced pluripotent stem cell lines 1-3

DGC – Dystrophin glycoprotein complex

DMD1-3 – Duchenne Muscular Dystrophy human induced pluripotent stem cell lines 1-3

DMD – Duchenne Muscular Dystrophy

E6 – Essential 6 media

E8 – Essential 8 media

EGF – Epidermal growth factor

EGFR – Epidermal growth factor receptor

EV – Extracellular vesicles

FACS – Fluorescence activated cell sorting

FAPs – Fibro-adipogenic progenitors

FGF2 – Basic fibroblast growth factor

FOXC1/2 – Forkhead box C1/2

FZD7 – Frizzled Class Receptor 7

GFP – Green fluorescent protein

GSK3β – Glycogen synthase kinase-3 beta

hESC – Human embryonic stem cell

HGF – Hepatocyte growth factor

hiPSC – Human induced pluripotent stem cell

IGF-1 – Insulin-like growth factor 1

MARK2 – Microtubule affinity regulating kinase 2

MEOX1/2 – Mesenchyme Homeobox 1/2

MESP2 - Mesoderm posterior protein 2

MHC – Myosin heavy chain

MRF4 – Myogenic regulatory factor

MSGN1 – Mesogenin 1

MYF5 – Myogenic factor 5

MYOD – Myoblast determination protein

MYOG – Myogenin

NCAM – Neural cell adhesion molecule

NSG – NOD scid gamma mouse

PAX3 – Paired box gene 3

PCP – Planar cell polarity

PSM – Presomitic mesoderm

RA – Retinoic Acid

Shh – Sonic hedgehog signaling

SSEA-4 – Stage-specific embryonic antigen-4

T3 - Thyroid hormone

TA – Tibialis anterior

TBX6 - T-Box transcription factor 6

VANGL2 – Van-Gogh like 2

WNT – Wingless

ACKNOWLEDGEMENTS

I am grateful to Dr. Michael Rudnicki for providing me with the incredible opportunity to work in his laboratory during my undergraduate and master's degree. His unwavering support and guidance enabled me to truly grow and mature as a student researcher. I also extend my gratitude to Dr. Morten Ritso for his mentorship and collaboration on this project. His prior work laid the foundation for this project's success, and his patient teaching enabled me to undertake the meticulous task of hiPSC growth, maintenance, and differentiation.

I would like to express my appreciation to the Rudnicki lab members for their constant collaboration and support. I always felt like I was part of a team. Special thanks to Dr. Derek Hall for his invaluable guidance with the Columbus and R Studio scripts, Ricardo Carmona for his Western Blot expertise, and Stephen Baird for performing all the high-content imaging with the Opera Phenix High-Content Screening System. Thank you to Marie Esper for revising this thesis.

Lastly, I would like to extend my sincere gratitude to all the current and past members of Dr. William Stanford's laboratory. The Human Pluripotent Stem Cell Facility was my second home for four years, and the Stanford lab members were always available to support me and my project. Working in such an amazing environment was a privilege, and I am grateful for the opportunity.

1 INTRODUCTION

1.1 SKELETAL MUSCLE STEM CELL REGENERATION AND SATELLITE CELL DIVISION MECHANISMS

Striated skeletal muscle is the most abundant tissue in the human body, accounting for roughly 40% of total body mass (1). Controlled by the somatic nervous system, skeletal muscle contributes to a variety of bodily functions (2). Mechanically, skeletal muscle converts chemical energy into mechanical energy in order to generate force and power, maintain posture, and produce movement (1). Metabolically, skeletal muscle contributes to basal energy metabolism, stores important substrates such as amino acids and carbohydrates, produces heat for core temperature maintenance, and consumes most of the oxygen and fuel used during physical activity and exercise (1).

Skeletal muscle has a remarkable ability to regenerate (2, 3). Following injury, exercise, or weight-related trauma, skeletal muscle can completely restore its structure and function (2, 4). The crucial mediators of muscle regeneration are skeletal muscle stem cells, termed satellite cells (2, 5). These mononucleated cells were first discovered in 1961 and named satellite cells due to their sublaminar location and intimate association with the sarcolemma of myofibers (5, 6). Satellite cells are characterized by their ubiquitous expression of the paired box transcription factor PAX7 (7).

PAX7 is required for the postnatal growth, maintenance, and regeneration of skeletal muscle. PAX7-null mice show marked muscle wasting and a progressive loss of functional satellite cells through precocious differentiation, which lead to death within 2 weeks after birth (2, 7, 8). PAX7 depletion in adult mice using inducible *PAX7 Cre-ER^{T2}* tamoxifen-treated mice dramatically reduced the number of satellite cells and prevented muscle

regeneration, indicating its essential role in adult myogenesis. (2, 3, 9). Similarly, conditionally depleting satellite cells by expressing a human diphtheria toxin receptor under the control of the murine PAX7 locus resulted in significant muscle tissue loss and failure to regenerate skeletal muscle (2, 10, 11). Notably, muscle regeneration could be rescued by satellite cell transplantation into the depleted muscle (10).

In resting skeletal muscle, satellite cells remain mitotically quiescent, however, they can become activated in response to exercise, injuries, or disease. They enter the cell cycle, fuse, and differentiate – a process that is controlled by the sequential expression of transcription factors (12). Myogenic factor 5 (MYF5), Myogenic Differentiation (MYOD), Myogenin (MYOG), and Myogenic Regulatory Factor 4 (MRF4) are the four transcription factors that comprise the myogenic regulatory factor family (MRF). These MRFs direct muscle progenitor cells through the skeletal muscle lineage (13). Once activated, the satellite cells re-enter the cell cycle to proliferate. These committed satellite cells are referred to as myoblasts and they express PAX7, and/or MYF5, and/or MYOD (2, 7, 14). After many rounds of proliferating, these myoblasts exit the cell cycle and differentiate into mature myocytes. This terminal differentiation program is characterized by a decrease in PAX7 and MYF5 expression, and by an increase in MYOG and MRF4 levels (2, 4). Finally, the myocytes can fuse to form new multinucleated myotubes and/or fuse to damaged myofibers. At this point, MYOD levels decline as the expression of myosin heavy chain (MHC) and other contractile proteins escalate. The balance of various MRFs is essential for regulating cell fate (2, 4, 7).

A long-term self-renewing stem cell population that expresses PAX7 but not MYF5 ($PAX7^{+}/MYF5^{-}$) appears to make up around 10% of the satellite cell population.

Transplantation and serial injury experiments have previously demonstrated that this population can replenish the satellite stem cell pool in addition to contributing to the committed progenitor pool (15). The remaining 90% of the satellite cell population are committed, MYF5-expressing cells ($PAX7^+/MYF5^+$) that appear to self-renew on a short-term basis (15, 16). Using a *Myf5-Cre* knock-in allele and a *ROSA-YFP* Cre reporter, Kuang et al. demonstrated that during muscle regeneration, satellite cells can undergo either asymmetric or symmetric division (15). During symmetric division, one $PAX7^+/MYF5^-$ satellite cell gives rise to two identical daughter $PAX7^+/MYF5^-$ cells in a planar (parallel) orientation relevant to the muscle fiber (15, 17). Conversely, in asymmetric division, one $PAX7^+/MYF5^-$ satellite cell gives rise to one daughter $PAX7^+/MYF5^-$ satellite cell and one $PAX7^+/MYF5^+$ committed myogenic progenitor cell. Asymmetric divisions of satellite cells typically occur in an apical-basal orientation (the polarity of cell division occurs at a right angle to the basal lamina), with the generation of a basal $PAX7^+/MYF5^-$ cell and an apical $PAX7^+/MYF5^+$ cell (15, 18). A tightly regulated balance between symmetric self-renewal and asymmetric division is required to maintain the satellite stem cell pool and generate enough committed progenitor cells for muscle regeneration (19).

The satellite stem cell niche plays a critical role in the establishment of apical-basal polarity for asymmetric division of satellite cells. These cells are situated within a niche between the sarcolemma and basal lamina of myofibers (20). Adhesion proteins such as M-cadherin and NCAM are polarized at the sarcolemmal surface of quiescent satellite cells, while high levels of dystroglycan and Integrin-α7 and -β1 are polarized at the basal level. Quiescent satellite cells interact with extracellular matrix components in their niche through the expression of heparan sulfate proteoglycans Sydecan-3 and Sydecan-4, which act as co-

receptors for Integrins, Notch, and Frizzled 7 (FZD7). This interaction with the basal lamina is thought to promote quiescence in satellite cells. During asymmetric cell division, the committed daughter progenitor cell is no longer in contact with the basal lamina, while the daughter satellite cell remains in the basal position to maintain niche interactions and return to quiescence (21).

Prior to asymmetric division, the partitioning defective (PAR) polarity complex is essential for determining the polarity of the satellite cell. The PAR-complex plays a key role in establishing polarized centrosomes and facilitating the formation of mitotic spindles at these sites to drive asymmetric division. Adhesion factors expressed by the satellite cell affect the localization of the PAR-complex through the dystrophin-glycoprotein-complex (DGC), which serves to connect the surrounding extracellular matrix and the basal lamina (21).

1.2 Embryonic and Fetal Myogenesis

Embryonic myogenesis occurs post-gastrulation, following the formation of the primitive streak, when the cells ingress into the primitive streak and form the ectoderm, mesoderm, and endoderm germ layers (22). The mesoderm is subdivided anatomically into three distinct regions: the paraxial, intermediate, and lateral plate, with the paraxial mesoderm giving rise to the presomitic mesoderm tissue (PSM). The PSM is composed of two regions, the immature posterior, and the committed anterior region, with the latter forming the segmented somites. The formation of somites is a result of morphogen gradients that exist at both ends of the PSM. To regulate the production of somites, the segmentation clock, a molecular oscillator, generates periodic pulses of Notch, FGF, and WNT signaling

(23). The posterior end of the presomitic mesoderm is highly exposed to WNT/FGF signaling, where cells exhibit the expression of paraxial mesoderm markers such as *MSGN1*, *TBX6*, and *BRACHT*. These markers are known to be key targets of WNT and FGF signaling. When the cells move towards the anterior side of the presomitic mesoderm, they reach the determination front, where they encounter increased concentrations of retinoic acid (RA) signaling originating from the anterior somitic region. RA signaling opposes the effects of WNT/FGF signaling, triggering metabolic and transcriptional alterations in the cells, leading to the expression of *MESP2*, *PAX3*, *FOXC1/2*, and *MEOX1/2* expression. A somite boundary is formed at the tip of the anterior PSM when MESP2 activates Eph-ephrin signaling, which creates a new furrow (Figure 1) (22).

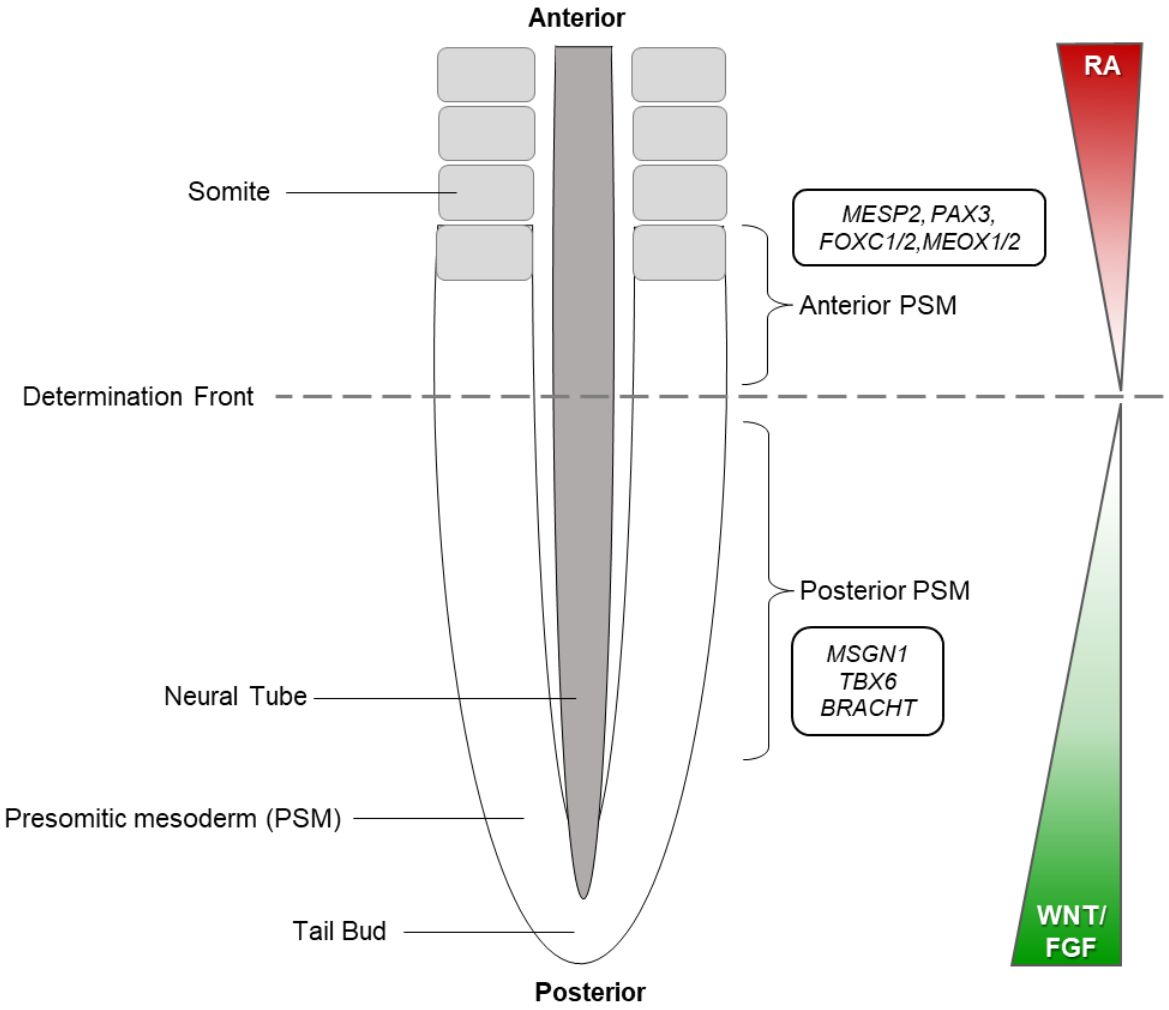

Figure 1. Simplified diagram of somitogenesis. In embryonic vertebrates, the formation of a somite begins in the immature, posterior presomitic mesoderm (PSM). The posterior end is exposed to high levels of WNT and FGF signaling (as demonstrated by the green gradient). As the PSM cells reach the determination front (the dashed line), they encounter an opposing gradient of retinoic acid (RA, in red) signaling originating from the anterior segmented region. In lateral pairs, the now epithelial like somites bud off and further differentiate into the sclerotome, dermomyotome, and myotome. The genes that characterize the anterior and posterior PSM are shown in boxes.

The newly formed somite gives rise to the dermomyotome, sclerotome, and myotome. The ventral compartment of the somite gives rise to the sclerotome, while the dorsal compartment generates the dermomyotome and myotome. In the ventral compartment, Sonic hedgehog signaling (Shh) acts as a morphogen and triggers the expression of paired box 1 (*PAX1*) and *PAX9* in the sclerotome, which later develops into cartilage and bone (23, 24). In the dorsal compartment, the dermomyotome cells produce skeletal muscle, excluding certain head muscles, and are distinguished by their expression of *PAX3*, *PAX7*, and low levels of *MYF5* (24). The expression of *PAX3/7* in the dermomyotome is induced by WNT signaling originating from the neural tube and ectoderm (25).

Primary myogenesis begins when the cells at the middle dorsal dermomyotome express the myogenic transcription factors *MYF5* and *MYOD1*. These committed myogenic cells, termed myoblasts, proliferate and further differentiate and fuse into primary myotubes that form the primary myotome (26). β-catenin binds its receptor WNT1/3A in the myotome to induce myogenic differentiation. Wnt signaling regulates Shh signaling to also induce myogenic commitment through up-regulation of *MYF5* and *MYOD* (27). After the myotome is formed, the dermomyotome disintegrates, and its PAX3-positive cells migrate into the myotome to remain as precursors for later phases of myogenic differentiation (23). Conversely, some PAX3-positive cells from the lateral dermomyotome migrate into the trunk and limb buds and differentiate into various tissues, including limb muscles, lymphatic endothelia, and vascular tissues.

During secondary, or fetal, myogenesis, a subset of PAX3 positive myogenic progenitors downregulate PAX3 expression and upregulate PAX7. These PAX7 positive cells fuse together to form larger secondary fibers and can even fuse along the surface of

primary myotubes as a template. A portion of this PAX7+ myogenic precursor population are enveloped into developing myofibers and remain as satellite cells in postnatal skeletal muscle (Figure 2) (24).

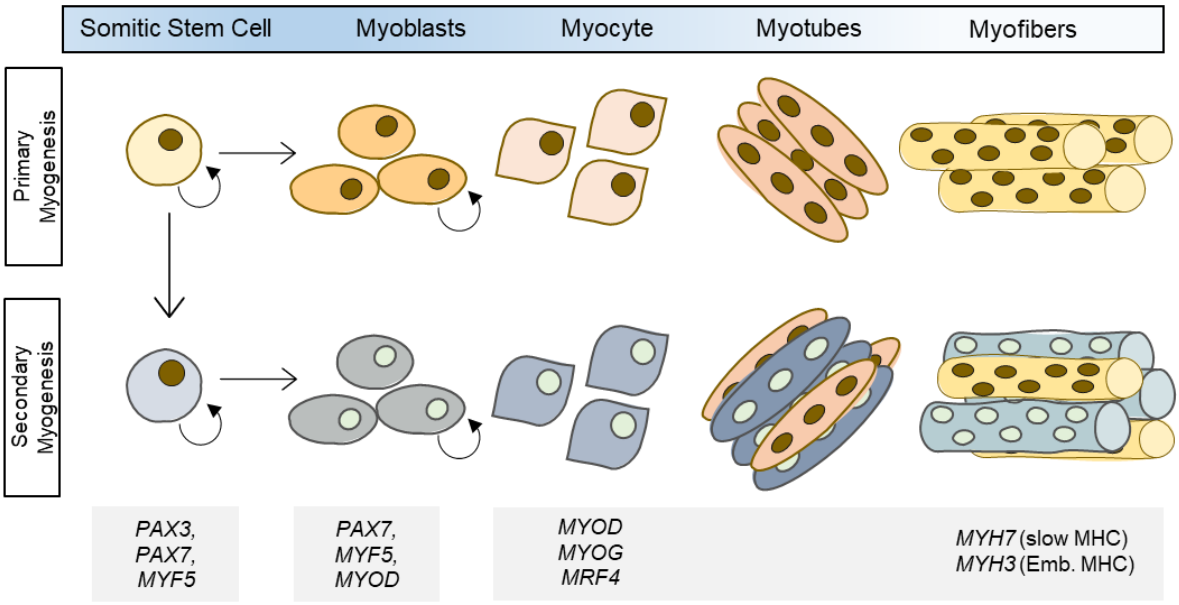

Figure 2. Summary of primary and secondary myogenesis. Primary myogenesis (summarized in the first row) is the formation of the first wave of skeletal muscle fibers which occurs during embryonic development. Myoblasts derived from the somitic stem cell proliferate, differentiate, and fuse to form primary myotubes (depicted in yellow). Secondary myogenesis (second row) occurs during fetal stages of development. The $PAX7^{+}$ fetal stem cell proliferates and then fuses either amongst themselves or along the surface of primary myofibers generated during primary myogenesis. The grey boxes at the bottom indicate the myogenic genes that are specified in each stage.

Skeletal myogenesis can be recapitulated *in vitro* from human pluripotent stem cells through directed differentiated (more on this later). Intriguingly, a couple of studies have tried to emulate the segmental clock and derive somites from pluripotent stem cells, including mouse embryonic stem cells, and human pluripotent stem cells, and yet these models seem to lack *PAX7* or *MYF5* expression in the dermomyotome (28–30).

1.3 Duchenne Muscular Dystrophy and Dystrophin Expression in Satellite Cells

Duchenne muscular dystrophy (DMD) is a devastating genetic muscular disorder that is characterized by progressive muscle weakness and wasting. This fatal disease affects around 1 in 3500 male births and ultimately results in death by the second or third decade of life due to respiratory insufficiency or cardiomyopathy in early childhood (31). DMD is caused by mutations in the *DMD* gene which encodes for the dystrophin protein. Dystrophin is a 3600-residue rod-shaped protein that is expressed in differentiated myofibers and connects the myofiber cytoskeleton to the extracellular matrix through the dystrophin-associated glycoprotein complex (DGC) (19). In the absence of dystrophin, muscle fibers are greatly weakened and muscle contraction-induced stress results in constant cycles of muscle regeneration and degeneration, leading to a loss of muscle mass and function (2, 32). There is currently no cure for DMD, however, glucocorticoid treatment along with cardioprotective treatment, ventilatory support, and physical therapy help delay the progression of the disease (31).

Previous studies have postulated that human DMD progression is a consequence of muscle stem cell exhaustion caused by the repetitive cycles of degeneration and regeneration (33–35). However, multiple studies have indicated an increase in the number of satellite cells

in mouse and human dystrophic muscle suggesting that the depletion of satellite cells is not the primary cause for impaired muscle regeneration (36, 37).

In 2015, Dumont and colleagues made a remarkable discovery regarding the role of satellite stem cells in the mouse model for DMD, hereafter referred to as *mdx* mice (19). Our lab discovered that *DMD* is highly transcribed in activated satellite cells, and dystrophin associates with the kinase MARK2 to regulate internal cell polarity. Furthermore, we discovered that PARD3 is distributed in a polarized manner at the opposite end of satellite cell along the apicobasal axis. This primes the satellite cell to undergo asymmetric division and give rise to a daughter satellite stem cell (for its self-renewal) and a daughter myogenic precursor cell (for myogenic commitment). Therefore, in *mdx* mice with dystrophin-deficient satellite cells, we observed a downregulation of MARK2, a loss of PARD3 polarization, and consequently reduced asymmetric cell division that resulted in the gradual loss of committed progenitors and a satellite stem cell hyperplasia. This decrease in myogenic precursor production leads to inefficient muscle regeneration. These findings importantly demonstrate that muscle wasting in DMD is not only caused by myofiber fragility – but also the inability of satellite cells to perform asymmetric division. Hence, interference in the homeostasis of symmetric divisions to asymmetric divisions notably contributes to DMD pathology.

1.4 WNT7A Induces Symmetric Expansion of Satellite Cells

As previously mentioned, Wnt signaling pathways play essential roles in regulating embryonic myogenesis. Wnt signaling from the dorsal neural tube or ectoderm can initiate and progress myogenesis in the presomitic mesoderm and early somites (38, 39). Additionally, Wnt signaling can regulate the expression of myogenic transcription factors

including *PAX3/7*, *MYF5*, and *MYOD* in embryonic myogenic progenitors to induce commitment and differentiation (26, 39). In the post-natal muscle, the roles of Wnt signaling during muscle regeneration have been controversial. After injury, satellite cells undergo a proliferative phase prior to fusing together to form new myofibers. One study indicated that Wnt proteins dramatically increase satellite-cell proliferation through the canonical Wnt/β-catenin pathway during muscle regeneration (39, 40). Conversely, another study demonstrated that satellite cells differentiate after exogenous Wnt treatment, due to a switch from Notch signaling to Wnt signaling through the canonical pathway (41). In a more recent comprehensive genetic study, Murphy et al. demonstrated that silencing, rather than activating, the canonical Wnt/β-catenin signaling pathway in adult satellite cells is important for muscle regeneration (39, 42).

Our lab has made significant advances in the role of WNT7A signaling in muscle growth and regeneration. Particularly, we have demonstrated that Frizzled 7 (FZD7), a G-protein-coupled transmembrane Wnt receptor, is expressed at high levels in quiescent satellite cells, suggesting a possible involvement of non-canonical Wnt signaling (17). Further analysis revealed that WNT7A was upregulated during muscle regeneration and binds to the FZD7 receptor at the surface of satellite cells. Interestingly, stimulation with WNT7A did not activate the canonical Wnt/β-catenin signaling pathway. Instead, we found that WNT7A binds to FZD7 and activates the non-canonical planar-cell-polarity (PCP) pathway, leading to symmetric expansion of satellite cells and accelerated muscle regeneration (39). The activation of the PCP pathway with WNT7A also leads to the polarized distribution of the PCP effector, Vangl2, at either pole of the satellite cell

undergoing symmetric planar cell division. Inhibition of Vangl2 expression abolishes the effects observed by WNT7A on the expansion of satellite stem cells.

Overexpression of WNT7A during TA (tibialis anterior) muscle regeneration of mice resulted in an impressive enhancement of the regeneration process and the creation of more fibres of bigger caliber. Importantly, Maltzahn et al. investigated the therapeutic potential of WNT7A in *mdx* mice (43). They discovered that WNT7A treatment efficiently induced satellite cell expansion and myofiber hypertrophy as well as significantly increasing muscle strength in treated muscles in *mdx* mice. The ability of WNT7A to drive muscle growth with satellite cell expansion and productive hypertrophy suggests that WNT7A may be used as a potential therapeutic for dystrophic muscles in DMD. Although we do observe satellite stem cell hyperplasia in adult *mdx* mice, WNT7A treatment is thought to increase the absolute number of asymmetric divisions as the total number of satellite cells would increase. Furthermore, Maltzahn et al. demonstrated that WNT7A can act on differentiated myofibers and activate the AKT/mTOR pathway which can have a protective effect in *mdx* mice (44).

1.5 EGF Induces Asymmetric division of Satellite Cells

Previous research has suggested that the epidermal growth factor receptor (EGFR) plays a role in myogenic differentiation. For example, Olwin et al. demonstrated that downregulation of EGFR was necessary for differentiation in mouse myoblasts (45). Similarly, Leroy et al. found that EGFR is a key regulator of human myoblast differentiation and is downregulated during the early stages of differentiation (46).

In a recent study, our lab characterized the role of EGFR in satellite cells. Through an *in-niche* muscle stem cell screen, we revealed that the activation of epidermal growth factor

receptor (EGFR) and the mitotic spindle assembly protein, aurora kinase A (Aurka), are key determinants of asymmetric division of satellite stem cells (47). We found that quiescent satellite cells express EGFR at their basal surface, and following treatment with epidermal growth factor (EGF), activated EGFR phosphorylated on Tyr1068 (p-EGFR) recruits Aurka, and drives the asymmetric division of satellite cells. This, in turn, increased the number of MYOG-expressing committed myogenic progenitors. Importantly, we observed that EGF stimulation or inhibition of EGFR did not affect the cell cycle re-entry, rate of mitosis, or total cell numbers *in vitro*. This indicated that EGFR acts as a determinant of satellite stem cell fate and is not acting as a mitogen (47). Furthermore, our research uncovered that the EGFR polarity pathway operates independently of the dystrophin-mediated polarity determination and can rescue the deficit in asymmetric division observed in dystrophin-deficient satellite cells. Notably, treatment with EGF in *mdx* muscles, resulted in increased generation of myogenic progenitors, improved regeneration potential, and ameliorated disease progression. These findings highlight the potential of EGF and EGFR as therapeutic targets for enhancing muscle regeneration in conditions such as DMD.

1.6 Disease Modeling with Duchenne Muscular Dystrophy Patient Derived hiPSCs

Perhaps a major challenge currently hindering the development of effective therapies for DMD is the lack of an animal model that closely recapitulates the disease progression in humans (48). Many of the aforementioned studies used the *mdx* mouse as a model for DMD. However, *mdx* mice exhibit only a mild dystrophic phenotype as they live a near-normal lifespan and reproduce normally (49). Their muscles appear normal at birth, but around 4-8 weeks, they undergo only a transient period of muscle degeneration and regeneration and

never exhibit the profound loss of muscle strength and death observed in human DMD patients (50). Therefore, there is a critical need to recapitulate the pathophysiological mechanisms of DMD in a human preclinical model. Takahashi et al. opened an avenue to generate patient and disease-specific pluripotent stem cells by reprogramming human adult fibroblasts into pluripotent stem cells (51). There have been many protocols developed to differentiate human pluripotent stem cells, such as induced pluripotent stem cells (iPSCs), to skeletal myofibres *in vitro* (52, 53). iPSCs derived from DMD patients are expected to be a better source for modelling DMD *in vitro* because they can be derived from the patients, and they have the ability to show key disease features. Patient-specific iPSCs are thus a useful platform and complement current animal models of DMD to study the underlying pathological mechanisms of DMD as well as testing therapeutic treatments.

There are currently two main approaches to inducing myogenic differentiation of hiPSCs: 1) the reprogramming and 2) chemically defined methods of myogenic induction. In 1) reprogramming protocols, hiPSCs are differentiated into the myogenic lineage by the overexpression of the myogenic transcription factors *PAX3, PAX7,* or *MYOD1*. To introduce these genes into the genome of hiPSCs, lentiviral systems and piggyback systems can be used, and selective transcription of these genes can be induced by gene expression systems such as tetracycline or tamoxifen (54). The cells that express these genes can be sorted and purified using fluorescent activated cell sorting (FACS), especially if they have a fluorescent reporter gene integrated such as GFP (green fluorescent protein) or mCherry.

In the 2) non-reprogramming approach, hiPSCs are differentiated through unique culture conditions and sequential addition of growth and differentiation factors to recapitulate the defined transitions from early embryonic myogenesis to fetal and post-natal

myogenesis (55). This study used the 2016 Shelton et al. protocol, which starts the differentiation program by treating a monolayer of hiPSCs with CHIR99021, a potent GSK3β (glycogen synthase kinase-3) inhibitor, to activate Wnt signalling and induce the formation of the paraxial mesoderm and form presomitic mesoderm progenitors (52). CHIR99201 significantly enhances the expression of mesoderm genes such as *TBX6*, *MSGN1*, and *MESP1* during the first week of differentiation (52, 54). FGF2 is added to the cultures beginning on day twelve. This factor acts on the dermomyotome progenitors to support their commitment to the myogenic lineage and promotes progenitor cell proliferation (52). Therefore, around day twelve of the differentiation process, the cells start to upregulate muscle specification genes such as *PAX3* and *PAX7*. By day twenty-one, there are a significant number of myogenic-like cells expressing the different MRFs and the differentiation continues until the endpoint, which is day fifty.

Several studies have demonstrated myogenic differentiation of human embryonic stem cells (hESCs) or hiPSCs through *MYOD1* overexpression (54, 56–58). However, this method bypasses early embryonic differentiation stages and initiates myogenesis at the myoblast stage, making it challenging to study early myogenesis. Moreover, these cells do not follow the defined myogenic developmental stages and may not accurately represent mature skeletal muscle tissue (55). More importantly, *MYOD1*-reprogrammed iPSCs cannot replenish the muscle stem cell niche, as they do not express *PAX3* or *PAX7*, and lack the regenerative potential of adult stem cells (55).

In the context of therapeutic applications, the chemically defined method of myogenic induction is superior to reprogramming methods. While reprogramming methods can produce myogenic progenitors more quickly and generate approximately 90% of

myogenic-like cells, the use of exogenous DNA can lead to genetic instability and disruption of cellular processes (54, 55). This is a significant concern for cell-based therapies, particularly for patients with DMD, and may raise additional regulatory considerations.

After induction of hiPSCs into the myogenic lineage, these myogenic progenitors can be transplanted into mice to promote the regeneration of new muscle fibers. In 2012, Darabi et al. induced PAX7 expression in hESCs and hiPSCs to derive myogenic progenitors (59). They incorporated a GFP reporter downstream of the *PAX7* gene and purified the PAX7+GFP+ cells through FACS. After expanding this sorted population, they transplanted the hESC/hiPSC-derived myogenic progenitors into NSG (NOD/SCID gamma-c mice, an immunodeficient strain of mice) -*mdx* mice. Two months after transplantation, they observed significant engraftment of human-derived myofibers and significant functional improvement in the NSG-*mdx* mice.

In a recent 2022 study, Sun et al. derived myogenic progenitors from hiPSCs using a chemically defined media procedure and a PAX7-specific fluorescent reporter system (60). After purifying the PAX7+GFP+ cells through FACS, they transplanted them into NSG and NSG-*mdx* mice to study their regenerative capacity. They found that these cells contributed to the regeneration of new myofibers and, more importantly, engrafted and matured into local quiescent satellite cells. These cells maintained PAX7 expression and self-renewed to replenish the satellite stem cell pool following injury. They demonstrated long-term self-renewal properties, which is crucial for muscular degenerative disorder therapeutics.

DMD patient-derived hiPSCs can also reveal important pathophysiological mechanisms underlying DMD. For example, Mournetas et al. conducted a comprehensive multi-omics study where they revealed that differentiated DMD hiPSCs show transcriptional

defects at the somite stage, even before the expression of myogenic markers and the expression of muscular dystrophin (61). The DMD hiPSCs were able to enter the mesoderm lineage unimpaired, however, many somite markers were dysregulated. The authors found that DMD onset starts at day ten of the differentiation process, where they observed dysregulation of mitochondrial genes, early induction of the sonic hedgehog signaling, and an upregulation of fibrosis and collagen-related genes.

Overall, hiPSC-derived myogenic progenitors from DMD patients have immense potential for advancing our understanding of the underlying mechanisms of DMD pathology and developing effective therapeutic interventions. These cells provide an invaluable human platform for modeling disease pathogenesis and trialing new therapies.

1.7 THESIS OBJECTIVES

To date, little is known about the modulatory capacity of WNT7A and EGF on the division of human satellite cells in healthy or dystrophic conditions, as many of the aforementioned studies have mainly utilized transgenic mouse models. Therefore, in this study, we employed a modified and thoroughly optimized version of the 2016 Shelton et al. protocol to derive myogenic progenitors from DMD-patient and healthy control individual hiPSCs (52). We performed WNT7A or EGF treatment on these hiPSC-derived myogenic progenitors and hypothesized that the treatments could modulate human satellite cell division dynamics in the same way as reported by Wang et al., and Le Grand et al. (see summary Figure 4) (17, 47). Here, we delve into the differences in myogenic differentiation between the healthy and DMD-patient derived hiPSCs. More importantly, we provide the

first evidence that WNT7A and EGF treatment can alter the division dynamics of hiPSC-derived myogenic progenitors.

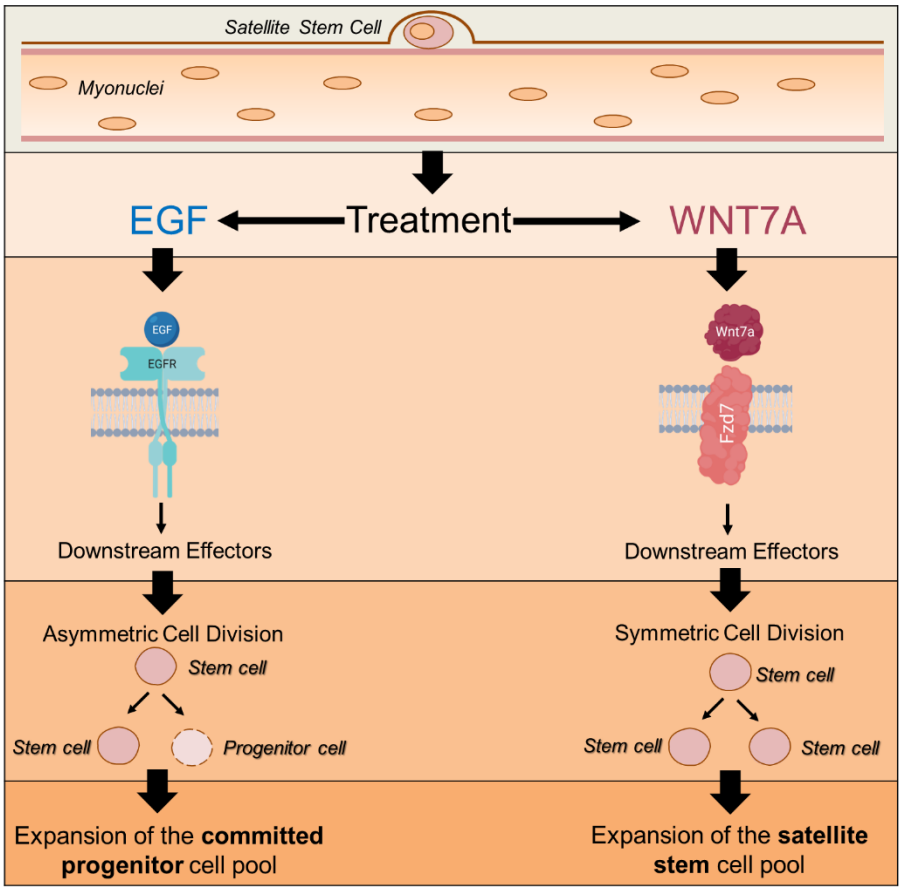

Figure 3. The division modulatory abilities of WNT7A and EGF. WNT7A induces symmetric cell division in satellite cells and expands the satellite stem cell pool through the non-canonical planar cell polarity pathway. EGF induces asymmetric division and expands the committed myogenic progenitor cell pool through the EGFR-AURKA signaling pathway.

2 MATERIALS AND METHODS

2.1 HUMAN INDUCED PLURIPOTENT STEM CELL CULTURE

This study was conducted under the Stem Cell Oversight Committee's approval of using human pluripotent stem cells. The IRB Approval Code is Protocol #2011706-01H - Use of Induced Pluripotent Stem Cells. Dr. Morten Ritso, a post-doctoral fellow from our laboratory, obtained myoblasts from 2 patients with DMD and 3 healthy control individuals from the UK MRC Biobank Centre for Neuromuscular Diseases in Newcastle upon Tyne, United Kingdom. The first DMD line (DMD1) carried a nonsense mutation in exon 6 at codon 637, and the second line (DMD2) carried a C>T mutation in codon 5899 of exon 41. The myoblasts were reprogrammed into hiPSCs at the Ottawa Hospital Research Institute, Human Pluripotent Stem Cell Facility through episomal reprogramming. Dr. Ritso conducted all the hiPSC characterization, including immunostaining for pluripotency markers, karyotyping, spontaneous *in vitro* differentiation assays to monitor their ability to generate all three germ layers, alkaline phosphatase assays, and teratoma assays (Morten Ritso & Michael Rudnicki; unpublished).

A third DMD-patient hiPSC line was provided to us by Dr. Nicolas Dumont. The Dumont laboratory obtained peripheral blood mononuclear cells from a DMD patient, carrying a depletion of exons 48-52, and reprogrammed them into hiPSCs at the CHU Sainte-Justine Stem Cell Core Facility using integration-free based Sendai virus. Following transduction, emerging clones were manually picked and cultured under feeder-free conditions using Matrigel (Corning 3542341)-coated dishes and mTeSR™ Plus medium (STEMCELL Technologies 00-0276) for a minimum of 15 passages to ensure stable pluripotency. The hiPSCs were characterized to show a normal karyotype and express the human *SSEA-4*, *SOX2*, *OCT4* and *TRA1-60* makers (Philippe Campeau, Morten Ritso, and Nicolas Dumont; unpublished). The identity of each hiPSC line used in this study is further characterized in Table 7 in the Results section 3.1.

All hiPSC lines were initially cultured in mTeSR™ Plus medium (hereon referred to as mTeSR™). They were maintained in Matrigel-coated (Corning 3542341) 6-well tissue culture plates (Greiner 657165 or Falcon 353046) in a feeder-free and serum-free

environment. The hiPSCs were routinely passaged every 3 days using 500µM EDTA in Dulbecco's phosphate-buffered saline (DPBS, ThermoFisher 14190144), at a split ratio of 1:6. After the hiPSCs have reached the desired confluency (around 80-90% confluent), they were slowly transitioned into Essential 8 media (E8). The components of E8 are outlined in Table 1. The hiPSCs were weaned onto E8 by 25% increments. The first day, they would be placed in 75% mTeSR™ and 25% E8. The next day, it would be 50% mTeSR™ and 50% E8. And the following day (the third day), it would be 25% mTeSR™ and 75% E8. On the third day, the hiPSCs would be ready to be passaged, and they would be passaged in the media composition of that day. The weaning onto E8 would resume the following day. After the hiPSCs have reached only E8 media, they would be passaged 2-3 times in pure E8 over the course of about 2 weeks. They were split at a ratio of 1:3 using EDTA. The cells would be fed every day and incubated at 37°C in a 10% CO_2 5% O_2 hypoxic environment. Additionally, the hiPSCs would be monitored daily under a dissection microscope for spontaneous differentiation. These differentiated cells would appear darker and without defined colony borders, and would be "picked away" with a pipette tip (52, 62).

Two of the DMD hiPSC lines and one healthy control line (all derived from Dr. Morten Ritso) were tested for mycoplasma and were found to be negative for contamination (Figure 4).

Table 1. Media components for hiPSC growth and differentiation. The first column indicates the base medium and the factors, the second column indicates the supplier and catalogue number, and the last column indicates the final concentration of each component. Note that E6 media contains the same components as E8 but lacks the pluripotency factors bFGF and human TGFβ1.

E8/E6 Media		
DMEM/F12	LifeTech 11330107	100%
Components		
Ascorbic acid	Sigma A8960-5G	64µg/ml
Sodium bicarbonate	Sigma S5761	543µg/ml
Recombinant human insulin	Wisent 511-016-CM	19.4µg/ml
Sodium Selenite	Sigma S5261-10G	14 ng /ml
Human holo-transferrin	Sigma T0665-1G	10.7µg/ml
Gentamicin sulphate	Wisent 450-135-XL	5 µg/mL
bFGF (E8 only)	LifeTech PHG0263	100 ng/mL

Human TGFβ1 (E8 only)	LifeTech PHG9202	2 ng/mL

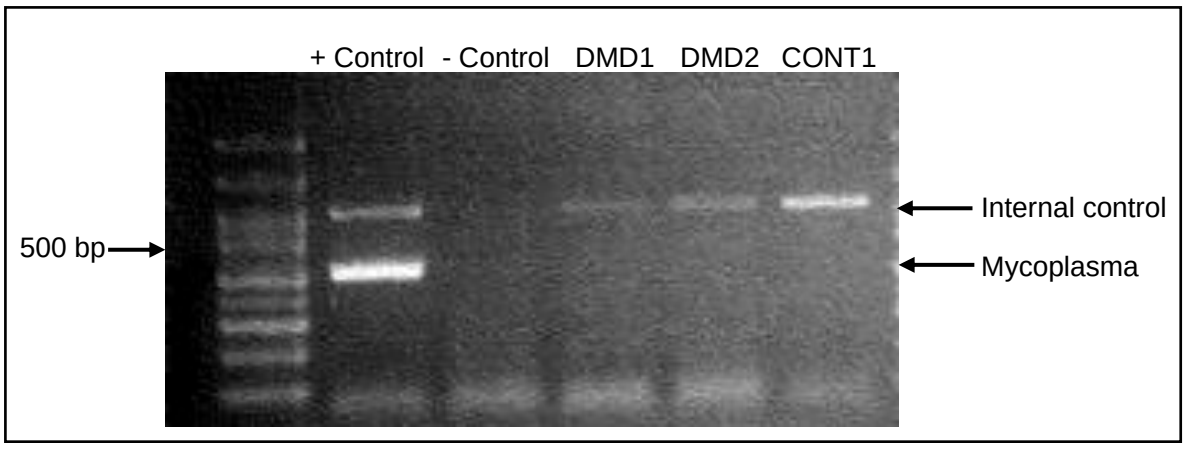

Figure 4. Absence of mycoplasma contamination in DMD1-2 and CONT1 hiPSCs. DMD1-2 and CONT1 (healthy control cell line 1) hiPSCs were grown and maintained in antibiotic free E8 media for 2 weeks and subsequently tested for mycoplasma contamination through PCR at The Ottawa Hospital Human Pluripotent Stem Cell Facility.

2.2 MYOGENIC DIFFERENTIATION OF HIPSCS AND OPTIMIZATION PROCEDURE

This study employed the 2016 Shelton et al. protocol for myogenic differentiation of hiPSCs (52). We followed a modified version of this protocol in three iterations, with each subsequent iteration an optimized version of the previous.

In the first iteration, the hiPSCs were cultured in pure mTeSR™ until they reached 90% confluency prior to differentiation (without prior culture in E8 media). On the day of differentiation, the hiPSCs were treated with 10μM ROCK inhibitor (Sigma Y0503) for 1 hour to minimize dissociation-induced apoptosis. After 1 hour, the hiPSCs were "cleaned" to remove any spontaneously differentiated cells and washed with PBS (Gibco 10010-023). Next, the colonies were dissociated into individual cells using Accutase (ThermoFisher A1110501) and incubated at 37°C in a 10% CO_2 5% O_2 hypoxic environment for 20 minutes. The disassociated hiPSCs were then re-plated onto a Matrigel-coated 12-well tissue

culture dish (Thermoscientific 130184) at a density of 2.0×10^5 cells per well and fed with mTeSR™ supplemented with 10μM ROCK inhibitor. Roughly 24 hours later, the hiPSCs were induced into the mesoderm lineage with 10μM CHIR99021 (Tocris 4423) supplemented in TeSR™-E6 Medium (STEMCELL Technologies 05947). The induction medium was added very slowly to avoid disrupting the fragile hiPSCs. The cells were then placed into a 5% CO_2 normoxic incubator overnight at 37°C. The following day, the same induction medium was added in a very slow manner and the cultures were returned to the incubator. For the next 10 days, the differentiating cultures were fed everyday with TeSR™-E6 without any other supplements. Starting from day 12, the cells were fed with TeSR™-E6 medium supplemented with 5ng/ml human recombinant basic fibroblast growth factor (FGF2, ThermoFisher GF003AFMG) on a daily basis. On day 21, the differentiating cells were dissociated into single-cells with Accutase, and seeded onto a new 12-well, Matrigel coated dish at a lower density of 1.5×10^5 cells per well. Dr. Morten Ritso has previously demonstrated that passaging the differentiating hiPSCs on day 21 leads to an enrichment of the myogenic population and enhances their engraftment potential in mice (Morten Ritso & Michael Rudnicki; unpublished). From day 21 to 50, the cells were fed every other day with TeSR™-E6 medium supplemented with 5ng/ml of FGF2.

For the second iteration of optimizing the myogenic differentiation protocol, all previously mentioned steps were maintained constant except for the replacement of TeSR™-E6 medium with Essential 6 (E6) medium. Table 1 provides an overview of the components of E6 medium.

For the third and final iteration, the hiPSCs were slowly transitioned from pure mTeSR™ to E8 media over the course of 2-3 passages as outlined earlier. Furthermore, a 24-well glass-

bottom tissue culture dish (Ibidi 82426) was used instead of a plastic 12-well plate as it was better suited for high-resolution imaging. Therefore, after dissociating the hiPSCs with Accutase, they were re-plated in the Matrigel-coated 24-well plate at a density of 8.2×10^4 cells per well. The optimal seeding density for all three DMD hiPSC lines required up to 9×10^4 cells per well as they were more sensitive to the CHIR99021 treatment. The replated cells were fed with E8 media supplemented with 10μM ROCK inhibitor. The next day, the hiPSCs were slowly fed with E6 media supplemented with 7.5μM of CHIR99021 as opposed to 10μM. This step was repeated the following day. From day 2 to 21, the protocol was the same as the first iteration, with the exception of using E6 media instead of TeSR™-E6. On day 21, the differentiating cells were dissociated using Accutase, and plated in a new 24-well Matrigel coated dish at a density of 6.1×10^4 cells per well. From day 21 to 50, they were fed every other day with E6 medium supplemented with 5ng/ml of FGF2. It is important to passage the differentiating cells by day 21 as the crowded colonies in the well can hinder their growth as they reach day 50. Re-plating the cells at a lower density enables the formation of uniform spindle-like structures by day 50, as depicted in Figure 5.

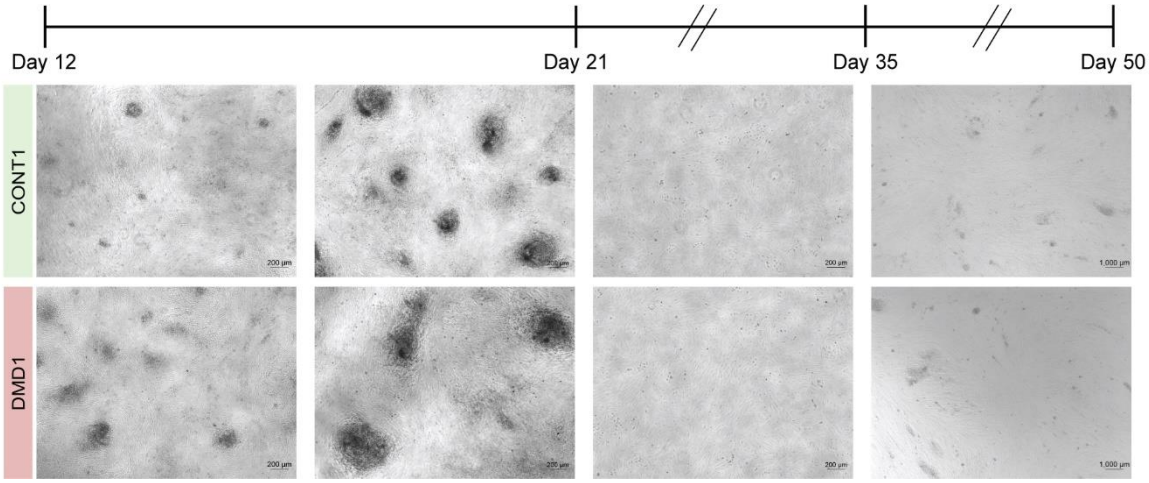

Figure 5. Formation of colony structures in twenty-one-day differentiated healthy control and DMD hiPSCs. Brightfield images of the differentiating cultures taken on day 12 (first column), day 20 (second column), day 30 (third column) and day 40 (last column) of the differentiation process. The first row are the healthy control hiPSCs and the second row are the DMD-patient hiPSCs that were both differentiated. The dark, dense structures in the first two columns are the colonies that have formed. Note the spindle like cells that formed by day 40 in the last column. Scale bar = 1000 μm in each image.

2.3 TREATMENT WITH WNT7A OR EGF

Starting from day 12 up to day 50 with the third iteration of the differentiation protocol, certain wells were treated with either 100ng/mL WNT7A (ThermoFisher 34-8694-166) or 100ng/mL of human recombinant Epidermal Growth Factor (EGF; Miltenyi Biotech 130-093-825) in E6 medium supplemented with 5ng/ml FGF2. The untreated control wells would just be fed with E6 and FGF2. The cells would either be fed everyday, or every other day from day 21 onwards.

2.4 IMMUNOFLUORESCENCE STAINING

On day 21, 35, and 50, the differentiated DMD and healthy control cells were washed twice with PBS (Gibco 10010-023) to remove any residual media. The cells were then fixed with 4% PFA in PBS for 10 minutes, followed by permeabilization with 0.5% TritionX-100

and 100mM glycine in Tris-buffered saline (TBS, 50mM Tris and 150mM NaCl, pH 7.6) for 10 minutes. All samples were subsequently blocked for 1 hour with a blocking solution made up of 2% bovine serum albumin (BSA, Sigma A7906), 5% goat serum (ThermoFisher 16210064), and 0.1% Tween20 in TBS. Primary antibodies (described in Table 2) diluted in the blocking buffer were applied to the cells and left to incubate overnight at 4°C. The next day, fluorophore-conjugated secondary antibodies (described in Table 3) were added to the cells for 1 hour at room temperature. Nuclei were counter stained with DAPI (Sigma-Aldrich 28718-90-3) at 1 μg/mL or 2.5 μg/mL Hoechst 33342 (SigmaMillipore B2261) diluted in TBS buffer with 0.1% Tween20 for 20 minutes at room temperature. The samples were either mounted with PermaFluor (ThermoScientific TA-006-FM) or plain PBS was added. Images of the differentiated cells were captured using an Axio Observer.Z1 microscope (Zeiss). The images were analyzed using the Zen Blue software (Zeiss).

Table 2. List of Primary Antibodies Used for Immunofluorescence Staining

Antigen	Supplier	Ig Type	Dilution
PAX7	Developmental Studies Hybridoma Bank	Mouse IgG1	1:4
MYOD	Abcam 133627	Rabbit IgG	1:500
MYOG	R&D Systems MAB66861	Mouse IgG2a	1:500
MF20	Developmental Studies Hybridoma Bank	Mouse IgG2b	1:5

Table 3. List of Secondary Antibodies Used for Immunofluorescence Staining

Fluorophore	Supplier	Ig Type	Dilution
AlexaFluor-546	Invitrogen Life Technologies A21123	Goat anti-mouse IgG1	1:1000
AlexaFluor-647	Invitrogen Life Technologies A21244	Goat anti-rabbit IgG	1:1000
AlexaFluor-488	Invitrogen Life Technologies A21131	Goat anti-mouse IgG2a	1:1000

AlexaFluor-488	Invitrogen Life Technologies A21141	Goat anti-mouse IgG2b	1:1000

2.5 AUTOMATED HIGH CONTENT IMAGING AND IMAGE PROCESSING

The 21, 25, and 50 day differentiated DMD and healthy control hiPSCs were fixed and stained in a 24-well glass bottom plate for PAX7, MYOD, and MYOG as previously described. The PerkinElmer Opera Phenix Plus High-Content Screening System was used for high-throughput and high-content image acquisition using either a 10X or 20X water immersion lens in confocal mode. For each replicate and condition, 143 to 144 fields of view were imaged, using the HOECHST 33342, Alexa 488, Alexa 546, and Alexa 647 nm channels.

The PerkinElmer Columbus Image Data Storage and Analysis System (v2.9.1) was used to store the image data and perform the initial image analyses. A script was created using the Columbus building blocks to first exclude the colony regions in the differentiated cultures (as we could not obtain the expression of each marker for all the individual cells within the colonies). We then programmed the script to find all the nuclei and extract certain morphological properties, including the nucleus area and roundness. Finally, we obtained the intensity properties for each fluorophore – specifically its mean, median, sum, maximum, and minimum intensity. A batch analysis was conducted using this script on all the differentiated hiPSC conditions/replicates (Table 4).

Table 4. PerkinElmer Columbus Image Analysis building blocks script to remove colony structures from differentiated hiPSC cultures, obtain morphology characteristics from the nuclei, and obtain intensity properties from each myogenic marker. Parameters were created with the help of Dr. Derek Hall, a post-doctoral fellow from the Rudnicki Lab. Table adapted from Lange et al. (63).

Cell Feature	Columbus Building Block	Specifics	Method	Output Name
Colony Structures	Input Image	Flatfield correction: basic Brightfield correction: yes Stack Processing: maximum projection		
	Find Image Region	Channel: HOECHST 33342	Method: Common Threshold Threshold: 0.8 Split into Objects: Yes Area: >800 µm	Output population: Colony Image Region
	Select Region	Population: whole image Region: whole image	Method: Restrict by M Population: Colony Image Mask region: Image Region Use Inverted Mask: Yes	Output Region: Analysis Region
Nuclei	Find Nuclei	Channel: HOECHST 33342 ROI Population: Whole Image ROI Region: Analysis Region	Method: C Common Threshold: 0.2 Area: 5 μm^2 Splitting Coefficient: 3 Individual Threshold: 0.4 Contrast: 0.1	Output Population: Nuclei
	Calculate Morphology Properties	Population: Nuclei Region: Nucleus	Method: Standard, area, roundness (in µm)	Property Prefix: Nucleus
PAX7+	Calculate Intensity Properties	Channel: Alexa 546 Population: Nuclei Region: Nucleus	Method: Standard, mean, standard deviation, mean, median, maximum, minimum	Property Prefix: af546

MYOD+	Calculate Intensity Properties (2)	Channel: Alexa 647 Population: Nuclei Region: Nucleus	Method: Standard, mean, standard deviation, mean, median, maximum, minimum	Property Prefix: af647
MYOG+	Calculate Intensity Properties (3)	Channel: Alexa 488 Population: Nuclei Region: Nucleus	Method: Standard, mean, standard deviation, mean, median, maximum, minimum	Property Prefix: af488

The results from these analyses were subsequently brought into R Studio (version 4.1.2). Table 2 outlines in detail the R studio scripts used for each step. Briefly, the nuclei were filtered based on their area and roundness (Table 2, steps 4-8). Then, the optimal metrics were identified to select the PAX7+, MYOD+, and MYOG+ cells (Table 2, steps 9-10). The cells were then classified by their myogenic marker (steps 11-12), and the total number of cells expressing each marker was determined (Table 2, step 13).

These results were exported to Excel to determine the percentage of cells that express PAX7+, MYOD+, MYOG+ and PAX7+/MYOD+ double positive out of the total population (note that the total population was determined in Table 2, step 7 of the R Studio script). In addition to the total population, we assessed the expression of each marker within the myogenic population. The myogenic population consisted of the cells that expressed PAX7 as well as cells that expressed MYOG.

The proportions of each myogenic marker within the total population and within the myogenic population were then imported into GraphPad Prism 8 (version 8.2.1) to generate the figures and conduct the statistical testing.

Table 5. R Studio scripts to filter nuclei based on area and roundness, and to determine the number of cells that expressed each myogenic marker. Scripts were created with the help of Dr. Derek Hall, a post-doctoral fellow in the Rudnicki lab.

Step	R Studio Script	Description/Comments of Script

1	if (!require(tidyverse)) {
	  install.packages("tidyverse")
	}
	
	if (!require(data.table)) {
	  install.packages("data.table")
	}
	
	library(tidyverse)
		To install the dependent packages.

2	path <- "./2021-11-22 iPSC 121D D21.result.A1[249990].Population - Nuclei.txt"	To designate the path to the Columbus output file.
3	data <- data.table::fread(path, nrows = 1206074)	To load data derived from the Columbus output file. The "nrows" designates the number of nuclei or the number of objects scanned through the Opera Phenix.
4	colnames(data)[grepl("Nuclei - Nucleus Area", colnames(data))] <- "Nuclei - Nucleus Area" colnames(data) <- gsub("Nuclei - ", "", colnames(data)) colnames(data) <- gsub(" ", "_", colnames(data))	To tidy variable names to facilitate use in downstream functions.
5	ggplot(data, aes(x=1, y = Nucleus_Roundness)) + geom_violin()	To generate a violin plot to visualize the distribution of nuclei roundness and determine the cut-offs.
6	ggplot(data, aes(x=1, y = log(Nucleus_Area))) + geom_violin()	To generate another violin plot and determine the cut-offs for the nucleus area.

7	data <- data %>% mutate(nucleus_selected = ifelse(
	  Nucleus_Area > 20 &
	  Nucleus_Area < 150 &
	  Nucleus_Roundness > 0.75,
	  yes = "selected",
	  no = "rejected"
	))
		To set the cut-offs for the nucleus area and roundness.

8	table(data$nucleus_selected)	To determine how many nuclei are selected for further analysis.

9	data %>%
	  filter(nucleus_selected == "selected") %>%
	  ggplot(aes(x = log(af546_Mean), y = log(af488_Mean))) +
		This generates a scatter plot to assess the log mean intensity of cells expressing PAX7 against the log mean intensity of cells

	geom_point() + labs(y = "log(Mean-Myog)", x = "log(Mean-Pax7)")	expressing MYOG. The cut-offs for each myogenic marker are determined by visual selection.
10	data %>% filter(nucleus_selected == "selected") %>% ggplot(aes(x = log(af546_Mean), y = log(af647_Mean))) + geom_point() + labs(y = "log(Mean-Myod)", x = "log(Mean-Pax7)")	This generates a scatter plot to assess the log mean intensity of cells expressing PAX7 against the log mean intensity of cells expressing MYOD. The cut-offs for each myogenic marker are determined by visual selection.
11	data <- data %>% mutate(pax7 = ifelse(af546_Mean > exp(7), yes = "pax7_pos", no = "paxy_neg"), myod = ifelse(af647_Mean > exp(7), yes = "myod_pos", no = "myod_neg"))	This classifies the cells that are PAX7+ and cells that are MYOD+. The number within the "exp" function designates the cut-offs that were determined in step 9.
12	data <- data %>% mutate(pax7 = ifelse(af546_Mean > exp(6.25), yes = "pax7_pos", no = "pax7_neg"), myog = ifelse(af488_Mean > exp(6.5), yes = "myog_pos", no = "myog_neg"))	This classifies the cells that are PAX7+ and cells that are MYOG+. The number within the "exp" function designates the cut-offs that were determined in step 8.
13	table(data$pax7, data$myod) table(data$pax7, data$myog)	These two tables summarize the total number of cells for each myogenic marker, including the cells that express both PAX7 and MYOD or PAX7 and MYOG.

2.6 GENE EXPRESSION ANALYSIS THROUGH QUANTITATIVE REAL-TIME PCR

On day 0 (before the CHIR99021 was added to the hiPSCs), and on days 12, 21, 35, and 50 of the differentiation program, RNA was harvested from the cells for gene expression analysis through reverse transcription quantitative PCR (RT-qPCR). Total RNA was isolated using the NucleoSpin RNA II kit (Macherey-Nagel 740955.250) according to the manufacturer's guidelines. The nucleic acid concentration and purity was determined using the NanoDrop One Microvolume UV-Vis Spectrophotometer (Thermo Scientific 840274100). The RNA was then retrotranscribed using the iSCRIPT cDNA Synthesis Kit

(Bio-Rad 1708891). The master mix was created with the appropriate primer combination (listed in Table 6) and SYBR Green Master Mix (Bio-Rad 1708884). The final reaction volume was 10µl per well, with 1ng/µl cDNA, and 500nM forward and reverse primers. The qPCR was conducted in technical triplicate for each sample and gene. The thermocycler (Bio-Rad CFX384) reaction parameters were as follows: 95°C for 3min, 40 cycles with 95° C for 10s and 55°C for 30s, then 95°C for 10s, and gradient melt curve from 65°C to 95°C with 5s steps. The data was analyzed through the **ΔΔ**Ct method: The Cq values for each gene were averaged, and then normalized to the average Ct values of the housekeeping genes *GAPDH* and *RPLP0*. The **Δ**Ct samples were then normalized to the **Δ**Ct day 0 samples or untreated samples and represented as fold change. The data represents 1-6 biological replicates as independent differentiations, as indicated in each figure legend.

Table 6. List of Human qPCR Primers

Gene	Forward Sequence	Reverse Sequence
GAPDH	AGGTCGGAGTCAACGGATTTG	TGTAAACCATGTAGTTGAGGTCA
RPLP0	GCTTCCTGGAGGGTGTCC	GGACTCGTTTGTACCCGTTG
PAX7	GTGTGCAGGTCTGGTTCAGT	CCTGGCAGAAGGTGGTTGAA
MYF5	TACTATAGCCTGCCGGGACA	CATTCGGGCATGCCATCAGA
MYOD	CGGCATGATGGACTACAGCG	CAGGCAGTCTAGGCTCGAC
MYOG	TGCCATCCAGTACATCGAGC	CAGATGATCCCCTGGGTTGG
TUBB3	TCATCTTTGGTCAGAGTGGGG	GGCAGTCGCAGTTTTCACAC
FZD7	GCGCTCATGAACAAGTTCGG	TAGGGCGCGGTAGGGTAG
EGFR	TTGCCGCAAAGTGTGTAACG	GAGATCGCCACTGATGGAGG
OCT4	TCAGCCAAACGACCATCTGCCG	AGCAAGGGCCGCAGCTTACA
SOX2	TACAGCATGTCCTACTCGCAG	GAGGAAGAGGTAACCACAGGG
PAX3	CTCACCTCAGGTAATGGGACT	CGTGGTGGTAGGTTCCAGAC
MEOX1	GCAGGGGGTTCCAAGGAAAT	GTCAGGTAGTTATGATGGGCAAA
MSGN1	AACCTGCGCGAGACTTTCC	ACAGCTGGACAGGGAGAAGA
BRACHYURY (T)	TTCATAGCGGTGACTGCTTATCA	CACCCCCATTGGGAGTACC
TBX6	CATCCACGAGAATTGTACCCG	AGCAATCCAGTTTAGGGGTGT

2.7 WESTERN BLOT ANALYSIS

Total protein was extracted from the 21-day differentiated CONT1, and DMD1-2 hiPSCs following the first iteration of the differentiation protocol. The cells were washed twice with PBS to remove any residual media and debris. RIPA buffer (Life Technologies PI89900) supplemented with a protease inhibitor (Sigma Roche Diagnostics 4693132001) and phosphatase inhibitor (Sigma-Aldrich 04906837001) was added to lyse the cells. The harvested cells were then centrifuged at 14,000 rpm for 10 minutes at 4°C. The supernatant was collected, and the protein concentration was detected through the Bradford Reagent Protein Assay kit (Bio-Rad 5000006) and by comparing the values to the measured concentration of BSA samples. 4X Laemmli buffer (20% SDS, 0.4% bromophenol blue, 40% glycerol, 200mM Tris pH 6.8, 20% β- mercaptoethanol) was added to the samples and they were boiled at 100°C for 3 minutes. The samples were loaded into an 8% gradient tris-glycine SDS-polyacrylamide gel electrophoresis (SDS-PAGE) and the gel ran at 140V constant voltage for 1 hour and 10 minutes. The gel was transferred to an Immobilon PVDF membrane (Millipore IPVH00010) at 110V constant voltage for 1 hour and 30 minutes. The membrane was subsequently blocked for 1 hour at room temperature in 5% milk powder in TBS-T (TBS with 0.1% Tween20) and incubated with primary antibodies at 4°C overnight. The primary antibodies and their dilution in the blocking buffer were the following: PAX7 (1:10, Developmental Studies Hybridoma Bank) and GAPDH (1:1000, Sigma PLA0302). The next day, the samples were probed with the following secondary fluorophore antibodies: AlexaFluor-546-conjugated donkey anti-goat IgG (1:1000, Invitrogen Life Technologies A11056), and Starbright Blue 700 goat anti-mouse IgG (1:2000, Bio-Rad 12004158). The blot was visualized using the ChemiDoc MP Imaging System (Bio-Rad 12003154).

2.8 STATISTICAL ANALYSIS

This study employs each independent differentiation as a biological replicate. The biological replicates for each experiment are indicated in the figure legends, and the results are presented as the mean ± standard error of the mean (SEM). Statistical comparisons between two matched conditions were made using a two-tailed Student's t test. The statistical analysis was performed using GraphPad Prism (version 8.2.1). p-vales <0.05 were considered statistically significant, and the level of significance is indicated as follows: $*p < 0.05$, $**p < 0.01$, $***p < 0.001$.

3 RESULTS

3.1 OPTIMIZATION OF THE HIPSC MYOGENIC DIFFERENTIATION PROTOCOL THROUGH ALTERATION OF CHEMICALLY DEFINED MEDIA AND CHIR99201 CONCENTRATION

The main goal of this study was to evaluate whether WNT7A and EGF, which are known to promote symmetric and asymmetric satellite cell division, respectively, in adult skeletal muscle, similarly modulate muscle stem cells derived from hiPSCs. To test the effects of these two compounds, we needed to first generate muscle stem cells and myogenic progenitors from DMD patient and healthy control hiPSCs.

For this study, primary myoblasts from two DMD patients and three normal, healthy control persons with a wild-type dystrophin allele, were reprogrammed into hiPSCs by a post-doctoral fellow, Dr. Morten Ritso, from our laboratory. He validated the hiPSC lines through gene expression analysis and immunostaining for the pluripotency markers *OCT4, SOX2,* and *NANOG,* and monitored their genomic integrity through karyotyping. Teratoma assays and alkaline phosphatase staining were also performed by Dr. Ritso to ensure pluripotency of the cell lines (Morten Ritso & Michael Rudnicki; unpublished). A third DMD-patient derived hiPSC line was provided to us by Dr. Nicolas Dumont from the Université de Montréal, CHU Sainte-Justine Research Center (Philippe Campeau, Morten Ritso, and Nicolas Dumont; unpublished). The Dumont laboratory characterized this cell line, and it demonstrated a normal karyotype, expressed the human *SSEA-4*, *SOX2*, *OCT4* and *TRA1-60* makers, and were passaged for a minimum of 15 times to ensure stable pluripotency. The different hiPSC lines are further characterized Table 7. From here

onwards, each DMD cell line will be referred to as DMD1, DMD2, and DMD3, while each healthy control cell line will be referred to as CONT1, CONT2, CONT3.

Table 7. Characterization of hiPSC lines used in this study. DMD1-2, and CONT1-3 were episomally reprogrammed in-house at The Ottawa Hospital Pluripotent Stem Cell Facility by Dr. Morten Ritso. DMD3 was obtained from Dr. Nicolas Dumont which was generated at the Université de Montréal Platform of Cell Reprogramming of CHU Sainte-Justine (Philippe Campeau, Morten Ritso and Nicolas Dumont; unpublished).

Unique Stem Cell Line Identifier	Alternative Name of Stem Cell Line	Gender, and Age at Biopsy	Original Cell Type	Clinical Diagnosis	Method of Reprogramming	Mutation
DMD1	M121	Male, Age: 10	Myoblast	Duchenne Muscular Dystrophy	Episomal Plasmid	Nonsense mutation c637 G>A (W143x) in exon 6
DMD2	M129	Male, Age: 8	Myoblast	Duchenne Muscular Dystrophy	Episomal Plasmid	c5899 C>T, pArg 1967x in exon 41
DMD3	F0640.1	Male, Age: <18 years old	Peripheral Blood Mononuclear Cells	Duchenne Muscular Dystrophy	Integration-Free Based Sendai Virus	Exon Depletion 48-52
CONT1	M262	Male, Age:21	Myoblast	N/A	Episomal Plasmid	Wild-type dystrophin
CONT2	M040	Male, Age: 20	Myoblast	N/A	Episomal Plasmid	Wild-type dystrophin
CONT3	M177	Male, Age:20	Myoblast	N/A	Episomal Plasmid	Wild-type dystrophin

The DMDl and DMD2 (DMD1-2) hiPSCs, as well as the CONT1 hiPSCs, were differentiated into the myogenic lineage using a modified version of the previously published Shelton et al. procedure (52). Modification was necessary to optimize the differentiation yield for the newly derived hiPSCs. Briefly, the hiPSCs were grown and maintained in mTeSR™ for one to two weeks. mTeSR™ was used as opposed to Essential 8 media, as mTeSR™ has been shown in numerous studies to promote superior iPSC growth and morphology followed by robust myogenic differentiation (26, 59, 64–69). After reaching confluency, the hiPSC lines were single-celled, and seeded at the density of 2 x 10^5 cells per well of a 12-well tissue culture plate. To remain consistent with the TeSR™ media-based workflow, TeSR-E6™ media was used to differentiate the hiPSCs into the myogenic lineage. The hiPSCs were then treated with 10 μM of CHIR99021 supplemented in TeSR-E6™ for two days. For the next ten days, the cells were fed daily with TeSR-E6™ media. From day twelve to day twenty-one, the differentiation medium was supplemented with 5ng/mL of FGF2 (Figure 6A).

After twenty-one days of differentiation, immunofluorescence imaging, RT-qPCR, and Western Blot analysis were performed to assess the efficiency of the differentiation process. Specifically, the differentiated DMD1-2 and CONT1 cells were fixed and stained for PAX7, and imaging analysis revealed sparse areas of muscle stem cells, particularly in the differentiated DMD1 line (Figure 6B). Additionally, gene expression analysis showed downregulation of *PAX7, MYF5, MYOD,* and *MYOG* compared to day zero, and PAX7 protein expression was not detectable (Figure 6C-D).

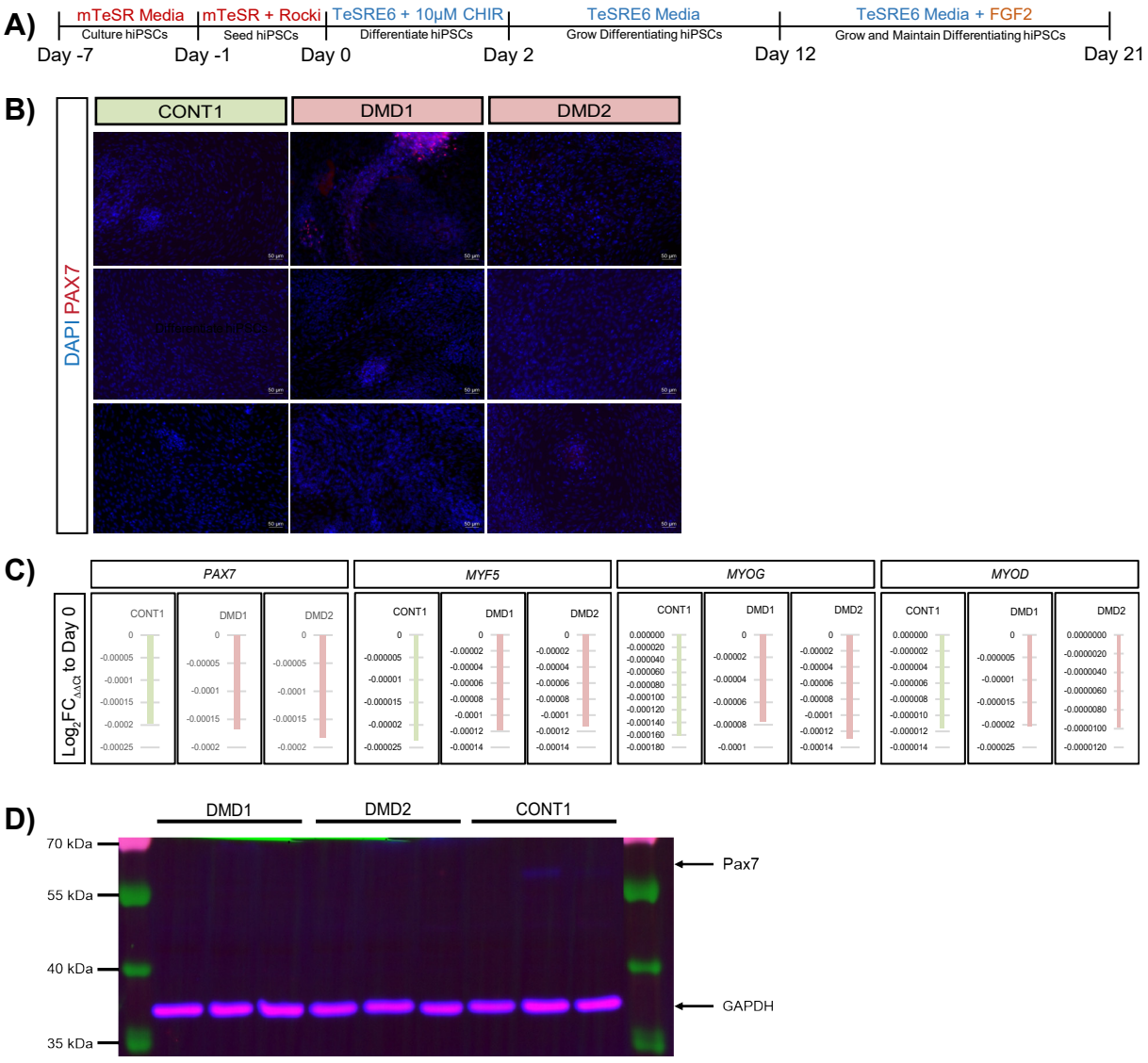

Figure 6. Inefficient myogenic differentiation with mTeSR™ hiPSC media and TeSR-E6™ differentiation media. (A) Schematic timeline of the twenty-one-day differentiation protocol with media and components used on the top of timeline and the directions of the differentiation below the timeline. (B) DMD1-2, and CONT1 hiPSC lines were differentiated for twenty-one days and stained for PAX7 (in red) and DAPI (in blue). Each panel represents a different field of view. Scale bar = 50 μm in all panels. (C) The expression of various myogenic marker genes at day twenty-one of the differentiation process was measured by RT-qPCR, normalized to *GAPDH* and *RPLP0* as the housekeeping genes, and plotted as Log_2 fold-change (FC) relative to day zero (before differentiation). The pink graphs represent DMD1 and DMD2, and the light green graph represents the CONT1 line. n=1. (D) Western blot analysis for PAX7 and GAPDH protein expression at day twenty-one of the differentiation process. n=3, where DMD1-2, and CONT1 were differentiated three independent times for 3 biological replicates.

In an effort to enhance the muscle stem cell yield, we explored the use of Essential 6 (E6) media instead of TeSR-E6™, which had been previously used for differentiating human embryonic stem cells (hESCs) into the myogenic lineage (52) (Figure 7A). On day twenty-one, the differentiated DMD1-2, and CONT1 cells were stained again for PAX7, and immunofluorescence imaging revealed a slight increase in the number of muscle stem cells (Figure 7B). We also tested different hiPSC seeding densities, but no significant differences were visibly observed (Figure 7C). We examined other myogenic precursor markers, including MYOD and MYOG, and observed the presence of myogenic precursor cells in all the differentiated cell lines (Figure 7D) (24).

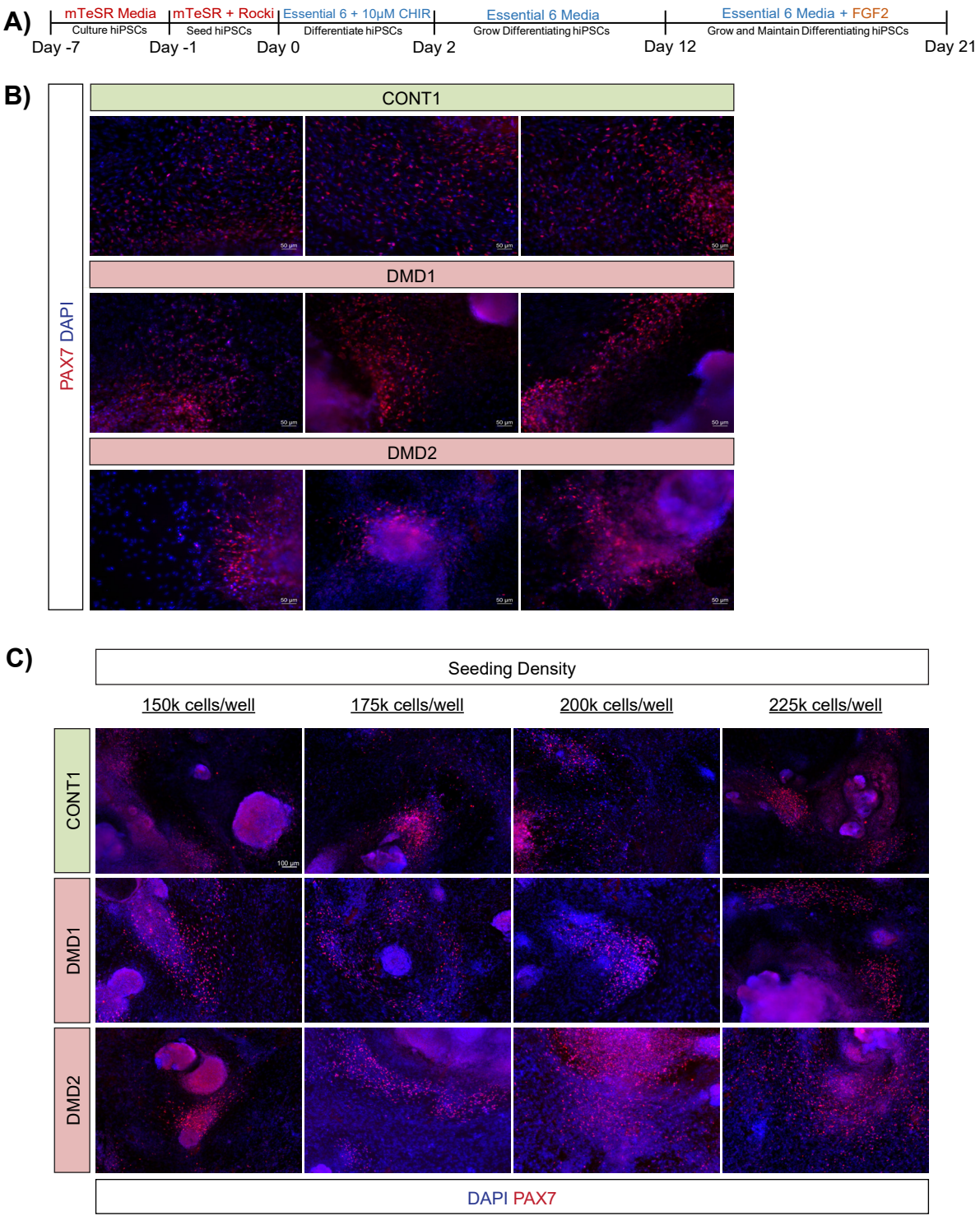
A)
mTeSR Media
Culture hiPSCs
Day -7
mTeSR + Rocki
Seed hiPSCs
Day -1
Essential 6 + 10μM CHIR
Differentiate hiPSCs
Day 0
Essential 6 Media
Grow Differentiating hiPSCs
Day 2
Essential 6 Media + FGF2
Grow and Maintain Differentiating hiPSCs
Day 12
Day 21
B)
PAX7 DAPI
CONT1
DMD1
DMD2
C)
Seeding Density
150k cells/well
175k cells/well
200k cells/well
225k cells/well
CONT1
DMD1
DMD2
DAPI PAX7

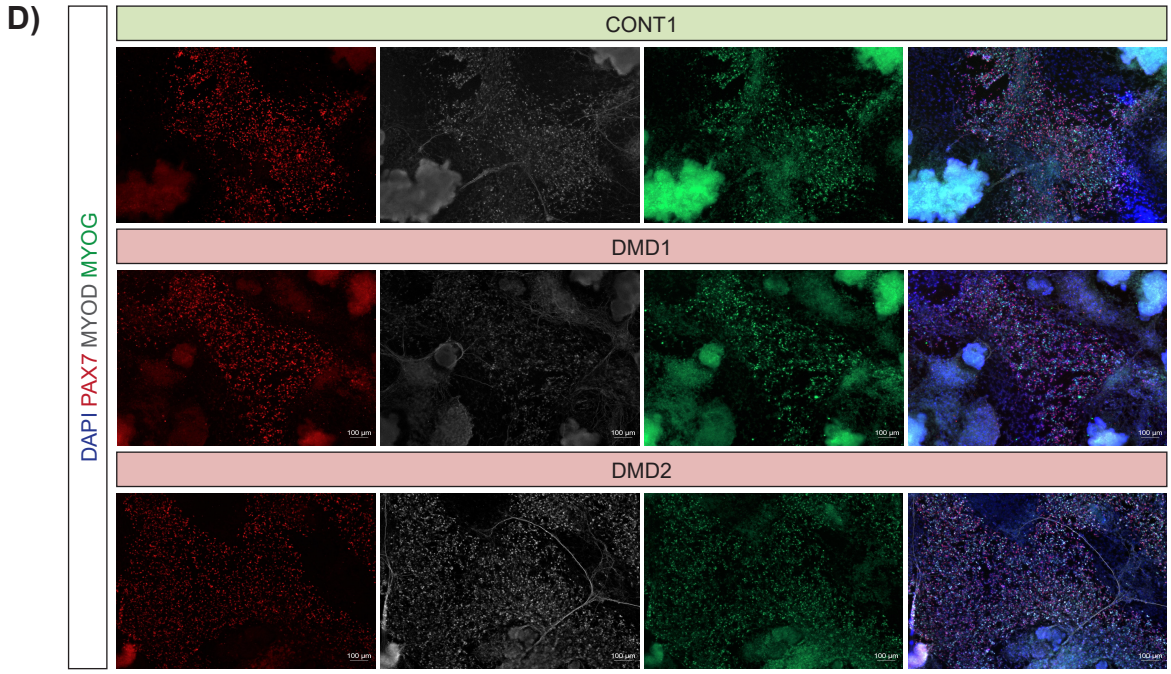

Figure 7. A slight increase in myogenic cell yields following differentiation with Essential 6 media. (A) Schematic timeline of the twenty-one-day differentiation protocol with media and components used on the top of timeline and the directions of the differentiation below the timeline. (B) DMD1-2 and CONT1 hiPSC lines were differentiated for twenty-one days using Essential 6 media, with FGF2 when necessary, and stained for PAX7 (in red) and DAPI (in blue). Each panel represents a different field of view. Scale bar = 50 µm in all panels. (C) DMD1-2 and CONT1 hiPSC lines were single-celled and seeded at various cell densities, as indicated in the top panel. They were differentiated for twenty-one days and immunostained for DAPI (in blue), and PAX7 (in red). Scale bar = 100 µm in all images. (D) DMD1-2 and CONT1 hiPSC lines were differentiated for twenty-one days using Essential 6 media, with FGF2 when necessary, and subsequently visualized by immunofluorescence for DAPI (in blue), PAX7 (in red), MYOD (in grey-white), and MYOG (in green). Scale bar = 100 µm in all images.

The Shelton et al. protocol used Essential 8 (E8) media to grow and maintain the hESCs prior to differentiation (52). However, abruptly changing the hiPSC growth media from mTeSR™ to E8 resulted in drastic hiPSC death and unwanted differentiation. Therefore, to maximize the yield of myogenic differentiation while minimizing cell death resulting from significant changes in media composition, we adopted a gradual transition approach. The DMD1 and CONT1 hiPSC lines were transitioned from mTeSR™ media to E8 media over two or three passages prior to differentiation. This was followed by treatment with 10 μM of CHIR99021 supplemented in E6 medium for two days (Figure 8A). After twenty-one days of differentiation, the cells were fixed, stained, and imaged, and revealed a notably higher yield of PAX7, MYOD, and MYOG-positive cells. Specifically, passaging the DMD1 and CONT1 hiPSCs three times in E8 media prior to differentiation resulted in a more uniform layer of myogenic cells across the tissue-culture dish, in contrast to passaging the hiPSCs twice in E8 media, which only yielded pockets of myogenic cells (Figure 8B-C).

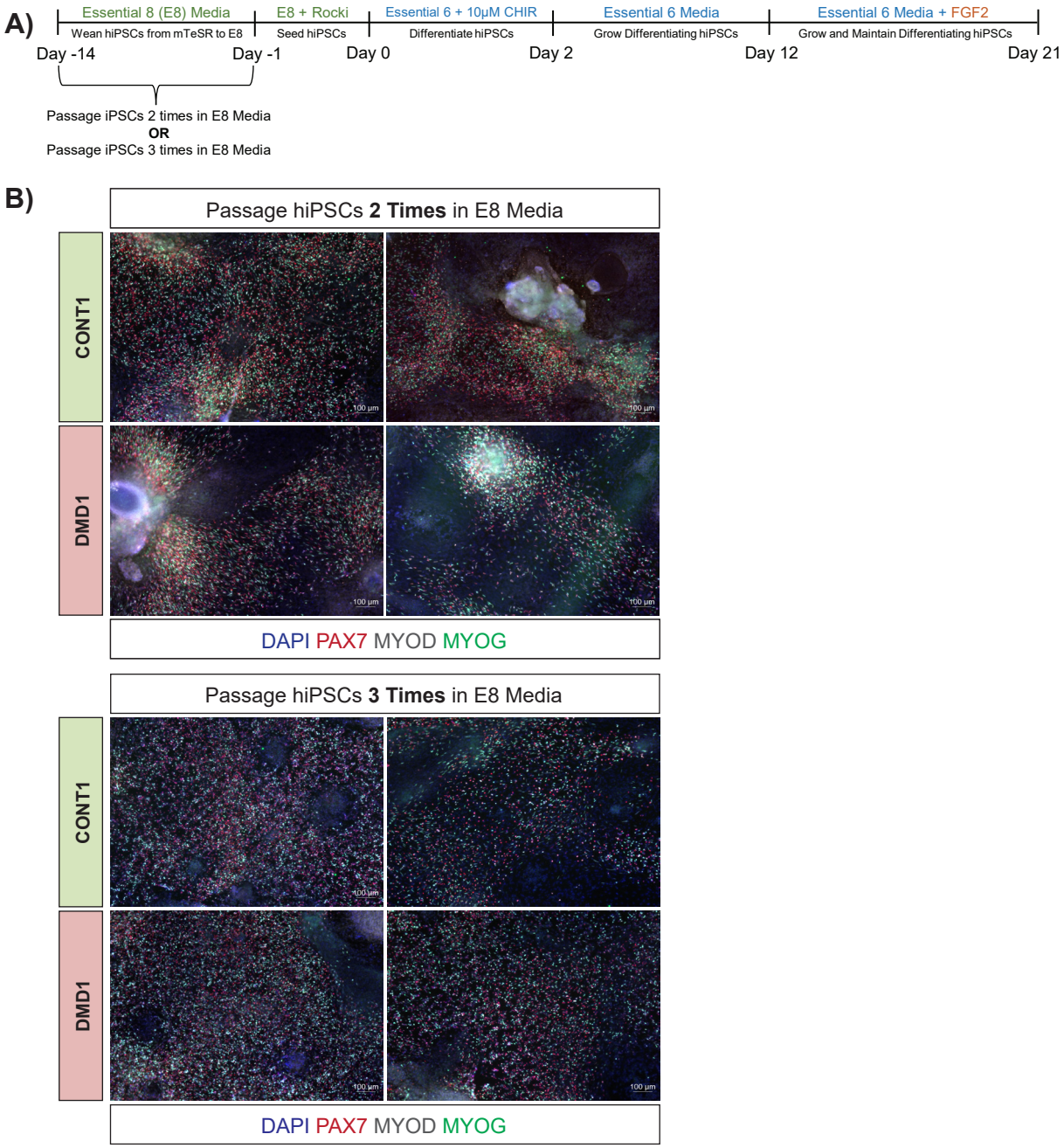

Figure 8. Enhanced myogenic differentiation with Essential 8 hiPSC media and Essential 6 differentiation media. (A) Schematic timeline of the twenty-one-day differentiation protocol with media and components used on the top of timeline and the directions of the differentiation below the timeline. (B) CONT1 and DMD1 hiPSC lines were gradually weaned from mTeSR™ to Essential 8 media and then passaged in pure Essential 8 media twice, or (C) three times. They were then differentiated into the myogenic lineage with Essential 6 as the differentiation media. Twenty-one days later, they were immunostained and visualized for DAPI (in blue), PAX7 (in red), MYOD (in grey-white), and MYOG (in green). Each panel represents a different field of view. Scale bar = 100 μm in all images.

Finally, we wanted to determine the optimal concentration of CHIR99021 for efficient myogenic differentiation of both DMD and healthy control patient-derived hiPSCs. Too high a concentration of CHIR99021 can be toxic, while too low a concentration may not yield myogenic progenitors effectively (52, 70). Previously, we showed that a concentration of 7.5 μM of CHIR99021 was optimal for differentiating hESCs into the myogenic lineage (71). Hence, we tested this specific concentration to assess if it could result in a higher number of myogenic cells. The DMD1 and CONT1 hiPSCs were passaged in E8 media three times, dissociated into single cells, and treated with either 7.5 μM or 10 μM of CHIR99021 in E6 media for two days (Figure 9A). Subsequently, the cells were differentiated for twenty-one days and immunostained for PAX7, MYOD, and MYOG (Figure 9B). Immunostained images were analyzed using the Opera Phenix™ Confocal High Content Screening System and the data was brought into R Studio to determine the fluorescent intensity of each relevant myogenic marker, which was then used to quantify the number of cells expressing each marker. We observed that the CONT1 line treated with 7.5 μM of CHIR99021 had almost three times more PAX7+ and MYOD+ cells compared to the 10 μM treatment. Similarly, the DMD1 line treated with 7.5 μM of CHIR99021 showed nearly two times more PAX7+ and MYOD+ cells (Figure 9C). Gene expression analysis demonstrated a trend of approximately two-fold increase in *MYOD* expression with 7.5 μM of CHIR99021 treatment in the CONT1 line (Figure 9D).

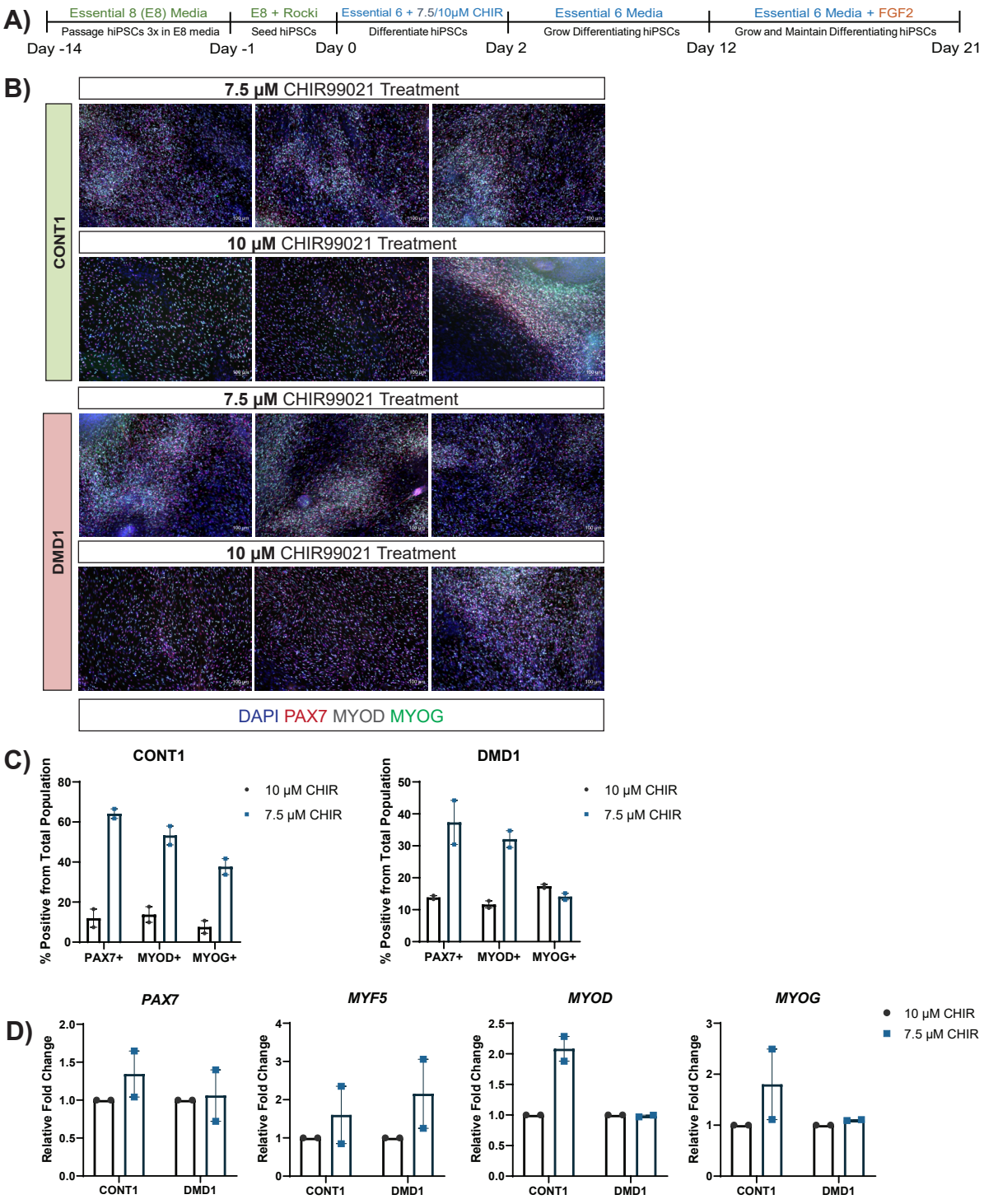

Figure 9. A CHIR99021 concentration of 7.5 μM rather than 10 μM yields more muscle stem cells and myogenic cells. (A) Schematic timeline of the twenty-one-day differentiation protocol with media and components used on the top of timeline and the directions of the differentiation below the timeline. (B) The CONT1 and DMD1 hiPSC lines were gradually weaned from mTeSR™ to Essential 8 media and then passaged in pure E8 media three times. The hiPSCs were then single-celled, seeded, and treated with either 7.5 μM or 10 μM

of CHIR99021 for two days. The cells were differentiated using Essential 6 media and twenty-one days later, they were immunostained and visualized for DAPI (in blue), PAX7 (in red), MYOD (in grey-white), and MYOG (in green). Each panel represents a different field of view. Scale bar = 100 μm in all images. (C) Immunofluorescence images were captured on day twenty-one using the Opera Phenix™ High-Content Screening System and the quantification of the percentage of each myogenic marker was conducted using the Columbus Image Data Storage and Analysis System and R Studio, as described in the Materials and Methods section. Data is expressed as a percentage from the total population of the differentiating cultures. n=2. The CONT1 and DMD1 hiPSC lines were differentiated two independent times for two biological replicates. Error bars are S.E.M. (D) The expression of various myogenic marker genes at day twenty-one of the differentiation process was measured by RT-qPCR, normalized to *GAPDH* and *RPLP0* as the housekeeping genes, and plotted as relative fold change to 10 μM of CHIR99021 treatment. The CONT1 and DMD1 hiPSC lines were differentiated two independent times for two biological replicates. Error bars are S.E.M.

Using this specific concentration of CHIR99201 and the aforementioned media changes (Figure 10A), we observed successful *in vitro* replication of myogenesis in both the healthy control (CONT1) and DMD patient (DMD1) hiPSC lines at day twenty-one (Figure 10B), thirty-five (Figure 10C), and fifty (Figure 10D) of the differentiation process as evidenced by robust immunofluorescence expression of PAX7, MYOD, and MYOG.

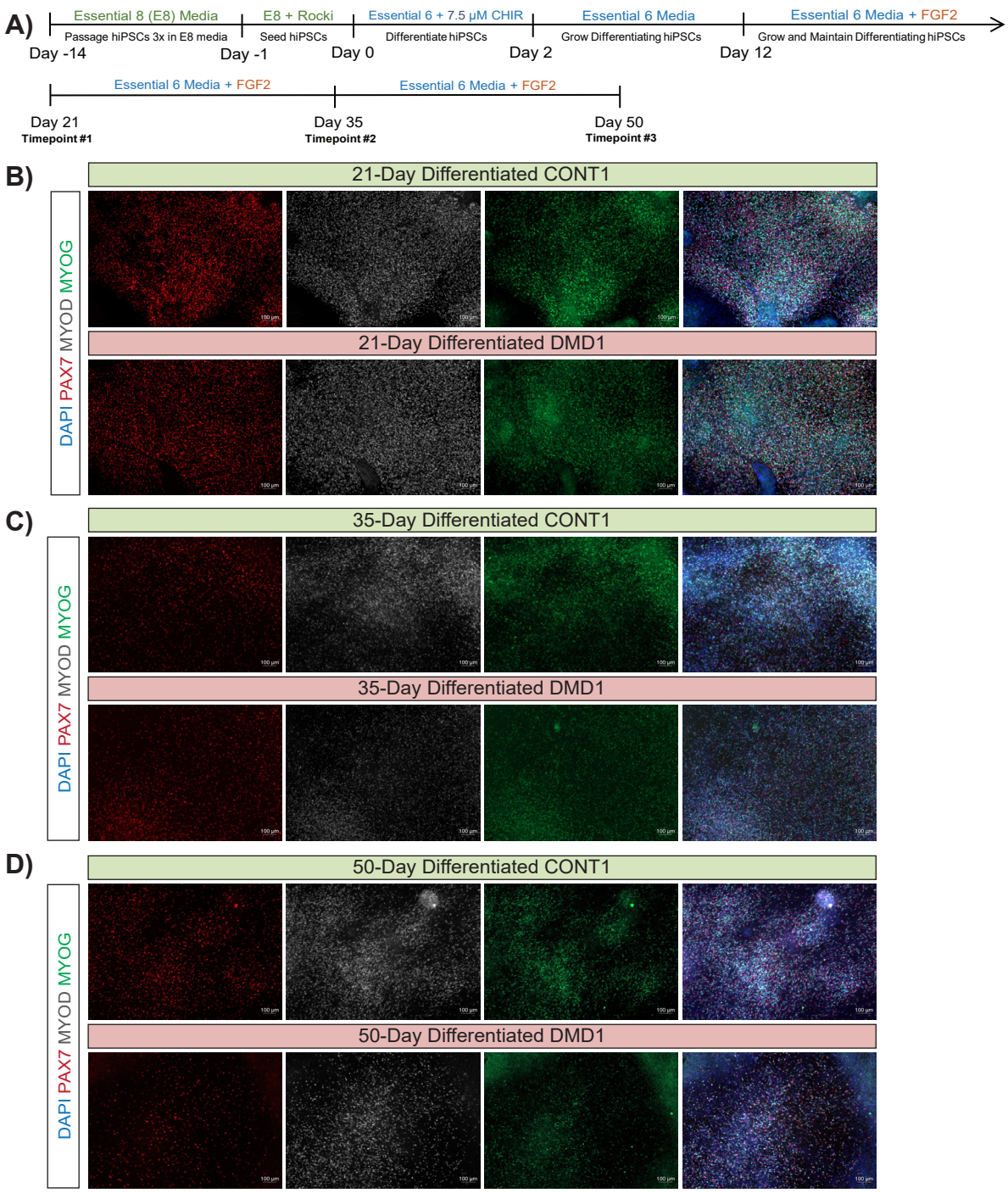

Figure 10. Robust myogenic differentiation observed with Essential 8 hiPSC media, 7.5 µM of CHIR99021 treatment, and Essential 6 differentiation media. (A) Schematic timeline of the 50-day differentiation protocol with media and components used on the top of timeline and the directions of the differentiation below the timeline. (B) The CONT1 and DMD1 hiPSC lines were differentiated into the myogenic lineage and immunostained at day twenty-one, thirty-five (C), and fifty (D) for DAPI (in blue), PAX7 (in red), MYOD (in grey-white), and MYOG (in green). Scale bar = 100 µm in all images.

We also tracked the myogenic differentiation process using stage-specific markers. RT-qPCR was used to assess various developmental genes, including the pluripotency markers *OCT4* and *SOX2*, the early mesodermal markers *Brachury T (BRACHT)*, *MSGN1*, and *TBX6*, the somite markers *PAX3* and *MEOX1*, as well as the myogenic markers *PAX7*, *MYF5, and MYOD* at day zero and day twelve of the myogenic differentiation program. Within each line, *MSGN1* expression was significantly increased by day twelve, indicating the presence of paraxial mesoderm cells that possess skeletal myogenic potential (Figure 11A-B) (52). Additionally, broad expression of the somite marker *PAX3* was significantly increased by day twelve in the DMD line (Figure 11B).

By day twenty-one, the pluripotency marker *OCT4* had significantly decreased (Figure 11C). The somite marker *PAX3* showed an increased trend by day twelve and twenty-one. More notably, the myogenic markers *PAX7*, *MYOD*, and *MYOG* were all significantly increased by day twenty-one. In order to rule out undesirable hiPSC differentiation into alternative lineages, the neuronal marker *TUBB3* expression was also investigated. We observed a small elevation in *TUBB3* in the healthy control patient hiPSCs that were differentiated for twelve days. In the DMD patient line, these changes were variable across technical replicates and consequently not significant (Figure 11C).

In summary, our findings suggest that robust myogenic differentiation can be achieved when the hiPSCs are grown and maintained in E8 media for three passages, treated with a concentration of 7.5 μM of CHIR99021 in E6 media for two days, and differentiated in E6 media with FGF2 when necessary.

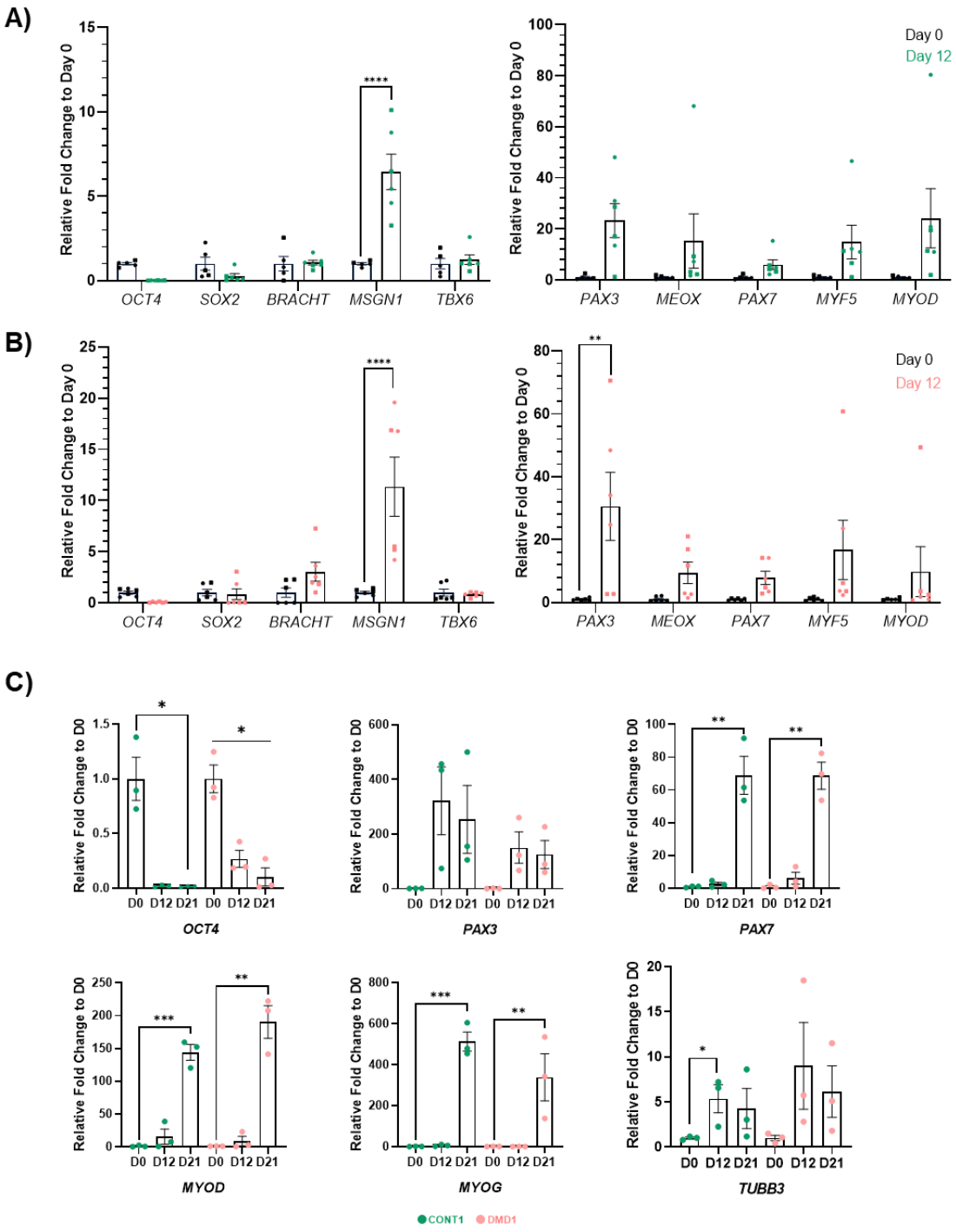

Figure 11. Enrichment of myogenic genes in the twenty-one-day differentiated healthy control and DMD-patient derived hiPSCs. (A) The CONT1 (represented as circles) and CONT2 (represented as squares) hiPSCs were differentiated for twelve days and RNA was harvested for gene expression analysis by RT-qPCR. *OCT4* and *SOX2* are pluripotency markers, *BRACHT*, *MSGN1*, and *TBX6* are early mesodermal markers, *PAX3* and *MEOX1* are somite markers, and *PAX7*, *MYF5*, and *MYOD* are the myogenic markers. Data is

presented as relative fold change to the day zero samples for the indicated developmental genes. n=5 for day 0, and n=6 for day 12, with with 4-6 biological replicates as independent differentiations. Error bars represent S.E.M. (B) The DMD1 (represented as circles) and DMD2 (represented as squares) hiPSCs were differentiated for twelve days and RNA was harvested for gene expression analysis by RT-qPCR. Data is presented as relative fold change to the day zero samples for the indicated developmental genes. n=5 for day 0, and n=6 for day 12, with 4-6 biological replicates as independent differentiations. Error bars represent S.E.M. ****$p < 0.0001$, **$p < 0.01$. (C) The CONT1 (in green) and DMD1 hiPSCs (in pink) were differentiated into the myogenic lineage and RNA was harvested on day zero, day twelve, and day twenty-one for gene expression analysis by RT-qPCR for the indicated developmental genes. Data is presented as relative fold change to day zero. n=4, with 4 biological replicates as independent differentiations. Error bars represent S.E.M. *$p < 0.05$, **$p < 0.01$, ***$p < 0.001$.

3.2 DMD-Patient Derived hiPSCs Precociously Differentiate Compared to Healthy Control hiPSCs

Previous studies utilized reprogramming methods to induce myogenic differentiation in hiPSCs derived from both healthy, normal individuals and patients with DMD, by overexpressing the key myogenic factors *PAX3/7* or *MYOD1* (56, 66). These studies have not revealed any significant differences in myogenic differentiation between the healthy, normal individual-derived hiPSCs and DMD patient-derived hiPSCs. Other studies using a non-reprogramming approach have demonstrated various outcomes in the DMD-patient derived myogenic differentiation efficiency (26, 72, 73). Here, we aimed to investigate whether there are any disparities in differentiation between healthy control and DMD-patient derived hiPSCs using our modified, non-reprogramming directed differentiation method utilizing CHIR99021.

To assess gene expression changes between the healthy control lines and the DMD-patient lines, we employed RT-qPCR to analyze pluripotency markers including *OCT4* and *SOX2*, early mesodermal markers including *BRACHT, MSGN1,* and *TBX6*, somite markers such as *PAX3* and *MEOX1*, as well as the myogenic markers *PAX7, MYF5,* and *MYOD* at day zero and day twelve of the myogenic differentiation program. Additionally, on day twenty-one, we specifically examined the expression of the MRFs *PAX7, MYF5, MYOD,* and *MYOG* to further elucidate differences in myogenic gene expression patterns between the two types of cell lines.

On day zero, there were no significant differences between the CONT1-2 and DMD1-2 hiPSC expression profiles (Figure 12A). Interestingly, on day twelve of the differentiation process, we observed a five-fold increase in *OCT4* expression in the DMD1-2

lines compared to the CONT1-2 lines. This could indicate that pluripotency was maintained in the DMD lines longer than the healthy controls (Figure 12B). On day twenty-one, there were no significant differences between the DMD1-3 and CONT1-3 lines (Figure 12C). However, we observed a trend where global *PAX7* expression was decreased in the DMD1-2 lines ($p=0.097$).

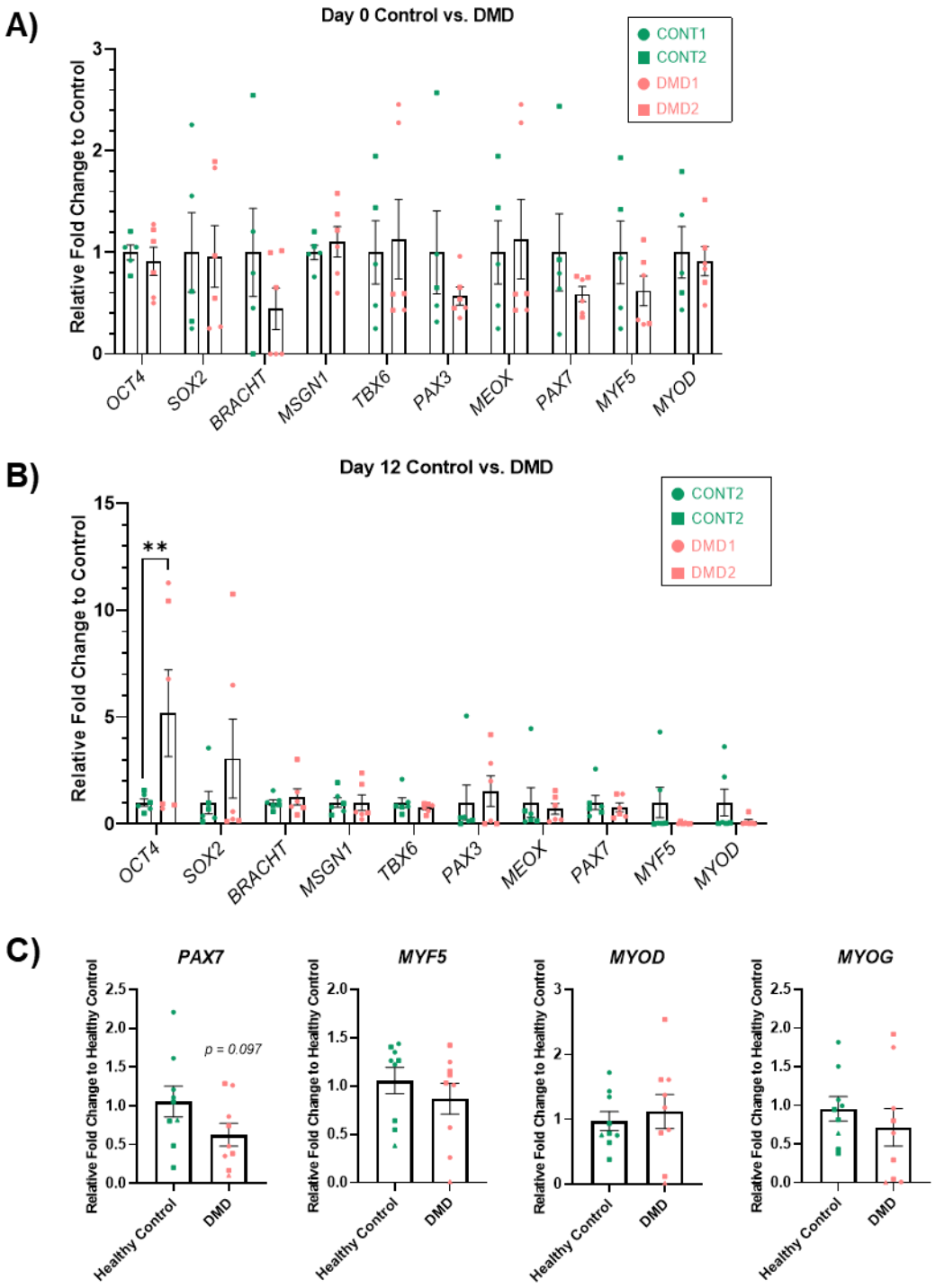

Figure 12. Twelve-day differentiated DMD hiPSCs retain pluripotency marker *OCT4* compared to twelve-day differentiated healthy control hiPSCs. (A) RNA was harvested from the CONT1-2 hiPSCs (in green circles and squares, respectively) and DMD1-2 hiPSCs (in pink circles and squares, respectively) on day zero for developmental gene expression analysis through RT-qPCR. *OCT4* and *SOX2* are pluripotency markers, *BRACHT, MSGN1*, and *TBX6* are early mesodermal markers, *PAX3* and *MEOX1* are somite markers, and *PAX7,*

MYF5, and *MYOD* are the myogenic markers. Data is presented as relative fold change to the healthy control hiPSCs. n=5 for CONT1-2, and n=6 for DMD1-2 with 4-6 biological replicates as independent differentiations. Error bars represent S.E.M. (B) CONT1-2 (in green circles and squares, respectively) and DMD1-2 hiPSCs (in pink circles and squares, respectively) were differentiated into the myogenic lineage and RNA was harvested on day twelve for gene expression analysis by RT-qPCR for the indicated developmental genes. Data is presented as relative fold change to the twelve-day differentiated healthy control hiPSCs. n=6, with 6 biological replicates as independent differentiations. Error bars represent S.E.M. $**p < 0.01$. (C) CONT1 (in green circles), CONT2 (in green squares), CONT3 (in green triangles) and DMD1 (in pink circles), DMD2 (in pink squares), and DMD3 (in pink triangles) hiPSCs were differentiated into the myogenic lineage. RNA was harvested on day twenty-one for gene expression analysis by RT-qPCR for the indicated myogenic genes. Data is presented as relative fold change to the twenty-one-day differentiated healthy control hiPSCs. n=9, with 9 biological replicates as independent differentiations. Error bars represent S.E.M.

To further elucidate the expression profiles of the myogenic markers in differentiated cells derived from DMD patients compared to healthy controls, we conducted immunostaining for PAX7, MYOD, and MYOG, and analyzed the immunostained images through high-content analysis. This analysis was performed at three time points during the differentiation process, specifically on day twenty-one, thirty-five, and fifty, to capture the dynamic changes in marker expression over time.

Interestingly, on day twenty-one, a significant decrease was observed in the proportion of PAX7+ cells in DMD1-2 compared to the CONT1-2 cells, which is consistent with the previously observed trend of reduced *PAX7* gene expression. Additionally, the DMD1-2 lines exhibited a significantly higher proportion of MYOG+ cells within the myogenic population (Figure 13A). On day thirty-five, the DMD1-2 lines continued to have a significantly lower proportion of PAX7+ cells and this phenomenon continued to day fifty (Figure 13B). However, intriguingly, on day fifty, both myogenic-precursor markers MYOD, and MYOG were significantly increased in the DMD1-2 lines (Figure 13C). These findings suggest that the hiPSCs derived from DMD patients that have been differentiated using our modified non-reprogramming approach have precociously differentiated compared to the CONT1-2 hiPSCs.

This finding is particularly noteworthy as it suggests a distinctive myogenesis program in hiPSCs derived from DMD patients, potentially different from adult dystrophin-deficient muscle stem cells which have an impaired ability to asymmetrically divide and therefore have reduced myogenic progenitor generation (19). This observed phenomenon could be attributed to the differentiation protocol employed or the intrinsic properties of the DMD patient-derived hiPSC lines.

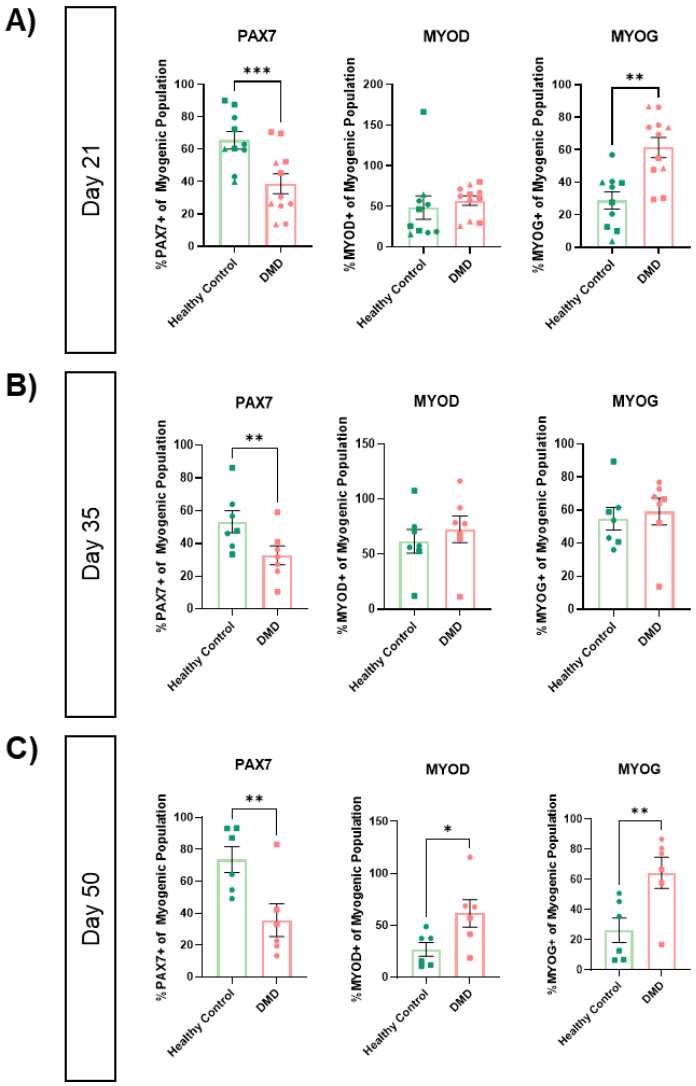

Figure 13. DMD-patient derived hiPSCs differentiate precociously compared to the healthy control hiPSCs. (A) CONT1 (in green circles), CONT2 (in green squares), CONT3 (in green triangles), and DMD1 (in pink circles), DMD2 (in pink squares), DMD3 (in pink triangles) hiPSCs were differentiated for twenty-one days. CONT1-2 (in green circles and squares, respectively) and DMD1-2 (in pink circles and squares, respectively) were differentiated for (B) thirty-five, and (C) fifty days. At all time points, the differentiated cells were stained for PAX7, MYOD, and MYOG. Immunofluorescence images were captured on day twenty-one, thirty-five, and fifty using the Opera Phenix™ High-Content Screening System and the quantification of the percentage of each myogenic marker was conducted using the Columbus Image Data Storage and Analysis System and R Studio, as described in the Materials and Methods section. The myogenic population represents cells that have expressed PAX7 and MYOG. n=10-11 for day twenty-one, with 10-11 biological replicates as independent differentiations. n=6 for day thirty-five and fifty, with with 6 biological replicates as independent differentiations. Error bars represent S.E.M. *$p < 0.05$, **$p < 0.01$, ***$p < 0.001$.

3.3 WNT7A Treatment Increases *PAX7* Gene Expression and Drives Expansion of the PAX7+ Stem Cell Pool in the DMD hiPSC Derived Muscle Stem Cells

Le Grand et al. previously reported that WNT7A, via the non-canonical planar cell polarity pathway, promotes symmetric expansion of satellite stem cells during muscle regeneration (17). Our myogenic cells derived from DMD-patient hiPSCs offer a unique "humanized" platform to investigate the potential division-modulating effects of WNT7A. We hypothesized that treating the healthy control and DMD-patient derived myogenic cells with WNT7A would result in the expansion of the PAX7 expressing muscle stem cell population through symmetric division.

To test this, we first differentiated DMD1-3 and CONT1-3 into the myogenic lineage, followed by treatment with 100 ng/mL of WNT7A from day twelve to day twenty-one of the differentiation process. We also continued differentiating and treating DMD1-2 and CONT1-2 until day fifty. On day twenty-one, thirty-five, and fifty, the cells were fixed, stained for myogenic markers, and analyzed via high-content immunofluorescence imaging. We specifically assessed the proportion of cells expressing PAX7, MYOD, MYOG, or both PAX7 and MYOD, within the myogenic population (which included cells that expressed PAX7 and cells that expressed MYOG), as well as within the total population of differentiating cells.

While we did not observe any significant changes in the CONT1-3 cells (Figure 14A-B), we found that treatment with WNT7A led to a significant two-fold increase in the proportion of PAX7+ cells within the myogenic population in the DMD1-3 lines (Figure 14C). This trend was consistent in the total population, where we observed a two-fold

increase in the proportion of PAX7+ cells (Figure 14D). Importantly, we also found that WNT7A treatment resulted in a decrease in the proportion of MYOD+ and MYOG+ expressing cells within the myogenic population, indicating that the treatment reduced the proportion of committed progenitor cells (Figure 14C).

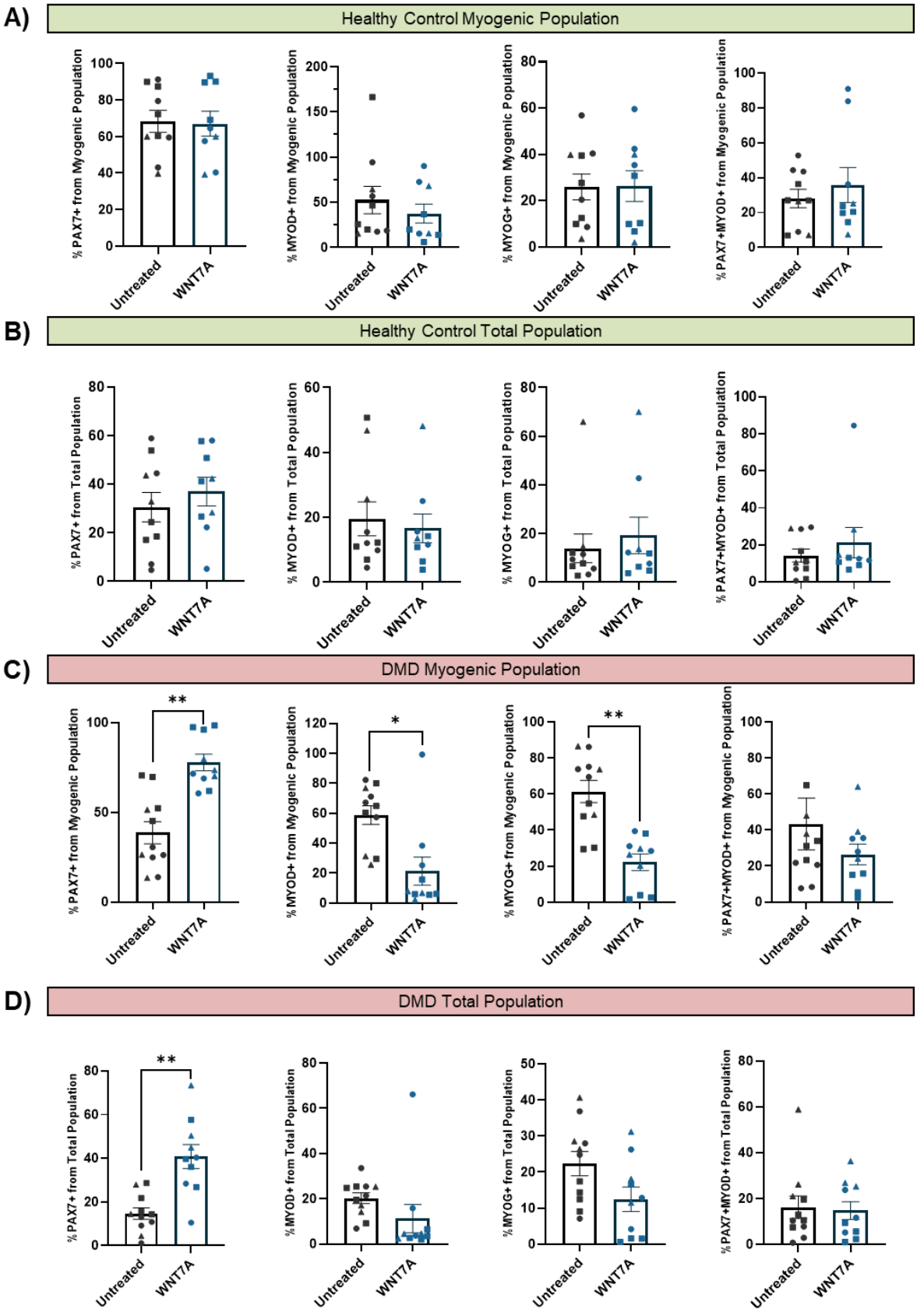
A)
Healthy Control Myogenic Population
% PAX7+ from Myogenic Population
% MYOD+ from Myogenic Population
% MYOG+ from Myogenic Population
% PAX7+MYOD+ from Myogenic Population
Untreated
WNT7A
B)
Healthy Control Total Population
% PAX7+ from Total Population
% MYOD+ from Total Population
% MYOG+ from Total Population
% PAX7+MYOD+ from Total Population
C)
DMD Myogenic Population
D)
DMD Total Population

Figure 14. WNT7A treatment expands the proportion of PAX7+ cells and decreases the proportion of MYOD+ and MYOG+ cells in the twenty-one day differentiated DMD-patient derived hiPSCs. The healthy CONT1-3 (A-B) and DMD1-3 (C-D) hiPSCs were differentiated for twenty-one days and treated with 100 ng/mL of WNT7A from day twelve to twenty-one. On day twenty-one the cells were stained for PAX7, MYOD, and MYOG and immunofluorescence images were captured using the Opera Phenix™ High-Content Screening System. Quantification of the percentage of each myogenic marker was conducted using the Columbus Image Data Storage and Analysis System and R Studio, as described in the Materials and Methods section. The myogenic population (A, C) represents cells that have expressed PAX7 and MYOG. The total population (B, D) refers to all the cells in the differentiated cultures. n=9-11, with with 9-11 biological replicates as independent differentiations. The circles (CONT1 or DMD1), squares (CONT2 or DMD2), and triangles (CONT3 or DMD3) represent the replicates for each cell line. Error bars represent S.E.M. *$p < 0.05$, **$p < 0.01$.

To gain further insights into the effects of WNT7A treatment on day twenty-one of the differentiation process, we conducted an RT-qPCR analysis to probe for the myogenic markers *PAX7, MYF5, MYOD, MYOG* and the WNT7A receptor, *Frizzled 7 (FZD7)*. Again, we did not observe any significant differences in the healthy CONT1-2 lines with the treatment (Figure 15A). However, in the DMD1-2 lines, we detected a significant increase in global *PAX7* gene expression upon WNT7A treatment, which is consistent with the previously observed increase in the proportion of PAX7+ cells within the total and myogenic population (Figure 15B). *FZD7* expression was relatively unchanged in both the healthy control and DMD patient lines with WNT7A treatment.

These results suggest that WNT7A treatment drove the symmetric expansion of the PAX7+ muscle stem cells in the DMD-patient derived cell lines.

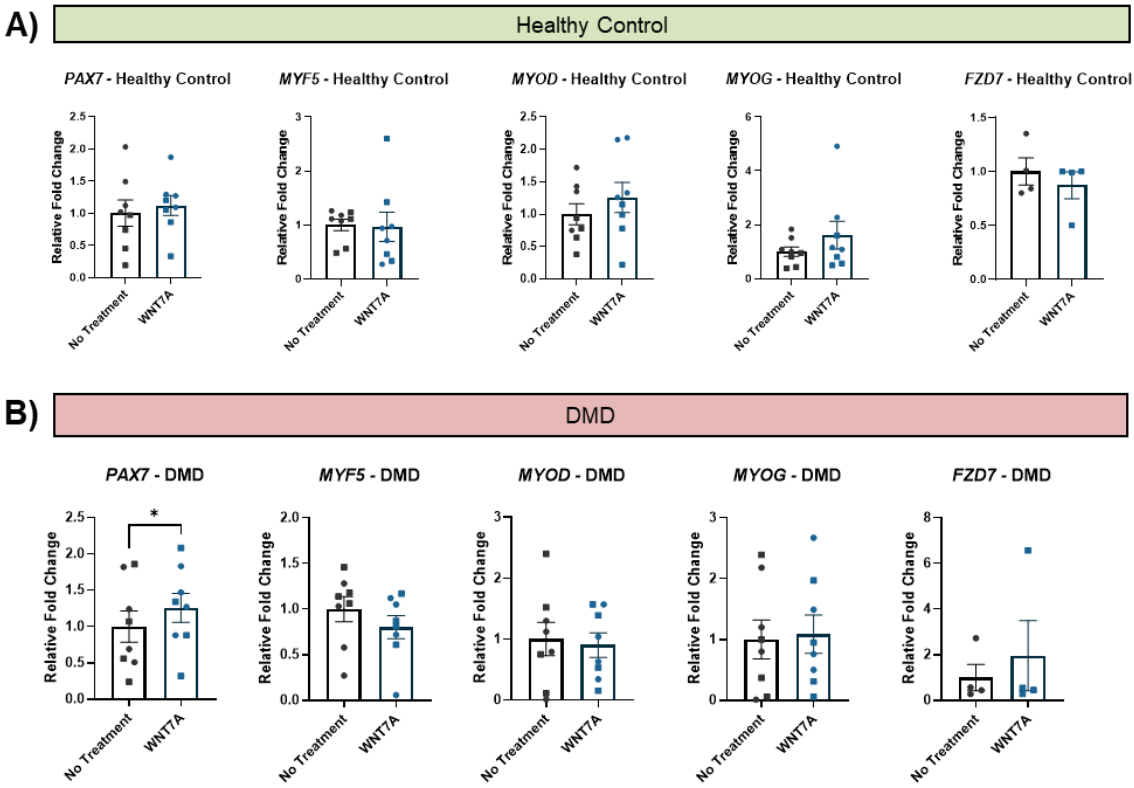

Figure 15. WNT7A treatment significantly increased *PAX7* global gene expression in twenty-one day differentiated DMD-patient hiPSCs. (A) The healthy CONT1-2 hiPSCs and (B) DMD1-2 hiPSCs were differentiated for twenty-one days and treated with 100 ng/mL of WNT7A from day twelve to twenty-one. The RNA was harvested on day twenty-one for gene expression analysis by RT-qPCR for the indicated myogenic genes, and *Frizzled 7 (FZD7)*, the receptor for WNT7A. Data is presented as relative fold change to the untreated control cells. n=8, with 8 biological replicates as independent differentiations for *PAX7*, *MYOD*, and *MYOG*. The circles (CONT1 and DMD1) and squares (CONT2 and DMD2) represent the replicates for each cell line. n=4, with 4 biological replicates for *FZD7*. Error bars represent S.E.M. *$p < 0.05$.

On day thirty-five of the differentiation process, we performed the same high content analysis (as described at the earlier timepoint) to assess the effects of WNT7A treatment (Figure 16A-D). Interestingly, we observed significant changes in the healthy CONT1-2 cells with WNT7A treatment, unlike at the earlier timepoint. Specifically, compared to the untreated cells, WNT7A treatment significantly decreased the proportion of MYOD+, MYOG+, and PAX7+MYOD+ double positive cells within the total population (Figure 16B). Similarly, in the DMD1-2 cell lines, we observed a significant decrease in the proportion of MYOD+ cells within the myogenic population, which was consistent with the findings at day twenty-one (Figure 16C).

By day fifty, we did not see many significant changes with long-term WNT7A treatment, except for a slight decrease in the proportion of MYOD+ cells from the total population in the healthy CONT1-2 lines (Figure 17A-D), possibly due to the shift towards terminal differentiation in these long-term cultures.

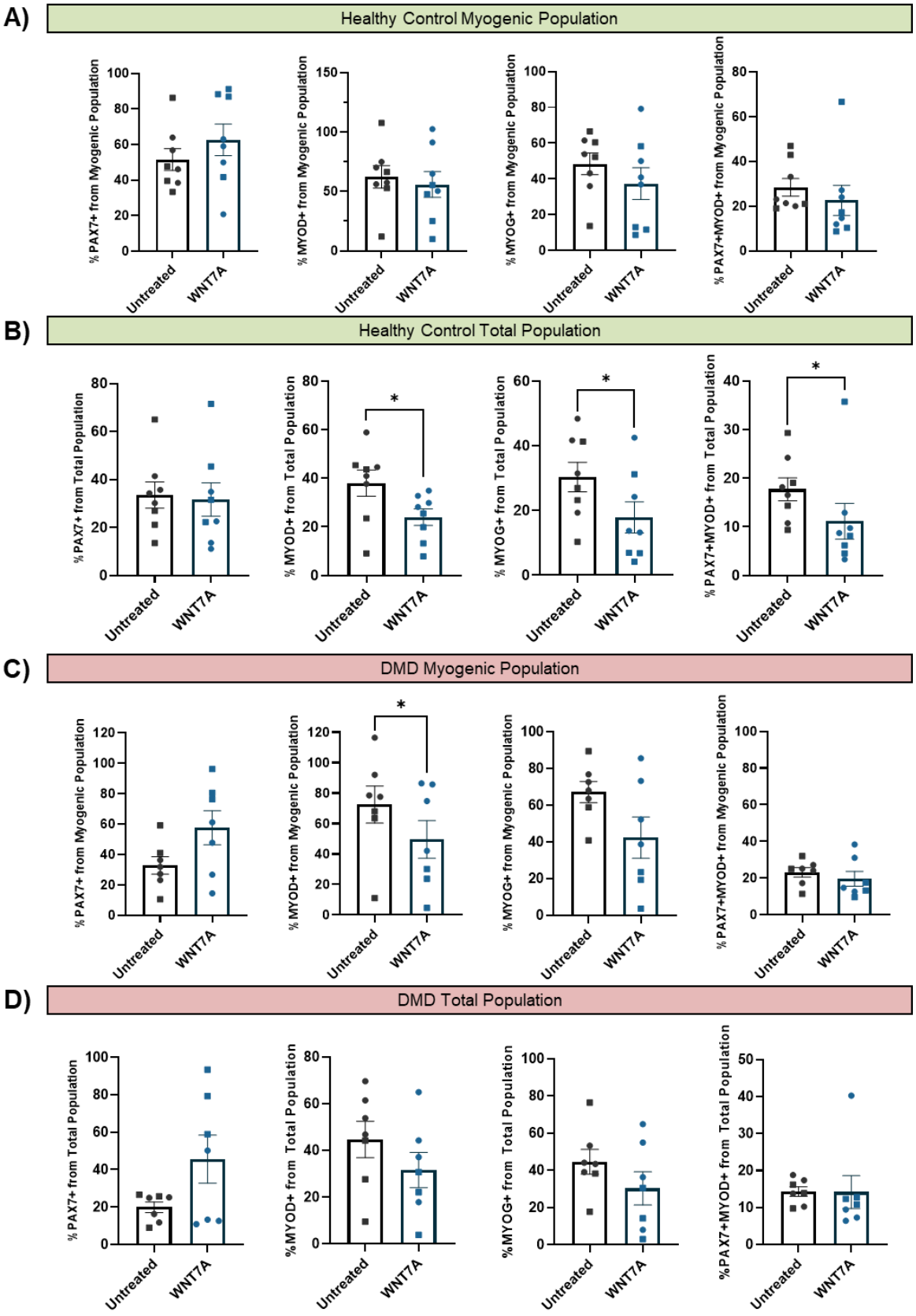
A)
Healthy Control Myogenic Population
% PAX7+ from Myogenic Population
% MYOD+ from Myogenic Population
% MYOG+ from Myogenic Population
% PAX7+MYOD+ from Myogenic Population
Untreated
WNT7A
B)
Healthy Control Total Population
% PAX7+ from Total Population
% MYOD+ from Total Population
% MYOG+ from Total Population
% PAX7+MYOD+ from Total Population
*
C)
DMD Myogenic Population
% PAX7+ from Myogenic Population
% MYOD+ from Myogenic Population
% MYOG+ from Myogenic Population
% PAX7+MYOD+ from Myogenic Population
D)
DMD Total Population
% PAX7+ from Total Population
%MYOD+ from Total Population
%MYOG+ from Total Population
%PAX7+MYOD+ from Total Population

Figure 16. WNT7A treatment significantly reduces the proportions of myogenic precursor cells in the thirty-five-day differentiated healthy control hiPSCs. The healthy CONT1-2 hiPSCs (A-B) and DMD1-2 hiPSCs (C-D) were differentiated for thirty-five days and treated with 100 ng/mL of WNT7A from day twelve to thirty-five. On day thirty-five the cells were stained for PAX7, MYOD, and MYOG and immunofluorescence images were captured using the Opera Phenix™ High-Content Screening System. Quantification of the percentage of each myogenic marker was conducted using the Columbus Image Data Storage and Analysis System and R Studio, as described in the Materials and Methods section. The myogenic population (A, C) represents cells that have expressed PAX7 and MYOG. The total population (B, D) refers to all the cells in the differentiated cultures. n=7, with 7 biological replicates as independent differentiations. The circles (CONT1 and DMD1) and squares (CONT2 and DMD2) represent the replicates for each cell line. Error bars represent S.E.M. *$p < 0.05$.

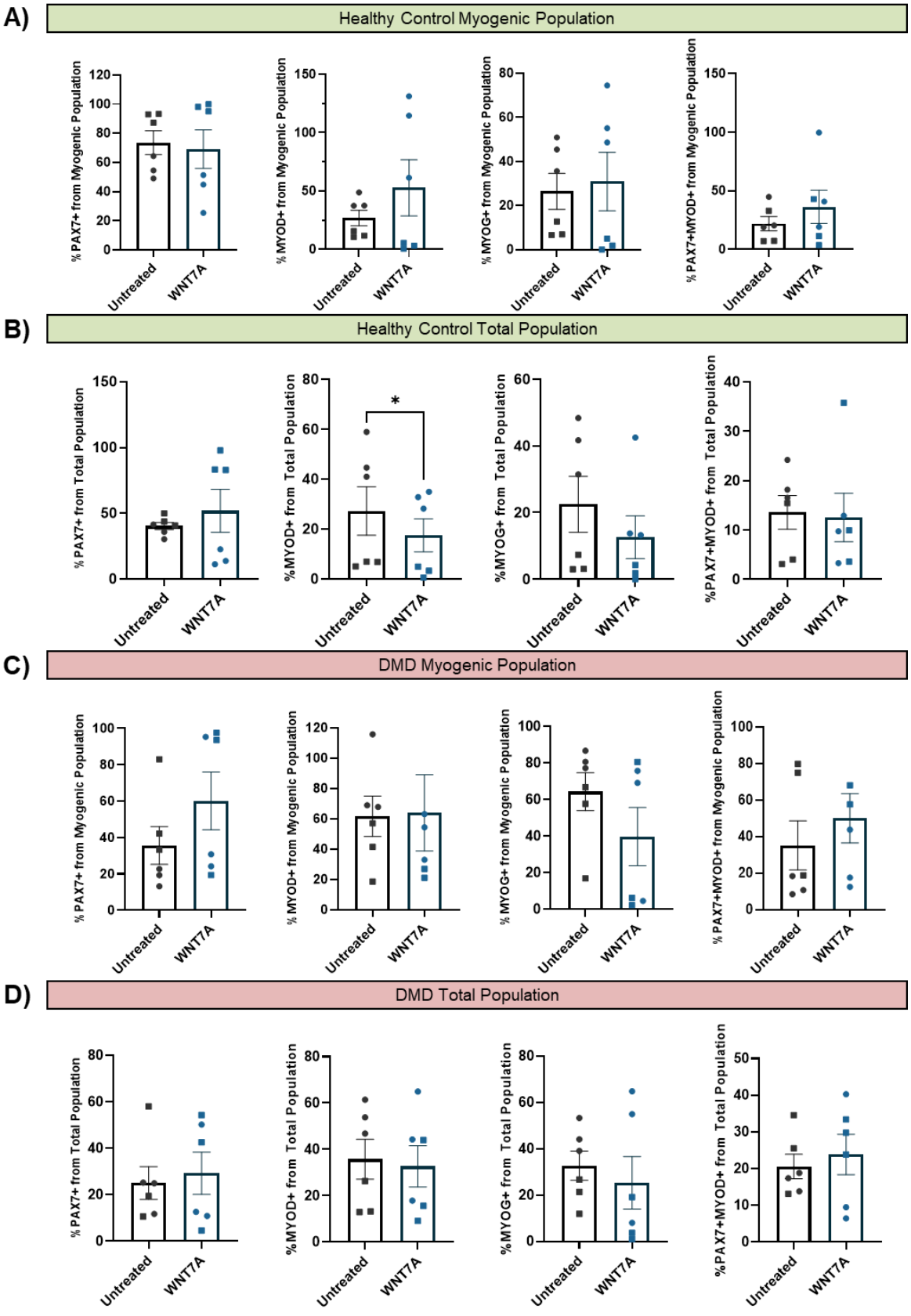
A)
Healthy Control Myogenic Population
% PAX7+ from Myogenic Population
% MYOD+ from Myogenic Population
% MYOG+ from Myogenic Population
% PAX7+MYOD+ from Myogenic Population
Untreated
WNT7A
B)
Healthy Control Total Population
% PAX7+ from Total Population
%MYOD+ from Total Population
%MYOG+ from Total Population
%PAX7+MYOD+ from Total Population
*
C)
DMD Myogenic Population
D)
DMD Total Population

Figure 17. WNT7A treatment reduces the proportion of MYOD+ expressing cells in the fifty-day differentiated healthy control hiPSCs. The healthy CONT1-2 hiPSCs (A-B) and DMD1-2 hiPSCs (C-D) were differentiated for fifty days and treated with 100 ng/mL of WNT7A from day twelve to fifty. On day fifty the cells were stained for PAX7, MYOD, and MYOG and immunofluorescence images were captured using the Opera Phenix™ High-Content Screening System. Quantification of the percentage of each myogenic marker was conducted using the Columbus Image Data Storage and Analysis System and R Studio, as described in the Materials and Methods section. The myogenic population (A, C) represents cells that have expressed PAX7 and MYOG. The total population (B, D) refers to all the cells in the differentiated cultures. n=7, with 7 biological replicates as independent differentiations. The circles (CONT1 and DMD1) and squares (CONT2 and DMD2) represent the replicates for each cell line. Error bars represent S.E.M. *$p < 0.05$.

Given that WNT7A appears to affect the differentiating hiPSC cultures, we sought to investigate if differentiation further along the myogenic lineage would be altered. To assess this, we performed immunostaining for Myosin Heavy Chain (MHC), which serves as a marker for multinucleated myotube formation. On day 21, we did not detect any significant differences in MHC expression with WNT7A treatment in both the healthy CONT2 line and DMD2 line (Figure 18A). However, by day 35, we observed an absence of MHC expression in the WNT7A treated cells, which is consistent with our high content analysis data showing a decrease in the proportion of cells expressing myogenic precursor markers upon WNT7A treatment (Figure 18B). By day 50, MHC expression was partially restored in the WNT7A treated cells, though to a lesser extent in the healthy control cell line (Figure 18C).

Here, we demonstrate that treatment with WNT7A led to a significant expansion of PAX7-expressing muscle stem cells on day twenty-one of the differentiation process, possibly through symmetric division. Notably, WNT7A treatment resulted in reduced myogenic differentiation on day thirty-five, as indicated by a significant decrease in myogenic precursor markers and the absence of MHC expression.

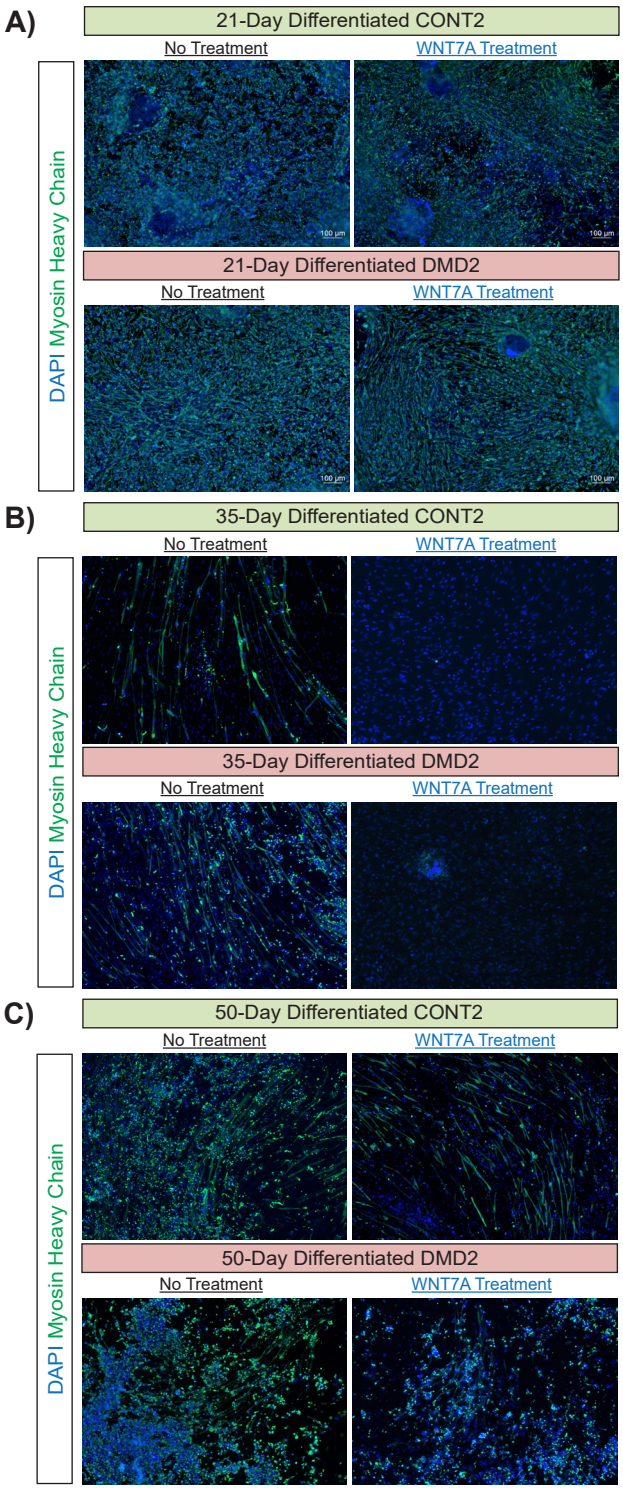

Figure 18. WNT7A treatment reduces MYH expression in thirty-five day and fifty day differentiated healthy control and DMD-patient hiPSCs. The healthy CONT2 and DMD2 hiPSC lines were differentiated into the myogenic lineage, treated with 100 ng/mL of WNT7A from day twelve to day fifty, and immunostained at day twenty-one (A), thirty-five (B), and fifty (C) for DAPI (in blue), and myosin heavy chain (MYH) (in green). Scale bar = 100 µm in all images.

3.4 EGF Treatment Decreases the PAX7+ Expressing Muscle Stem Cell Pool

In the study conducted by Dumont et al. in 2015, it was shown that dystrophin is expressed in activated satellite cells and interacts with regulators of cell polarity to promote asymmetric cell division (19). However, in Duchenne Muscular Dystrophy, which is characterized by the absence of dystrophin, satellite cells are unable to properly polarize, leading to a significant reduction in the number of asymmetric cell divisions (19). Our laboratory showed that supplementation with exogenous EGF substantially increased the number of asymmetric cell divisions in dystrophin-deficient satellite cells obtained from *mdx* mice (47).

We then aimed to investigate whether the addition of exogenous EGF during the differentiation of healthy control and DMD patient hiPSCs at day twenty-one, day thirty-five, or day fifty would alter the muscle stem cell division mechanisms to favor asymmetric cell division and expand the committed myogenic progenitor cell pool.

To test this, we differentiated the healthy CONT1-3 and DMD1-3 lines into the myogenic lineage using our aforementioned optimized myogenic differentiation protocol. The differentiating cells were then treated with 100 ng/mL of EGF every day from day twelve to day twenty-one of the differentiation process. We also continued differentiating and treating DMD1-2 and CONT1-2 until day fifty. The cells were fixed and stained on day twenty-one, thirty-five, and day fifty where we probed for expression of PAX7, MYOD, and MYOG at the population level using high-content analysis.

On day twenty-one, in the healthy control lines, we observed an increase in the proportion of MYOG+ cells within the myogenic population, which could indicate an

increase in committed myogenic progenitors due to enhanced asymmetric cell division (Figure 19A-B). However, we did not observe any significant changes in the DMD cells with EGF treatment (Figure 19C-D).

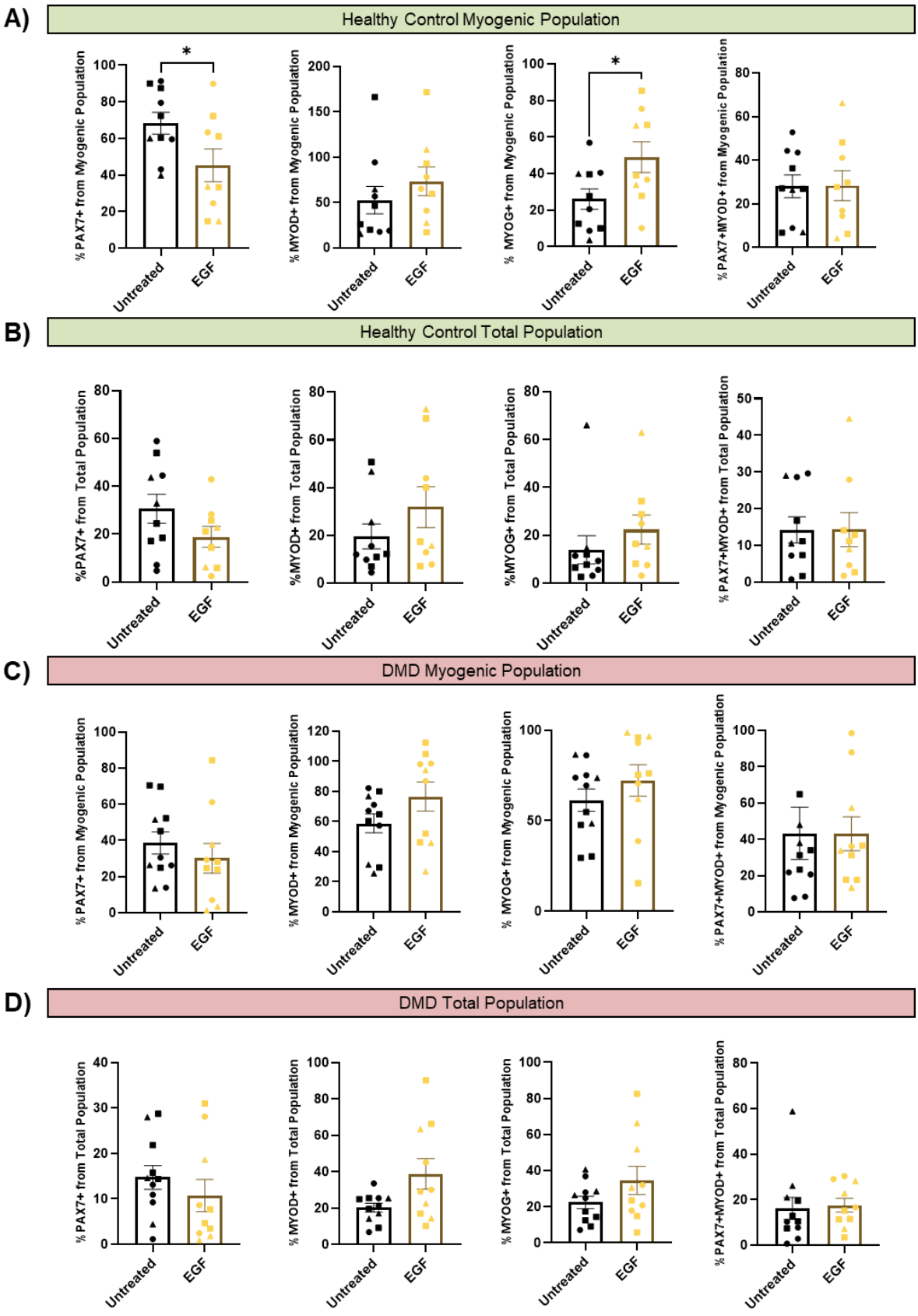
A)
Healthy Control Myogenic Population
% PAX7+ from Myogenic Population
% MYOD+ from Myogenic Population
% MYOG+ from Myogenic Population
% PAX7+MYOD+ from Myogenic Population
Untreated
EGF
B)
Healthy Control Total Population
%PAX7+ from Total Population
%MYOD+ from Total Population
%MYOG+ from Total Population
% PAX7+MYOD+ from Total Population
C)
DMD Myogenic Population
D)
DMD Total Population

Figure 19. EGF treatment reduces the proportion of PAX7+ cells and increases the proportion of MYOG+ cells in twenty-one-day differentiated healthy control hiPSCs. The healthy CONT1-3 (A-B) and DMD1-3 (C-D) hiPSCs were differentiated for twenty-one days and treated with 100 ng/mL of EGF from day twelve to twenty-one. On day twenty-one the cells were stained for PAX7, MYOD, and MYOG and immunofluorescence images were captured using the Opera Phenix™ High-Content Screening System. Quantification of the percentage of each myogenic marker was conducted using the Columbus Image Data Storage and Analysis System and R Studio, as described in the Materials and Methods section. The myogenic population (A, C) represents cells that have expressed PAX7 and MYOG. The total population (B, D) refers to all the cells in the differentiated cultures. n=9-11, with 9-11 biological replicates as independent differentiations. The circles (CONT1 or DMD1), squares (CONT2 or DMD2), and triangles (CONT3 or DMD3) represent the replicates for each cell line. Error bars represent S.E.M. *$p < 0.05$, **$p < 0.01$.

Additionally, we performed gene expression analysis using RT-qPCR on day twenty-one to evaluate changes in myogenic gene expression with EGF treatment. Although no significant differences were observed in the healthy CONT1-2 lines (Figure 20A), we did notice a decrease in *MYOD* gene expression with EGF treatment in the DMD1-2 patient lines (Figure 20B). This effect could be attributed to EGF reducing *MYOD* expression within the heterogeneous population of the differentiating cultures, as these cultures consist of various cell types and are not purely composed of myogenic cells.

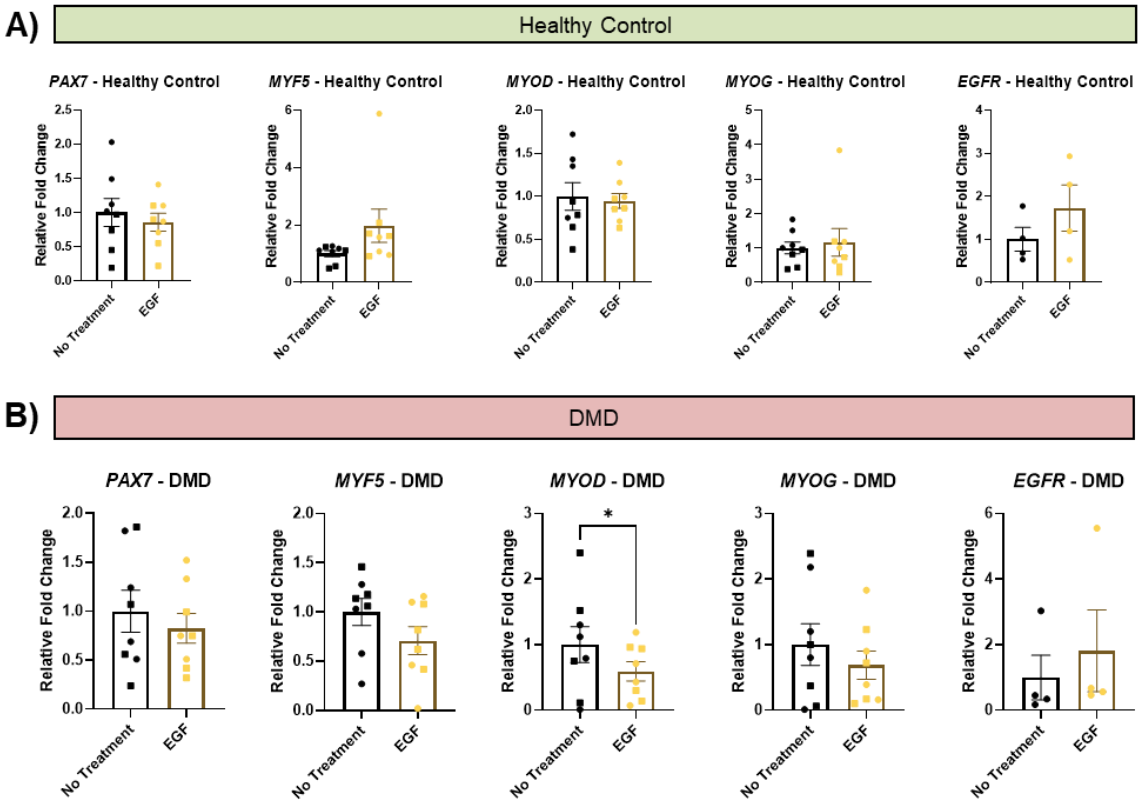

Figure 20. EGF treatment significantly reduces global *MYOD* gene expression in twenty-one-day differentiated DMD-patient hiPSCs. (A) The healthy CONT1-2 hiPSCs and (B) DMD1-2 hiPSCs were differentiated for twenty-one days and treated with 100 ng/mL of EGF from day twelve to twenty-one. RNA was harvested on day twenty-one for gene expression analysis by RT-qPCR for the indicated myogenic genes, and *EGFR*, the receptor for EGF. Data is presented as relative fold change to the untreated control cells. n=8, with 8 biological replicates as independent differentiations for *PAX7*, *MYOD*, and *MYOG*. The circles (CONT1 and DMD1) and squares (CONT2 and DMD2) represent the replicates for each cell line. n=4, with with 4 biological replicates as independent differentiations for *EGFR*. Error bars represent S.E.M. *$p < 0.05$.

On day thirty-five (Figure 21A-D), we observed that EGF treatment decreased the proportion of PAX7+ cells within the entire population in both the DMD1-2 lines and the healthy CONT1-2 lines (Figure 21B, D). This effect was also evident within the myogenic population of the DMD1-2 lines (Figure 21C). Interestingly, by day thirty-five, the proportion of MYOG+ cells within the myogenic population in the DMD1-2 lines was significantly increased (Figure 21C). This suggests that EGF may have stimulated asymmetric cell division, leading to an expansion of the committed progenitor cells expressing MYOG, particularly in the DMD patient lines.

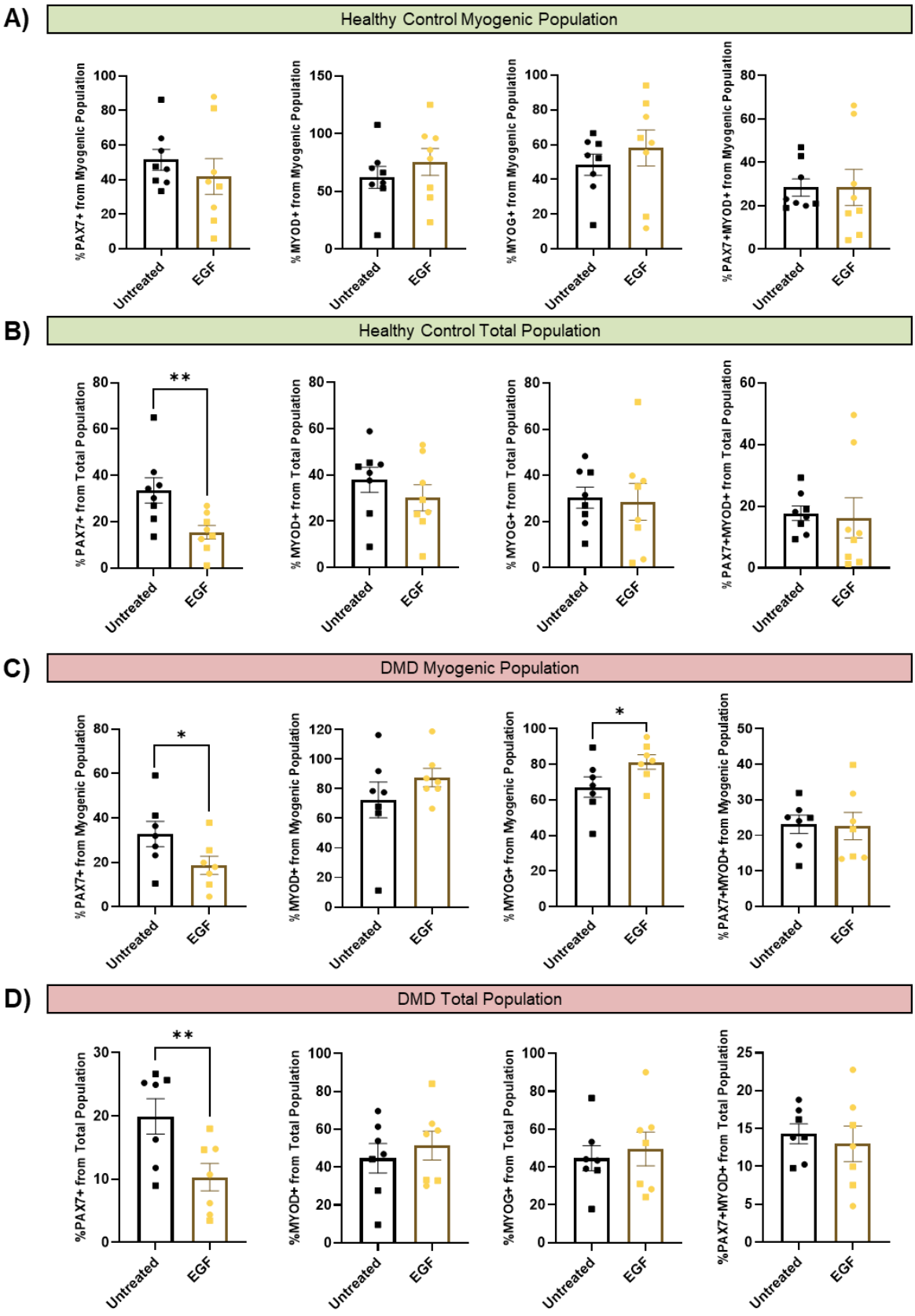
A)
Healthy Control Myogenic Population
% PAX7+ from Myogenic Population
% MYOD+ from Myogenic Population
% MYOG+ from Myogenic Population
% PAX7+MYOD+ from Myogenic Population
Untreated
EGF
B)
Healthy Control Total Population
% PAX7+ from Total Population
% MYOD+ from Total Population
% MYOG+ from Total Population
% PAX7+MYOD+ from Total Population
**
C)
DMD Myogenic Population
% PAX7+ from Myogenic Population
% MYOD+ from Myogenic Population
% MYOG+ from Myogenic Population
% PAX7+MYOD+ from Myogenic Population
*
D)
DMD Total Population
%PAX7+ from Total Population
%MYOD+ from Total Population
%MYOG+ from Total Population
%PAX7+MYOD+ from Total Population
**

Figure 21. EGF treatment reduces the proportion of PAX7+ cells and increases the proportion of MYOG+ cells in thirty-five-day differentiated DMD-patient hiPSCs. The healthy CONT1-2 hiPSCs (A-B) and DMD1-2 hiPSCs (C-D) were differentiated for thirty-five days and treated with 100 ng/mL of EGF from day twelve to thirty-five. On day thirty-five, the cells were stained for PAX7, MYOD, and MYOG and immunofluorescence images were captured using the Opera Phenix™ High-Content Screening System. Quantification of the percentage of each myogenic marker was conducted using the Columbus Image Data Storage and Analysis System and R Studio, as described in the Materials and Methods section. The myogenic population (A, C) represents cells that have expressed PAX7 and MYOG. The total population (B, D) refers to all the cells in the differentiated cultures. n=7, with 7 biological replicates as independent differentiations. The circles (CONT1 and DMD1) and squares (CONT2 and DMD2) represent the replicates for each cell line. Error bars represent S.E.M. $*p < 0.05$, $**p < 0.01$.

It is on day fifty (Figure 22A-D) where we see significant changes with EGF treatment in the healthy CONT1-2 lines within the myogenic population. EGF treatment increased the proportion of MYOD+ and MYOG+ expressing cells within the myogenic population, compared to the untreated control in the healthy CONT1-2 lines. This suggests that EGF may be facilitating asymmetric division in the fifty-day differentiated healthy control hiPSCs (Figure 22A). Similar to day thirty-five, EGF treatment led to a significant decrease in the proportion of PAX7+ cells in the CONT1-2 lines, as well as in the total population of the DMD1-2 patient lines (Figure 22B, D).

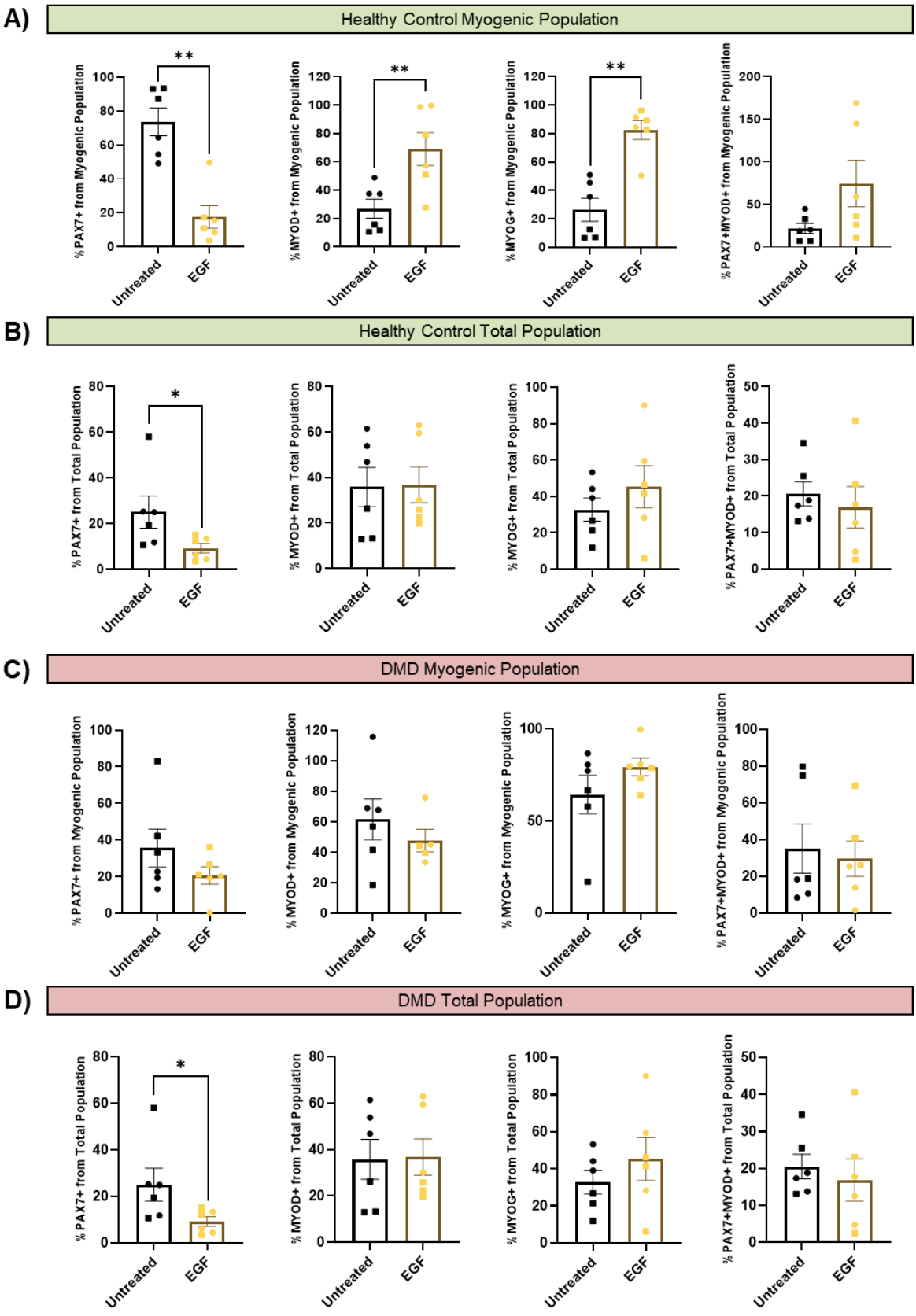
A)
Healthy Control Myogenic Population
% PAX7+ from Myogenic Population
% MYOD+ from Myogenic Population
% MYOG+ from Myogenic Population
% PAX7+MYOD+ from Myogenic Population
Untreated
EGF
B)
Healthy Control Total Population
% PAX7+ from Total Population
% MYOD+ from Total Population
% MYOG+ from Total Population
% PAX7+MYOD+ from Total Population
C)
DMD Myogenic Population
D)
DMD Total Population

Figure 22. EGF treatment increases the proportion of MYOD+ and MYOG+ cells in the fifty-day differentiated healthy control hiPSCs. The healthy CONT1-2 hiPSCs (A-B) and DMD1-2 hiPSCs (C-D) were differentiated for fifty days and treated with 100 ng/mL of EGF from day twelve to fifty. On day fifty the cells were stained for PAX7, MYOD, and MYOG and immunofluorescence images were captured using the Opera Phenix™ High-Content Screening System. Quantification of the percentage of each myogenic marker was conducted using the Columbus Image Data Storage and Analysis System and R Studio, as described in the Materials and Methods section. The myogenic population (A, C) represents cells that have expressed PAX7 and MYOG. The total population (B, D) refers to all the cells in the differentiated cultures. n=7, with 7 biological replicates as independent differentiations. The circles (CONT1 and DMD1) and squares (CONT2 and DMD2) represent the replicates for each cell line. Error bars represent S.E.M. $*p < 0.05$, $**p < 0.01$.

We also investigated whether EGF treatment would alter later myogenic differentiation stages, so we stained the differentiating CONT2 and DMD2 cultures with MYH. On day twenty-one, we did not observe any visible differences with the treatment (Figure 23A). However, by day thirty-five, we noticed that EGF treatment led to an increase in MHC-expressing myotubes, particularly in the DMD2 patient line (Figure 23B). This trend continued until day fifty and was also evident in the healthy CONT2 line (Figure 23C). It is possible that the increased formation of myotube structures was due to EGF acting as a mitogen and promoting the differentiation of more cells initially.

Altogether, EGF consistently reduced the proportion of PAX7 expressing cells in the differentiated healthy control and DMD patient hiPSCs. EGF treatment may have promoted asymmetric cell division in the DMD1-2 lines on day thirty-five and in the healthy CONT1-2 lines on day fifty of the differentiation process as we observed higher proportions of myogenic precursor markers.

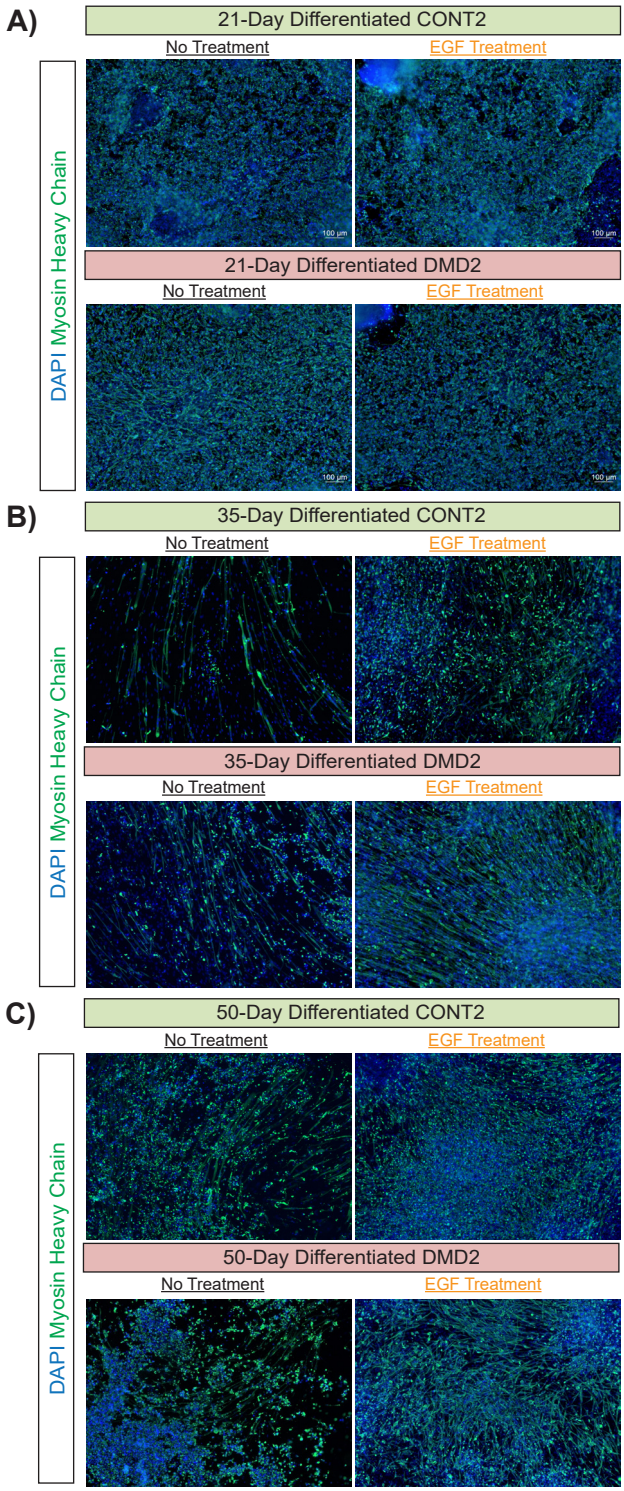

Figure 23. EGF treatment increases MYH expression in thirty-five day and fifty day differentiated healthy control and DMD-patient hiPSCs. The healthy CONT2 and DMD2 hiPSC lines were differentiated into the myogenic lineage, treated with 100 ng/mL of EGF from day twelve to day fifty, and immunostained at day twenty-one (A), thirty-five (B), and fifty (C) for DAPI (in blue), and myosin heavy chain (MYH) (in green). Scale bar = 100 µm in all images.

4 DISCUSSION

Satellite cells are indispensable for skeletal muscle regeneration (10, 11, 74). Upon injury, they become activated and can divide symmetrically to self-renew, or divide asymmetrically to expand the myogenic progenitor pool for repair of damaged myofibers (21).

Dystrophin is highly expressed in activated satellite cells and is required for sarcolemmal integrity (19). In the absence of dystrophin, satellite cells are unable to polarize and initiate asymmetric cell division (19). Fewer progenitor cells are generated, leading to satellite stem cell hyperplasia and contributing to the muscular degenerative disorder, DMD, which results in progressive muscle wasting and premature death.

Our lab discovered two compounds that have been shown regulate satellite cell division mechanisms as well as show therapeutic potential for DMD.

The first compound, WNT7A, modulates satellite cell division by promoting symmetric expansion. WNT7A binds to its receptor FZD7 in satellite cells, polarizes the distribution of the PCP effector VANGL2, and induces symmetric satellite cell expansion, as shown by Le Grand et al. (17, 74). Additionally, Wang et al. reported that EGF stimulation of satellite cells activates EGFR and recruits AURKA, a mitotic spindle assembly protein, to promote apicobasal asymmetric cell division (47).

Although extensively studied in mouse models, little is known about the division modulatory capacity of both compounds in a human context, and particularly in the human context of DMD. In this study, we confirm that WNT7A and EGF can modify the division mechanisms of satellite-like cells in myogenically differentiated hiPSCs derived from

healthy controls and DMD patients. Our study provides a comprehensive analysis of the myogenic differentiation strategy used to derive a high yield of myogenic cells, compares the differentiation characteristics of healthy donor and DMD patient derived hiPSCs, and evaluates the division effects of WNT7A or EGF treatment at day twenty-one, thirty-five, and fifty of the hiPSC differentiation program.

4.1 E8 MEDIA, E6 MEDIA, AND 7.5 UM CHIR ARE OPTIMAL FOR DMD AND HEALTHY CONTROL HIPSC DIFFERENTIATION.

Human modeling of DMD is challenging due to the limited availability of satellite cells that can be obtained from patient biopsy samples. Additionally, these satellite cells spontaneously differentiate *in vitro*, which is characterized by the irreversible expression of *MYF5, MYOD,* and *MYOG* (24, 56). More notably, these satellite cells and their derived myoblasts have reduced proliferative and regenerative capacities, making them difficult to manipulate as potential stem cell therapies for the diseased muscle (56, 75).

A promising alternative approach to DMD disease modelling is the use of hiPSCs derived from DMD patients to generate myogenic cells. Through hiPSC myogenic differentiation, we now have the unprecedented ability to generate numerous muscle stem cells, investigate the pathophysiological mechanisms of disease, and most importantly, trial therapeutics in a patient-specific manner (56, 66) .

The Shelton et al. protocol, is a well-established and reliable method previously used by the authors of this study with hESCs differentiated into the myogenic lineage (52, 71). This approach is not only simple and cost-effective but also yields a significant number of muscle stem cells capable of generating PAX7-expressing cells upon transplantation, as

demonstrated in the 2018 study by Hicks et al. (76). Therefore, this protocol was used to differentiate DMD and healthy control hiPSCs into the myogenic lineage. We initially cultured the healthy control and DMD-patient hiPSCs in the STEMCELL Technologies mTeSR™ hiPSC and ESC media. Consistency with the TeSR™ series was maintained throughout the study by differentiating the hiPSCs in TeSR-E6™ media, rather than using E8 media for hiPSC culture and E6 media for differentiation. However, we observed very few to no PAX7+ cells in all three cell lines during differentiation. Gene expression analysis showed a downregulation of all myogenic genes, and Western blot analysis revealed no PAX7 protein expression. These results indicated that the differentiation did not proceed to the early dermomyotome stage as expected.

The choice to use mTeSR™ and TeSR-E6™ media in this study was based on their successful application in previous myogenic differentiation protocols (26, 59, 64–69). Additionally, mTeSR™ has been shown to maintain hiPSC lines in a healthy morphology, characterized by compact colonies with distinct borders and large nuclei to plasma ratios (77). Truly, this media is regarded as the standard for hiPSC maintenance and is the most commonly published feeder-free cell culture medium for iPSCs and ESCs (78). It is crucial to carefully select the culture media prior to differentiation as the success and reproducibility of differentiation can be influenced by the quality of starting hiPSCs, which can in turn be impacted by their maintenance conditions.

A study similar to ours was conducted by Fabre et al. in 2022, where they used mTeSR™ to grow and maintain their DMD-patient and healthy control hiPSCs. They differentiated the hiPSCs into the myogenic lineage using TeSR-E6™ and CHIR99021 following a modified version of the Shelton et al. protocol. They observed the generation of

hiPSC-derived myogenic cells by day seven through immunofluorescence imaging of the dermomyotomal marker PAX3 and satellite stem cell marker PAX7. Additionally, they observed the expression of later myogenic markers MYOG and MHC by day thirty (79). One possible explanation for the difference in outcomes between our protocol and that of Fabre et al. is the duration and dosage of CHIR99021 treatment. Our protocol involved a two-day treatment of 10 μM CHIR99021, while Fabre et al. used a three-day treatment of 7 μM CHIR99021. It's possible that a longer treatment period and/or a lower concentration of CHIR99021 would have been more effective for our hiPSCs. It's also worth considering that our hiPSCs may have different characteristics or requirements for successful differentiation compared to the hiPSCs used in the Fabre et al. study.

To improve our differentiation protocol, we switched back to E6 media instead of TeSR-E6™ while keeping all other parameters constant. By day twenty-one, we observed a significant increase in the number of PAX7 expressing cells in the DMD1-2 and CONT1 lines. Additionally, we observed cells that have differentiated further into the myogenic lineage as they expressed MYOD and MYOG. Based on our findings, we hypothesized that we could generate more myogenic cells by transitioning the hiPSCs from mTeSR™ to E8 media, as originally suggested by the Shelton et al. protocol. Our observations showed that the longer the hiPSCs were cultured in pure E8 media, the more uniform and abundant the myogenic cells became. These results suggest that hiPSCs cultured in mTeSR™ may remain in a highly pluripotent state, making them resistant to differentiation. To address this issue, we had to gradually transition the hiPSCs out of mTeSR™ and into E8 media, allowing them to acclimate to the new conditions for two weeks to eliminate any residual effects of mTeSR™. After the two-week culture of hiPSCs in E8, we initiated differentiation using E6

media and found that 7.5 μM of CHIR was the optimal concentration for differentiating DMD and healthy control hiPSCs (71). With this specific concentration, we observed a three-fold increase in the number of PAX7+ cells in the healthy control line, and two-fold increase in the DMD line. It is worth noting that previous studies have shown that higher concentrations of CHIR, especially 10 μM for 2 days, can cause toxicity in hiPSC cultures (25, 54, 80). We also found that the optimal cell density had to be adjusted for each cell line, ranging from 200,000 cells/well to 400,000 cells/well, while maintaining the concentration of CHIR99021 at 7.5 μM.

While it was possible to extend the CHIR99021 treatment period beyond two days (as conducted in the Fabre et al. study), we opted to modify the media composition instead of solely relying on longer CHIR99021 treatment to induce myogenic differentiation of hiPSCs. This approach was not only cost-effective but also led to robust myogenic differentiation on day twenty-one, thirty-five, and fifty of the differentiation program.

By day fifty of the differentiation process, the cultures terminally differentiated and committed to the skeletal muscle lineage, with approximately 30-40% of cells expressing MYOD or MYOG. A study conducted by Baci et al. demonstrated an interesting method to increase the terminally differentiated population by using extracellular vesicles (EVs) derived from C2C12 myotubes (81). They co-cultured hiPSCs with CHIR99021 and EVs and found that the combination treatment synergistically enhanced terminal differentiation compared to CHIR99201 treatment alone. The CHIR99201 and EV combination treatment yielded a significantly higher fusion index and consistently increased the number of cells expressing MHC. Specifically, by day thirty, approximately 70-80% of their cells were

positive for MYOD or MYOG (81). This co-culture method could be used in future studies to increase our yield of terminally differentiated myogenic cells.

4.2 DMD HIPSCS PRECOCIOUSLY DIFFERENTIATE IN THE MYOGENIC LINEAGE.

In 2015, Dumont and colleagues made a remarkable discovery regarding the role of satellite stem cells in the disease etiology of *mdx* mice (19). Dystrophin-deficient satellite cells display a loss of polarity and exhibit a 5-fold reduction in the proportion of asymmetric division.

We hypothesized that DMD hiPSCs, lacking dystrophin, would display a similar phenomenon upon differentiation into the myogenic lineage with more muscle stem cells and fewer committed progenitor cells. However, our high-content analysis revealed fewer PAX7+ cells within the myogenic population at all time points, and an increased number of MYOG+ cells at day twenty-one and fifty compared to healthy control hiPSCs. These findings suggest that our DMD hiPSCs have an increased myogenic capacity and precociously differentiated compared to the healthy control hiPSCs.

This could be attributed to the pathological condition of hiPSCs derived from DMD patients. Mournetas et al. also differentiated DMD-patient derived hiPSCs into the myogenic lineage using a non-reprogramming approach (61). Their study involved a comprehensive multi-omics analysis to investigate the onset of DMD using hiPSC-derived skeletal muscle progenitors. Although the DMD hiPSCs differentiated normally into the mesoderm lineage, the researchers detected numerous genetic dysregulations at the somite stage – specifically dysregulations of mitochondrial genes. More notably, upon entering the skeletal muscle

compartment at day 17, the authors observed significant skeletal muscle-specific gene dysregulations, including the aberrant expression of various myomiRs (miRNAs specific to striated muscles).While we did not observe any somitic gene dysregulations in the twelve-day differentiated DMD cultures, we did observe that DMD1-2 had significantly higher levels of *OCT4* compared to the control cultures.

On the other hand, we postulated if we were seeing different effects due to our differentiated hiPSCs resembling embryonic or fetal-like muscle stem cells. Especially since the previously mentioned Dumont et al. study was conducted in adult *mdx* mice and therefore demonstrated satellite cell division defects in adult satellite cells. Indeed, a noteworthy study published in Cell Stem Cell in 2020 by Xi et al. confirmed the developmental stage of muscle stem cells derived from hiPSCs as transitioning from the embryonic phase to the fetal phase of human development. The group created a comprehensive human skeletal muscle atlas, which mapped the developmental trajectory of satellite cells and progenitors during various stages of myogenesis (82). Xi et al. utilized single-cell RNA sequencing to profile human skeletal muscle at various developmental stages, including embryonic, fetal, and post-natal stages. They also differentiated hiPSCs using three published protocols, including the Shelton et al. protocol, and mapped the derived myogenic progenitors to their developmental atlas. Intriguingly, they found that the hiPSC-derived progenitor cells align with the late embryonic to early fetal transition stage. In fact, these cells do not resemble postnatal or adult satellite cells and prolonging the differentiation protocol past seven weeks does not drive the hiPSC-derived skeletal muscle past the embryonic-to-fetal transition stage. Other studies also state that hiPSC-derived skeletal myocytes resemble an embryonic or fetal phenotype (54, 61).This is a particularly

important finding as it can affect our future translational hiPSC cell-based therapeutic studies for DMD patients.

Another possible reason for the observed differences between the myogenically differentiated DMD-patient hiPSCs and healthy control hiPSCs could be attributed to the non-transgene differentiation protocol used in this study. Recent advances in skeletal muscle differentiation from hiPSCs have led to two main types of protocols: reprogramming-mediated and non-reprogramming-mediated myogenic differentiation. Both methods produce varying myogenic yields in DMD hiPSCs compared to healthy control hiPSCs.

For example, Abujarour et al. used MYOD transfection with doxycycline to induce myogenic differentiation in both healthy and DMD-patient derived hiPSCs (56). They found no significant differences in %MYOG+ nuclei and fusion index between the DMD and healthy groups after seven days of differentiation. Additionally, in a more recent study, Caputo et al. used an enhanced version of the piggyBac transposon vector to induce expression of MYOD and BAF60C (encoded by the SMARCD3 gene) for myogenic differentiation (66). They found no difference in the differentiation potential of healthy and DMD-patient derived hiPSCs, with both forming phenotypically similar myotubes and expressing the same levels of myogenic markers.

Overall, studies utilizing reprogramming methods of myogenic differentiation, such as Abujarour et al. and Caputo et al., found no significant differences in differentiation between healthy and DMD-patient derived hiPSCs, as indicated by similar levels of myogenic markers and MHC-positive multinucleated myotubes.

Conversely, in 2016, Choi et al. used a chemical-compound, reprogramming-free method of hiPSC differentiation (72). Briefly, the group treated the hiPSCs with CHIR99021 and DAPT until day twelve, followed by growth and maintenance culturing conditions until day thirty. The resulting myogenic differentiation showed robust MHC and MYOG expressing cells, but when the protocol was used to differentiate DMD-patient derived iPSCs, the fusion index was significantly decreased compared to healthy controls. To confirm their findings, the group used the Shelton et al. protocol and found comparable robust myogenic differentiation, but with aberrant myotube formation with many branched arms in the DMD-patient derived cells. In our study, we did not notice any visual differences in MHC expression between the healthy control and DMD hiPSCs differentiated for twenty-one, thirty-five, and fifty days. However, future studies can further analyze myotube formation as measured by the fusion index.

Chal et al. used hESCs and hiPSCs to recapitulate myogenesis *in vitro* and this group also used CHIR99021 but added LDN193189 to induce progression into the paraxial mesoderm (26, 83). This was followed by addition of the growth factors IGF-1, HGF, and FGF2, and they cultured the cells for up to two months. They differentiated *mdx* mouse ES cell lines using this protocol and found no significant differences in multinucleated fiber length and diameter compared to control fibers. However, myofibers derived from the *mdx* hESCs showed significantly more lateral branches, without deficits in myotube fusion unlike the Choi et al. study.

An interesting, comprehensive study conducted by Al Tanoury et al. used CRISPR-Cas9 gene editing to generate two isogenic DMD-mutant hiPSC lines from a previously well-characterized wild-type line. They optimized the Chal et al. protocol by incorporating a

secondary differentiation strategy and observed a significant improvement in myogenic morphology with prednisolone treatment. However, around day 20 of the differentiation process, the authors reported a significant decrease in the number of MYOG+ cells in the two DMD lines, and reduced PAX7+ cells in one of the DMD line. Al Tanoury et al. suggested that a lack of dystrophin reduced the myogenic capacity of the differentiating cultures. Gene expression analysis also revealed a trend in reduced myogenic gene expression for *PAX7* in one of the DMD lines. In our study, we also found a trend for reduced *PAX7* gene expression in the twenty-one-day differentiated DMD1-2 compared to CONT1-2.

Unlike what Chal et al. and Choi et al. observed, Al Tanoury et al. demonstrated that the DMD hiPSCs that have been differentiated for 3-4 weeks show significantly more fusion of myocytes. Intriguingly, they also observed significantly more branching in the differentiated DMD myofibers. They suggested that increased fusion is a result of the constant regeneration that needs to happen because of the myofiber death observed in DMD patients.

Overall, in the hiPSC-skeletal muscle differentiation field, each protocol discussed had yielded varying outcomes, likely due to differences in the methods used, such as overexpression of myogenic factors or the use of chemically-defined culture conditions to induce myogenesis *in vitro*. Further experiments could explore fusion and branching of myocytes to compare our findings with those of others. As Al Tanoury et al. have mentioned, our *in vitro* model of myogenesis used three different DMD-patient derived hiPSC lines and then compared the myogenic yield with three different hiPSC lines from healthy individuals. Inherently, there was a great source of variability within and between

each line, and this could have significantly influenced the outcomes of the study. To address this issue, Al Tanoury and colleagues used CRISPR-Cas9 gene editing to introduce the DMD mutation into a well-characterized healthy parental line to create isogenic lines. Future studies could adopt this strategy before conducting the WNT7A and EGF treatment studies.

4.3 WNT7A EXPANDS THE MUSCLE STEM CELL POOL IN THE DMD- PATIENT DERIVED CELLS.

Our lab has previously shown that WNT7A modulates satellite cell division by stimulating their symmetric expansion. Le Grand et al. specifically demonstrated that WNT7A binds to its receptor FZD7 which leads to a polarized distribution of the PCP effector VANGL2, and then induces symmetric satellite cell expansion (17, 74). However, little is known about the ability of WNT7A to induce symmetric cell division in a human DMD model.

In contrast to *mdx* mice, patients with DMD demonstrate significantly reduced satellite cell proliferation potential and subsequent muscle regenerative issues (19, 43). In this respect, WNT7A treatment on the muscle stem cells derived from DMD-patient hiPSCs should increase their self-renewal capacity.

In this study, we show that WNT7A significantly increased *PAX7* gene expression and the proportion of PAX7+ cells in twenty-one-day differentiated DMD hiPSCs. At the same timepoint, WNT7A decreased the committed myogenic markers MYOD and MYOG, suggesting that WNT7A has expanded the muscle stem pool through symmetric cell division. Moreover, WNT7A reduced the proportion of cells expressing MYOD, MYOG, and the double positive PAX7+MYOD+ in thirty-five day differentiated healthy control

hiPSCs. Interestingly, immunofluorescence analysis showed a drastic reduction in MHC expression in both cell lines at day thirty-five and fifty. These results indicate that recombinant WNT7A protein treatment dramatically altered the myogenic differentiation program in both DMD-patient derived hiPSCs, and healthy control hiPSCs by reducing their myogenic commitment.

As previously mentioned, the twenty-one, thirty-five, and fifty-day differentiated DMD-patient cell lines demonstrated a significant reduction in the proportion of PAX7+ expressing cells when compared the healthy control lines at each of the timepoints. More specifically, the total number of cells that have expressed PAX7 out of the whole population was just below 20% at day twenty-one and thirty-five, and a little above 20% at day fifty. Notably, treatment with WNT7A significantly doubled the expression of PAX7, especially at day twenty-one, with a trend towards doubling at day thirty-five and fifty. These findings suggest that WNT7A treatment may have a positive effect on PAX7 expression in DMD-patient derived cells during myogenic differentiation.

Von Maltzahn and colleagues investigated the effect of WNT7A treatment on dystrophic mouse muscles, finding that it effectively caused satellite cell expansion and myofiber hypertrophy through activation of the AKT/mTOR pathway. This led to increased muscle strength and reduced contractile damage (43). In a recent study, Abujarour et al. overexpressed *MYOD* to direct DMD-patient hiPSCs into the myogenic lineage, and demonstrated that WNT7A treatment induced significant hypertrophy and increased myotube diameter in the resulting myoblasts. These findings align with those of Von Maltzahn, who also observed a significant increase in myotube diameter in human primary myoblasts treated with WNT7A (56).

Importantly, Bentzinger et al. showed that brief *ex vivo* exposure to WNT7A could activate the FZD7 receptor on satellite cells and myogenic progenitors, leading to a significant increase in cell polarization and migration. Moreover, when primary mouse satellite cells were treated with WNT7A and transplanted into *mdx* mice, their engraftment was enhanced due to improved cell dispersion. The authors observed the same effects in primary human myoblasts, where WNT7A treatment increased motility, hypertrophy, and engraftment.

Given that our WNT7A treatment resulted in a significant increase in the PAX7+ muscle stem cell pool for both DMD patient and healthy control hiPSCs, it would be valuable to investigate the regenerative potential of these cells *in vivo*. Transplantation of our WNT7A-treated muscle stem cells into *mdx* mice could provide insights into their ability to promote cell motility, hypertrophy, and regeneration in a dystrophic environment.

One very important thing to note is that we observed a significant reduction in MHC expression by day thirty-five and fifty, while MHC expression was rather unperturbed on day twenty-one. This finding may be attributed to the fact that our study involved a long-term treatment of WNT7A compared to previous studies, which usually involved short-term treatments lasting no more than 48 hours. It is possible that the prolonged exposure to WNT7A may have caused a reduction in myogenic commitment in the hiPSCs. For future engraftment studies, we recommend transplanting the day twenty-one muscle stem cells derived from DMD-patient hiPSCs, as they exhibited increased PAX7 expression, potentially mediated through WNT7A symmetric expansion.

We also observed some cell lines within the healthy control lines or within the DMD lines differentiate better into the myogenic lineage compared to others, and therefore could

have modified the results of the WNT7A treatment. For instance, the healthy control line CONT2 consistently exhibited a higher proportion of PAX7+ cells at all three timepoints, while a similar effect was observed in the DMD2 line. Moreover, the DMD1 hiPSC line yielded more committed progenitors at day thirty-five and fifty. These variations in differentiation between the patient lines may be attributed to the differentiation protocol utilized, as previously discussed, or could reflect inherent differences in the individuals themselves. Choi et al. performed therapeutic studies using hiPSC-derived myoblasts from DMD patients, and discovered that some patient-derived myoblasts did not exhibit a response to pharmacological interventions (72). The researchers suggested that *in vitro* cultures can reveal patient-specific differences in phenotypes and responses to therapeutic rescue, such as disease progression or variations in lifestyle factors (72, 84).

In summary, to test WNT7A as a therapeutic in a human, DMD context, it will be important to consider the WNT7A treatment length, and the differentiation efficiency of the DMD patient-derived hiPSCs prior to initiating engraftment studies.

4.4 EGF TREATMENT REDUCES PAX7 EXPRESSING CELLS IN THE TOTAL POPULATION AND WITHIN THE MYOGENIC POPULATION.

Wang et al. previously reported that EGF stimulation of mouse satellite cells activates its receptor EGFR and recruits the mitotic spindle assembly protein AURKA to promote apicobasal asymmetric cell division (47). In the context of DMD, the authors reported that *in vivo* EGF treatment in *mdx* mice significantly increased the number of asymmetric cell divisions, restored proper myogenic precursor levels, and enhanced muscle regeneration.

We found that EGF treatment on the differentiating hiPSCs consistently reduced the proportion of PAX7 expressing cells in the total population at all three time points. Consistent with the Wang et al. study, EGF may have induced asymmetric division to increase the proportion of committed myogenic precursors within the myogenic population as we saw a significant increase in MYOD and MYOG in the fifty-day differentiated CONT1-2. However, we only saw a modest increase in MYOG expression on day thirty-five for DMD1-2 and significant reduction in global *MYOD* gene expression on day twenty-one.

It is possible that EGF affected other non-myogenic cell populations, as EGF is known to stimulate the proliferation and survival of various cell types, including epithelial cells and neural stem cells. However, the specific effects of EGF on non-myogenic cells in the context of DMD or muscle regeneration are currently unknown and would require further investigation.

Xi et al. identified other cell types derived from hiPSCs using the Shelton et al. protocol (82). At week six-seven of the differentiation program, the authors used their single-cell RNA sequencing strategy to examine the cultures. They observed a population that might be involved in epithelial development as the cells robustly expressed genes related to cytokeratins or keratinization. They also identified a major subpopulation that lacked canonical expression of osteogenic, chondrogenic, or tenogenic lineages, but nonetheless expressed genes involved in skeletal development such as *COL1A1*, and *OGN*. This raises the possibility that EGF could be affecting multiple other cell populations.

Additionally, as previously mentioned, the Xi et al. group mapped the differentiating cultures from the Shelton et al. protocol to the late embryonic to early fetal transition of human myogenesis (82). Fung et al. conducted PAX7 lineage-tracing studies in mice during

embryogenesis and found that PAX7-expressing cells that do not commit to the myogenic lineage can give rise to embryonic fibro-adipogenic progenitors (FAPs) with bipotent potential towards dermal fibroblasts and brown adipocytes (85). Recent work from our lab found that EGFR ligands can affect FAP differentiation into adipocytes (Wen Pan & Michael Rudnicki, unpublished), further highlighting the importance of considering potential effects on non-myogenic cell populations when evaluating the division modulating potential of EGF. Another potential explanation to what we observed in our results was the expression of *TUBB3* indicating the presence of neural crest cells in both healthy and DMD-patient derived hiPSCs that were differentiated for twenty-one days. EGF treatment could have stimulated these cells, as well as other neuronal cells, and induced asymmetric division. Previous studies have suggested that neural crest cells, as well as neuroblasts, can undergo asymmetric divisions through similar molecular mechanisms as satellite stem cells (86, 87). Therefore, for future studies, it will be very important to purify the differentiating hiPSC cultures for the myogenic population prior to treatment with EGF.

Finally, this study solely looked at myogenic markers to determine whether EGF treatment expanded the committed progenitor pool. PARD3 staining of the hiPSC-derived muscle stem cells can also be conducted to properly enumerate asymmetric division events. Furthermore, to enhance the efficacy of therapeutic transplant studies, a two-step approach can be considered. First, WNT7A treatment could be used to increase the PAX7+ cell population. This could be followed by EGF treatment, which has the potential to induce asymmetric division in the expanded PAX7+ muscle stem cells and enhance the committed progenitor cell pool in both healthy control and DMD cell lines.

5.0 FUTURE STUDIES

In future studies, it would be useful to use CRISPR-Cas9 to generate isogenic dystrophin-null hiPSCs from a healthy donor line. This approach would allow for the identification of whether the differences in differentiation efficiency observed were due to the absence of dystrophin. Additionally, these isogenic lines could help determine whether the differences in response to WNT7A and EGF treatment between the healthy and DMD lines are specifically attributed to the dystrophin deficiency. To further characterize the differentiated hiPSCs, single-cell RNA sequencing can be conducted to delineate their identities and trajectory.

In the context of future therapeutic studies, it is essential to consider promoting the formation of adult satellite cells, since the muscle stem cells and progenitors derived from our hiPSC platform were at the late embryonic/fetal stage. One potential approach to induce the conversion of embryonic/fetal muscle stem cells to a more adult phenotype would be through thyroid hormone (T3) stimulation. Previous studies have shown that T3 directly targets MYOD and downstream myogenic factors to promote myogenic differentiation (88). More importantly, T3 plays a crucial role in the transition of fetal muscle fibers to adult myosin isoforms and stimulates myoblasts to terminal differentiation (89). We suggest conducting T3 treatment on the differentiating cultures around day thirty-five to fifty, as more myogenic progenitors were present towards the end of differentiation.

Lastly, to evaluate the potential therapeutic effect of WNT7A and EGF treatment on hiPSC-derived myogenic cells for DMD, transplantation studies in *mdx* mice would be necessary. As the differentiation process yields a heterogeneous cell population, fluorescence activated cell sorting can be used to enrich for the myogenic population prior to the

WNT7A/EGF treatment and transplantation. Markers such as VCAM1, CD34, NCAM1, CXCR4, and others that are extensively reviewed in Tey et al. can help to remove unwanted cell types that may lead to poor engraftment or teratoma formation *in vivo* (55, 90). Specifically transplanting the PAX7+ cells derived from the WNT7A treated condition can further explore their self-renewing and differentiation capacity.

6.0 CONCLUDING STATEMENTS

In summary, this study highlights the importance of customizing skeletal muscle differentiation protocols for different hiPSC lines. Furthermore, we provide evidence of the potential differences in differentiation capabilities of hiPSCs derived from healthy individuals versus DMD-patients. We suspect that DMD-patient hiPSC derived muscle stem cells precociously differentiate, however, more investigation is required. Most importantly, we demonstrate the potential of WNT7A and EGF to manipulate the division dynamics of muscle stem cells and progenitors derived from healthy and DMD-patient hiPSCs, providing a promising avenue for future therapeutic studies. We envisage that this project and future work will provide translational evidence for applying these therapeutic candidates to tackling DMD pathology.

References

1. Frontera WR, Ochala J. 2015. Skeletal Muscle: A Brief Review of Structure and Function. Calcif Tissue Int 96:183–195.

2. Dumont NA, Bentzinger CF, Sincennes M-C, Rudnicki MA. 2015. Satellite Cells and Skeletal Muscle Regeneration, p. 1027–1059. *In* Comprehensive Physiology. American Cancer Society.

3. von Maltzahn J, Jones AE, Parks RJ, Rudnicki MA. 2013. Pax7 is critical for the normal function of satellite cells in adult skeletal muscle. Proc Natl Acad Sci USA 110:16474–16479.

4. Bentzinger CF, Wang YX, Rudnicki MA. 2012. Building Muscle: Molecular Regulation of Myogenesis. Cold Spring Harb Perspect Biol 4:a008342.

5. Yin H, Price F, Rudnicki MA. 2013. Satellite Cells and the Muscle Stem Cell Niche. Physiol Rev 93:23–67.

6. Mauro A. 1961. SATELLITE CELL OF SKELETAL MUSCLE FIBERS. J Biophys Biochem Cytol 9:493–495.

7. Seale P, Sabourin LA, Girgis-Gabardo A, Mansouri A, Gruss P, Rudnicki MA. 2000. Pax7 Is Required for the Specification of Myogenic Satellite Cells. Cell 102:777–786.

8. Kuang S, Chargé SB, Seale P, Huh M, Rudnicki MA. 2006. Distinct roles for Pax7 and Pax3 in adult regenerative myogenesis. J Cell Biol 172:103–113.

9. Günther S, Kim J, Kostin S, Lepper C, Fan C-M, Braun T. 2013. Myf5-Positive Satellite Cells Contribute to Pax7-Dependent Long-Term Maintenance of Adult Muscle Stem Cells. Cell Stem Cell 13:590–601.

10. Sambasivan R, Yao R, Kissenpfennig A, Van Wittenberghe L, Paldi A, Gayraud-Morel B, Guenou H, Malissen B, Tajbakhsh S, Galy A. 2011. Pax7-expressing satellite cells are indispensable for adult skeletal muscle regeneration. Development 138:3647–3656.

11. Lepper C, Partridge TA, Fan C-M. 2011. An absolute requirement for Pax7-positive satellite cells in acute injury-induced skeletal muscle regeneration. Development 138:3639–3646.

12. Schmidt M, Schüler SC, Hüttner SS, von Eyss B, von Maltzahn J. 2019. Adult stem cells at work: regenerating skeletal muscle. Cell Mol Life Sci 76:2559–2570.

13. Zammit PS. 2017. Function of the myogenic regulatory factors Myf5, MyoD, Myogenin and MRF4 in skeletal muscle, satellite cells and regenerative myogenesis. Seminars in Cell & Developmental Biology 72:19–32.

14. Stockdale FE. 1992. Myogenic cell lineages. Developmental Biology 154:284–298.

15. Kuang S, Kuroda K, Le Grand F, Rudnicki MA. 2007. Asymmetric Self-Renewal and Commitment of Satellite Stem Cells in Muscle. Cell 129:999–1010.

16. Chen W, Datzkiw D, Rudnicki MA. 2020. Satellite cells in ageing: use it or lose it. Open Biology 10:200048.

17. Le Grand F, Jones AE, Seale V, Scimè A, Rudnicki MA. 2009. Wnt7a Activates the Planar Cell Polarity Pathway to Drive the Symmetric Expansion of Satellite Stem Cells. Cell Stem Cell 4:535–547.

18. Rudnicki MA, Grand FL, McKinnell I, Kuang S. 2008. The Molecular Regulation of Muscle Stem Cell Function. Cold Spring Harb Symp Quant Biol 73:323–331.

19. Dumont NA, Wang YX, von Maltzahn J, Pasut A, Bentzinger CF, Brun CE, Rudnicki MA. 2015. Dystrophin expression in muscle stem cells regulates their polarity and asymmetric division. Nat Med 21:1455–1463.

20. Bentzinger CF, Wang YX, von Maltzahn J, Soleimani VD, Yin H, Rudnicki MA. 2013. Fibronectin regulates Wnt7a signaling and satellite cell expansion. Cell Stem Cell 12:75–87.

21. Feige P, Brun CE, Ritso M, Rudnicki MA. 2018. Orienting Muscle Stem Cells for Regeneration in Homeostasis, Aging, and Disease. Cell Stem Cell 23:653–664.

22. Maroto M, Bone RA, Dale JK. 2012. Somitogenesis. Development 139:2453–2456.

23. Chal J, Pourquié O. 2017. Making muscle: skeletal myogenesis in vivo and in vitro. Development 144:2104–2122.

24. Bentzinger CF, Wang YX, Rudnicki MA. 2012. Building Muscle: Molecular Regulation of Myogenesis. Cold Spring Harb Perspect Biol 4:a008342.

25. Borchin B, Chen J, Barberi T. 2013. Derivation and FACS-Mediated Purification of PAX3+/PAX7+ Skeletal Muscle Precursors from Human Pluripotent Stem Cells. Stem Cell Reports 1:620–631.

26. Chal J, Oginuma M, Al Tanoury Z, Gobert B, Sumara O, Hick A, Bousson F, Zidouni Y, Mursch C, Moncuquet P, Tassy O, Vincent S, Miyanari A, Bera A, Garnier J-M, Guevara G, Hestin M, Kennedy L, Hayashi S, Drayton B, Cherrier T, Gayraud-Morel B, Gussoni E, Relaix F, Tajbakhsh S, Pourquié O. 2015. Differentiation of pluripotent stem cells to muscle fiber to model Duchenne muscular dystrophy. 9. Nature Biotechnology 33:962–969.

27. Jin W, Peng J, Jiang S. 2016. The epigenetic regulation of embryonic myogenesis and adult muscle regeneration by histone methylation modification. Biochemistry and Biophysics Reports 6:209–219.

28. Sanaki-Matsumiya M, Matsuda M, Gritti N, Nakaki F, Sharpe J, Trivedi V, Ebisuya M. 2022. Periodic formation of epithelial somites from human pluripotent stem cells. Nat Commun 13:2325.

29. Veenvliet JV, Bolondi A, Kretzmer H, Haut L, Scholze-Wittler M, Schifferl D, Koch F, Guignard L, Kumar AS, Pustet M, Heimann S, Buschow R, Wittler L, Timmermann B, Meissner A, Herrmann BG. 2020. Mouse embryonic stem cells self-organize into trunk-like structures with neural tube and somites. Science 370:eaba4937.

30. Yamanaka Y, Hamidi S, Yoshioka-Kobayashi K, Munira S, Sunadome K, Zhang Y, Kurokawa Y, Ericsson R, Mieda A, Thompson JL, Kerwin J, Lisgo S, Yamamoto T, Moris N, Martinez-Arias A, Tsujimura T, Alev C. 2023. Reconstituting human somitogenesis in vitro. 7948. Nature 614:509–520.

31. Sun C, Serra C, Lee G, Wagner KR. 2020. Stem cell-based therapies for Duchenne muscular dystrophy. Experimental Neurology 323:113086.

32. Goldstein JA, McNally EM. 2010. Mechanisms of muscle weakness in muscular dystrophy. J Gen Physiol 136:29–34.

33. Sacco A, Mourkioti F, Tran R, Choi J, Llewellyn M, Kraft P, Shkreli M, Delp S, Pomerantz JH, Artandi SE, Blau HM. 2010. Short Telomeres and Stem Cell Exhaustion Model Duchenne Muscular Dystrophy in mdx/mTR Mice. Cell 143:1059–1071.

34. Blau HM, Webster C, Pavlath GK. 1983. Defective myoblasts identified in Duchenne muscular dystrophy. Proc Natl Acad Sci U S A 80:4856–4860.

35. Webster C, Blau HM. 1990. Accelerated age-related decline in replicative life-span of Duchenne muscular dystrophy myoblasts: implications for cell and gene therapy. Somat Cell Mol Genet 16:557–565.

36. Kottlors M, Kirschner J. 2010. Elevated satellite cell number in Duchenne muscular dystrophy. Cell Tissue Res 340:541–548.

37. Jiang C, Wen Y, Kuroda K, Hannon K, Rudnicki MA, Kuang S. 2014. Notch signaling deficiency underlies age-dependent depletion of satellite cells in muscular dystrophy. Dis Model Mech 7:997–1004.

38. Ikeya M, Takada S. 1998. Wnt signaling from the dorsal neural tube is required for the formation of the medial dermomyotome. Development 125:4969–4976.

39. Rudnicki MA, Williams BO. 2015. Wnt signaling in bone and muscle. Bone 80:60–66.

40. Otto A, Schmidt C, Luke G, Allen S, Valasek P, Muntoni F, Lawrence-Watt D, Patel K. 2008. Canonical Wnt signalling induces satellite-cell proliferation during adult skeletal muscle regeneration. J Cell Sci 121:2939–2950.

41. Brack AS, Conboy IM, Conboy MJ, Shen J, Rando TA. 2008. A temporal switch from notch to Wnt signaling in muscle stem cells is necessary for normal adult myogenesis. Cell Stem Cell 2:50–59.

42. Murphy MM, Keefe AC, Lawson JA, Flygare SD, Yandell M, Kardon G. 2014. Transiently active Wnt/β-catenin signaling is not required but must be silenced for stem cell function during muscle regeneration. Stem Cell Reports 3:475–488.

43. Maltzahn J von, Renaud J-M, Parise G, Rudnicki MA. 2012. Wnt7a treatment ameliorates muscular dystrophy. PNAS 109:20614–20619.

44. von Maltzahn J, Bentzinger CF, Rudnicki MA. 2011. Wnt7a-Fzd7 signalling directly activates the Akt/mTOR anabolic growth pathway in skeletal muscle. Nat Cell Biol 14:186–191.

45. Olwin BB, Hauschka SD. 1988. Cell surface fibroblast growth factor and epidermal growth factor receptors are permanently lost during skeletal muscle terminal differentiation in culture. J Cell Biol 107:761–769.

46. Leroy MC, Perroud J, Darbellay B, Bernheim L, Konig S. 2013. Epidermal Growth Factor Receptor Down-Regulation Triggers Human Myoblast Differentiation. PLoS One 8:e71770.

47. Wang YX, Feige P, Brun CE, Hekmatnejad B, Dumont NA, Renaud J-M, Faulkes S, Guindon DE, Rudnicki MA. 2019. EGFR-Aurka Signaling Rescues Polarity and Regeneration Defects in Dystrophin-Deficient Muscle Stem Cells by Increasing Asymmetric Divisions. Cell Stem Cell 24:419-432.e6.

48. Bulfield G, Siller WG, Wight PA, Moore KJ. 1984. X chromosome-linked muscular dystrophy (mdx) in the mouse. Proc Natl Acad Sci U S A 81:1189–1192.

49. Allen DG, Whitehead NP, Froehner SC. 2016. Absence of Dystrophin Disrupts Skeletal Muscle Signaling: Roles of Ca^{2+}, Reactive Oxygen Species, and Nitric Oxide in the Development of Muscular Dystrophy. Physiological Reviews 96:253–305.

50. Morgan JE, Prola A, Mariot V, Pini V, Meng J, Hourde C, Dumonceaux J, Conti F, Relaix F, Authier F-J, Tiret L, Muntoni F, Bencze M. 2018. Necroptosis mediates myofibre death in dystrophin-deficient mice. 1. Nature Communications 9:3655.

51. Takahashi K, Tanabe K, Ohnuki M, Narita M, Ichisaka T, Tomoda K, Yamanaka S. 2007. Induction of Pluripotent Stem Cells from Adult Human Fibroblasts by Defined Factors. Cell 131:861–872.

52. Shelton M, Kocharyan A, Liu J, Skerjanc IS, Stanford WL. 2016. Robust generation and expansion of skeletal muscle progenitors and myocytes from human pluripotent stem cells. Methods 101:73–84.

53. Piga D, Salani S, Magri F, Brusa R, Mauri E, Comi GP, Bresolin N, Corti S. 2019. Human induced pluripotent stem cell models for the study and treatment of Duchenne and Becker muscular dystrophies. Ther Adv Neurol Disord 12.

54. Jiwlawat N, Lynch E, Jeffrey J, Van Dyke JM, Suzuki M. 2018. Current Progress and Challenges for Skeletal Muscle Differentiation from Human Pluripotent Stem Cells Using Transgene-Free Approaches. Stem Cells International 2018:e6241681.

55. Iberite F, Gruppioni E, Ricotti L. 2022. Skeletal muscle differentiation of human iPSCs meets bioengineering strategies: perspectives and challenges. 1. npj Regen Med 7:1–30.

56. Abujarour R, Bennett M, Valamehr B, Lee TT, Robinson M, Robbins D, Le T, Lai K, Flynn P. 2014. Myogenic Differentiation of Muscular Dystrophy-Specific Induced Pluripotent Stem Cells for Use in Drug Discovery. Stem Cells Transl Med 3:149–160.

57. Tanaka A, Woltjen K, Miyake K, Hotta A, Ikeya M, Yamamoto T, Nishino T, Shoji E, Sehara-Fujisawa A, Manabe Y, Fujii N, Hanaoka K, Era T, Yamashita S, Isobe K, Kimura E, Sakurai H. 2013. Efficient and Reproducible Myogenic Differentiation from Human iPS Cells: Prospects for Modeling Miyoshi Myopathy In Vitro. PLoS One 8:e61540.

58. Maffioletti SM, Gerli MFM, Ragazzi M, Dastidar S, Benedetti S, Loperfido M, VandenDriessche T, Chuah MK, Tedesco FS. 2015. Efficient derivation and inducible differentiation of expandable skeletal myogenic cells from human ES and patient-specific iPS cells. 7. Nat Protoc 10:941–958.

59. Darabi R, Arpke RW, Irion S, Dimos JT, Grskovic M, Kyba M, Perlingeiro RCR. 2012. Human ES- and iPS-Derived Myogenic Progenitors Restore Dystrophin and Improve Contractility upon Transplantation in Dystrophic Mice. Cell Stem Cell 10:610–619.

60. Sun C, Kannan S, Choi IY, Lim H, Zhang H, Chen GS, Zhang N, Park S-H, Serra C, Iyer SR, Lloyd TE, Kwon C, Lovering RM, Lim SB, Andersen P, Wagner KR, Lee G. 2022. Human pluripotent stem cell-derived myogenic progenitors undergo maturation to quiescent satellite cells upon engraftment. Cell Stem Cell 29:610-619.e5.

61. Mournetas V, Massouridès E, Dupont J, Kornobis E, Polvèche H, Jarrige M, Dorval ARL, Gosselin MRF, Manousopoulou A, Garbis SD, Górecki DC, Pinset C. 2021. Myogenesis modelled by human pluripotent stem cells: a multi-omic study of Duchenne myopathy early onset. J Cachexia Sarcopenia Muscle 12:209–232.

62. Beers J, Gulbranson DR, George N, Siniscalchi LI, Jones J, Thomson JA, Chen G. 2012. Passaging and colony expansion of human pluripotent stem cells by enzyme-free dissociation in chemically defined culture conditions. 11. Nat Protoc 7:2029–2040.

63. Lange J, Wood-Kaczmar A, Ali A, Farag S, Ghosh R, Parker J, Casey C, Uno Y, Kunugi A, Ferretti P, Andre R, Tabrizi SJ. 2021. Mislocalization of Nucleocytoplasmic Transport Proteins in Human Huntington's Disease PSC-Derived Striatal Neurons. Frontiers in Cellular Neuroscience 15.

64. Xu N, Wu J, Ortiz-Vitali JL, Li Y, Darabi R. 2021. Directed Differentiation of Human Pluripotent Stem Cells toward Skeletal Myogenic Progenitors and Their Purification Using Surface Markers. Cells 10:2746.

65. Xi H, Fujiwara W, Gonzalez K, Jan M, Liebscher S, Van Handel B, Schenke-Layland K, Pyle AD. 2017. In vivo Human Somitogenesis Guides Somite Development from hPSCs. Cell Rep 18:1573–1585.

66. Caputo L, Granados A, Lenzi J, Rosa A, Ait-Si-Ali S, Puri PL, Albini S. 2020. Acute conversion of patient-derived Duchenne muscular dystrophy iPSC into myotubes reveals constitutive and inducible over-activation of TGFβ-dependent pro-fibrotic signaling. Skeletal Muscle 10:13.

67. Selvaraj S, Mondragon-Gonzalez R, Xu B, Magli A, Kim H, Lainé J, Kiley J, Mckee H, Rinaldi F, Aho J, Tabti N, Shen W, Perlingeiro RC. 2019. Screening identifies small molecules that enhance the maturation of human pluripotent stem cell-derived myotubes. Elife 8:e47970.

68. Hosoyama T, McGivern JV, Van Dyke JM, Ebert AD, Suzuki M. 2014. Derivation of Myogenic Progenitors Directly From Human Pluripotent Stem Cells Using a Sphere-Based Culture. Stem Cells Transl Med 3:564–574.

69. Sakai-Takemura F, Narita A, Masuda S, Wakamatsu T, Watanabe N, Nishiyama T, Nogami K, Blanc M, Takeda S, Miyagoe-Suzuki Y. 2018. Premyogenic progenitors derived from human pluripotent stem cells expand in floating culture and differentiate into transplantable myogenic progenitors. 1. Sci Rep 8:6555.

70. van der Wal E, Herrero-Hernandez P, Wan R, Broeders M, in ’t Groen SLM, van Gestel TJM, van IJcken WFJ, Cheung TH, van der Ploeg AT, Schaaf GJ, Pijnappel WWMP. 2018. Large-

Scale Expansion of Human iPSC-Derived Skeletal Muscle Cells for Disease Modeling and Cell-Based Therapeutic Strategies. Stem Cell Reports 10:1975–1990.

71. Madana M, Ritso M, Yockell-Lelievre J, Carmona R, Rudnicki MA. 2020. Modulating human embryonic stem cell-derived satellite-like cell division with WNT7A and epidermal growth factor. Honours Thesis 1:21.

72. Choi IY, Lim H, Estrellas K, Mula J, Cohen TV, Zhang Y, Donnelly CJ, Richard J-P, Kim YJ, Kim H, Kazuki Y, Oshimura M, Li HL, Hotta A, Rothstein J, Maragakis N, Wagner KR, Lee G. 2016. Concordant but Varied Phenotypes among Duchenne Muscular Dystrophy Patient-Specific Myoblasts Derived using a Human iPSC-Based Model. Cell Reports 15:2301–2312.

73. Al Tanoury Z, Zimmerman JF, Rao J, Sieiro D, McNamara HM, Cherrier T, Rodríguez-delaRosa A, Hick-Colin A, Bousson F, Fugier-Schmucker C, Marchiano F, Habermann B, Chal J, Nesmith AP, Gapon S, Wagner E, Gupta VA, Bassel-Duby R, Olson EN, Cohen AE, Parker KK, Pourquié O. 2021. Prednisolone rescues Duchenne muscular dystrophy phenotypes in human pluripotent stem cell–derived skeletal muscle in vitro. Proc Natl Acad Sci USA 118:e2022960118.

74. von Maltzahn J, Chang NC, Bentzinger CF, Rudnicki MA. 2012. Wnt Signaling in Myogenesis. Trends Cell Biol 22:602–609.

75. Montarras D, Morgan J, Collins C, Relaix F, Zaffran S, Cumano A, Partridge T, Buckingham M. 2005. Direct isolation of satellite cells for skeletal muscle regeneration. Science 309:2064–2068.

76. Hicks MR, Hiserodt J, Paras K, Fujiwara W, Eskin A, Jan M, Xi H, Young CS, Evseenko D, Nelson SF, Spencer MJ, Van Handel B, Pyle AD. 2018. ERBB3 and NGFR mark a distinct skeletal muscle progenitor cell in human development and hPSCs. Nat Cell Biol 20:46–57.

77. Nagasaka R, Matsumoto M, Okada M, Sasaki H, Kanie K, Kii H, Uozumi T, Kiyota Y, Honda H, Kato R. 2017. Visualization of morphological categories of colonies for monitoring of effect on induced pluripotent stem cell culture status. Regenerative Therapy 6:41–51.

78. Ghaedi M, Niklason LE. 2019. Human Pluripotent Stem Cells (iPSC) Generation, Culture, and Differentiation to Lung Progenitor Cells. Methods Mol Biol 1576:55–92.

79. Assessment of Muscle Function Following hiPSC-Derived Myoblast Transplantation in Dystrophic Mice https://doi.org/10.1002/cpz1.356.

80. Shelton M, Metz J, Liu J, Carpenedo RL, Demers S-P, Stanford WL, Skerjanc IS. 2014. Derivation and Expansion of PAX7-Positive Muscle Progenitors from Human and Mouse Embryonic Stem Cells. Stem Cell Reports 3:516–529.

81. Baci D, Chirivì M, Pace V, Maiullari F, Milan M, Rampin A, Somma P, Presutti D, Garavelli S, Bruno A, Cannata S, Lanzuolo C, Gargioli C, Rizzi R, Bearzi C. 2020. Extracellular Vesicles from Skeletal Muscle Cells Efficiently Promote Myogenesis in Induced Pluripotent Stem Cells. Cells 9:1527.

82. Xi H, Langerman J, Sabri S, Chien P, Young CS, Younesi S, Hicks M, Gonzalez K, Fujiwara W, Marzi J, Liebscher S, Spencer M, Van Handel B, Evseenko D, Schenke-Layland K, Plath K, Pyle AD. 2020. A Human Skeletal Muscle Atlas Identifies the Trajectories of Stem and Progenitor Cells across Development and from Human Pluripotent Stem Cells. Cell Stem Cell 27:158-176.e10.

83. Chal J, Al Tanoury Z, Hestin M, Gobert B, Aivio S, Hick A, Cherrier T, Nesmith AP, Parker KK, Pourquié O. 2016. Generation of human muscle fibers and satellite-like cells from human pluripotent stem cells in vitro. 10. Nat Protoc 11:1833–1850.

84. Pegoraro E, Hoffman EP, Piva L, Gavassini BF, Cagnin S, Ermani M, Bello L, Soraru G, Pacchioni B, Bonifati MD, Lanfranchi G, Angelini C, Kesari A, Lee I, Gordish-Dressman H, Devaney JM, McDonald CM, Cooperative International Neuromuscular Research Group. 2011. SPP1 genotype is a determinant of disease severity in Duchenne muscular dystrophy. Neurology 76:219–226.

85. Fung CW, Zhou S, Zhu H, Wei X, Wu Z, Wu AR. 2022. Cell fate determining molecular switches and signaling pathways in Pax7-expressing somitic mesoderm. Cell Discov 8:61.

86. Chang NC, Chevalier FP, Rudnicki MA. 2016. Satellite Cells in Muscular Dystrophy - Lost in Polarity. Trends Mol Med 22:479–496.

87. Alhashem Z, Camargo-Sosa K, Kelsh RN, Linker C. 2022. Trunk Neural Crest Migratory Position and Asymmetric Division Predict Terminal Differentiation. Front Cell Dev Biol 10:887393.

88. Ambrosio R, De Stefano MA, Di Girolamo D, Salvatore D. 2017. Thyroid hormone signaling and deiodinase actions in muscle stem/progenitor cells. Molecular and Cellular Endocrinology 459:79–83.

89. Lee J-W, Kim N-H, Milanesi A. 2014. Thyroid Hormone Signaling in Muscle Development, Repair and Metabolism. J Endocrinol Diabetes Obes 2:1046.

90. Tey S-R, Robertson S, Lynch E, Suzuki M. 2019. Coding Cell Identity of Human Skeletal Muscle Progenitor Cells Using Cell Surface Markers: Current Status and Remaining Challenges for Characterization and Isolation. Front Cell Dev Biol 7:284.